Head involution in *Drosophila melanogaster*

On the role of supracellular actomyosin structures in tissue bending, spreading, and positioning

Natalia Dorota Czerniak

TESI DOCTORAL UPF / ANY 2015

DIRECTOR DE LA TESI
Jérôme Solon, Phd.
Cell and Developmental Biology Programme, CRG.

Rodzicom

Acknowledgements

First of all, I would like to thank Jérôme for the supervision. Thank you for letting me play and try out new things, and for having the patience when I was playing too much! :) Thank you for your guidance, teaching, and help in structuring my ideas. Thank you for your kindness and for always, always being there for me.

I would like to thank my thesis committee for reviewing my work and for all the great advice: Yogi Yaeger, Enrique Martin Blanco and Xavi Trepat.

A huge thank you to the microscopy facility at CRG, for constantly helping me, even when I almost crashed the double photon :) Thank you Arrate, Raquel, Xavi and Timo.

Thank you Jim and Jürgen for helping with the SPIM.

Special thanks to Julien Colombelli, for letting me use the laser cutter, for all the help and discussions. Thanks to Lidia, Anna, Maria and Sebastian at the Advanced Digital Microscopy Unit at IRB, for all the help and for making the trips to IRB such a nice time!

I would like to thank many people for productive discussions and lots of advice on my project; I wasn't suppose to write the acknowledgements the night before printing, so I can only hope that I won't forget anyone! Thanks to Marta Llimargas, Marco Milan, Andreu Casali, Hilde Janssens, Javier Terriente and Javier Diego Iñiguez.

I would like to thank Annick and Marta for the opportunity to teach, communicate science and to learn so much from it.

Warm thanks to Alba, Isabel, Rut, Sharon and Imma, for always being so helpful, especially the times I was running late with deadlines.

And, of course, the lab!!! For all the help, discussions and criticism. Thank you all so much for also making it an awesome time! For all the coffees and beers and tapas :) Thank you for letting me be myself, and also for helping me grow up.

Thanks to Doc, for introducing me to the world of research, for all the hints and advice, all the conversations, your positive energy and love.

Special thanks to Arturo. Monster! Thank you for teaching me, for being patient and kind, for all your help! Thanks for being playful and looking out for me at the same time. Thanks for the meetings at your wonderful apartment, for all the warmth and love.

Thanks to Petra, for all the help with the flies, for your patience and all the sweets :)

Piggies!!! Thank you for the study sessions, the sciencing, for all the silliness and laughs. Thank you for becoming amazing friends.

Angee, thank you for your sweetness, sincerity, for always being there and cheering me up.

Thanks to David for all the scripts, help with the english (the?), all the coffees in the morning, for always making sure we arrive on time :) Thanks for teaching me the diplomacy and for your kind heart.

Huge thanks to Kai! For all the theory and math, for showing me all the scientific values and being an incredible teacher. Thank you for reading, and re-reading this thesis. Thank you for always believing in me and convincing me that I, too, believe in myself.

Thanks to Yogi, for always reassuring me that I could do this :)

I would also like to thank Mirko, Jelena and Luciano for introducing me to CRG, and for the great times between the PRBB and la Paloma.

Thank you Alba for helping with the Catalan, for all your positive energy and for always wanting to go dancing!

Thanks to Andy and Tommaso for often listening to lots of complaints, for the good vibes, dinners and all the cheese :p

Thanks to my friends at CRG for all the great times and your positivity.

Gracias a Ale por ser tan incredible!

Gracias a Jose: sin ti no estuviera aqui preperandome para imprimir la tesis. Mil gracias por ayudarme en todo, por aguantar los berrinches, por creer en mi, y por siempre siempre motivarme para ser mejor.

Dziekuje Rodzicom! Nigdy bym nie zaszla tak daleko w spelnianiu swoich marzen bez waszej pomocy i wsparcia. Dziekuje za wszystko! Dziekuje za to, ze przez te wszystkie lata, podczas kazdego zakonczenia roku szkolnego byliscie ze mnie dumni i kazaliscie podnosic poprzeczke coraz wyzej. Kocham Was najmocniej jak sie da. Dziekuje Dagusi za to ze byla moja pierwsza nauczycielka :) Ponad dwadziescia piec lat pozniej, wreszcie koncze szkole!

Dziekuje grzedzie, za wysluchiwanie szlochow i skarg, za wsparcie i nieustajace slowa otuchy. Szczegolne podziekowania dla Grubego, za to, ze ciagle nagrywamy film :)

Thank you all for making this possible!

Natalia Dorota Czerniak
Barcelona 29th of April, 2015.

Abstract

Morphogenesis creates a plethora of complex shapes in plants and animals. We devote this work to the study of *Drosophila* head involution (HI), a late embryogenetic process, which involves complete rearrangement of the head tissues, internalization of the brain and spreading of the epidermis. We show, for the first time, the complete kinetics of HI with high spatial and temporal resolution.

We describe the movements leading to the internalization of the embryonic brain, its "sculpting" by apoptosis, and cell removal by hemocytes. We then focus on the epidermal progression over the head, which can be divided into two phases: rolling and sliding. We show that both phases are powered by a supracelullar actomyosin cable, which first exerts a pushing force and drives the rolling of tissue anterior to it, and then produces a pulling force when it becomes the leading edge cable. We also show that the spreading of the epidermis is spatially controlled resulting in segments of equal width being precisely positioned along the AP axis. This positional control is performed by patterned tensile forces along the epidermal layer regulated by hedgehog signaling. Our study reveals a mechanism by which genes involved in body segmentation are also regulating morphogenesis.

Resum

La morfogènesi crea una plètora de formes complexes en animals i plantes. Hem consagrat aquest treball a l'estudi de la involuciò del cap (head involution HI) de Drosophila, un procès embriogenètic tardiu, que implica un complet rearranjament dels teixits del cap, així com la internalització del cervell i la propagació de l'epidermis. Mostrem, pel primer cop, la cinètica completa de HI amb una alta resolució espacial i temporal.

Describim els moviments que porten a la internalitzaciò del cervell de l'embriò, així com el seu "sculpting" per apoptosi i l'eliminació de cèl.lules pels hemòcits. Seguidament, hem enfocat l'estudi en la progressió de l'epidermis sobre el cap de l'embrió, essent aquest un esdeveniment que es pot dividir en dues fases: rodolament i lliscament.

Mostrem que totes dues fases son impulsades per un cable d'actomyosina, que primer exerceix una força que empeny i condueix el rodolament del teixit anterior a aquesta i després, un cop el cable convertit en cable principal, produeix una forca que estira. També mostrem que la propagació de l'epidermis es troba espacialment controlada, tenint aquest control com a resultat la formació de segments de mateixa amplada posicionats de manera precisa al llarg the l'axis AP. Aquest control posicional és dut a terme per forces tènsils al llarg de la capa epidèrmica regulades per hedgehog. El nostre estudi revela un mecanisme pel qual els gens involucrats en la segmentació troncal regulen al seu torn la morfogènesi.

Contents

List of Figures

List of Movies

INTRODUCTION

Chapter 1

What is this life if, full of care,
We have no time to stand and stare.
No time to stand beneath the boughs
And stare as long as sheep or cows.
No time to see, when woods we pass,
Where squirrels hide their nuts in grass.
No time to see, in broad daylight,
Streams full of stars, like skies at night.
No time to turn at Beauty's glance,
And watch her feet, how they can dance.
No time to wait till her mouth can
Enrich that smile her eyes began.
A poor life this is if, full of care,
We have no time to stand and stare.

— WILLIAM HENRY DAVIES (1911)

1.1 Biomechanics of development

Historically, research in developmental biology was mainly motivated by questions regarding the mechanisms that bring about biological form [Müller and Newman, 2003]. The emergence of the precise features of an adult animal out of fertilized egg is a truly astonishing process at ev-

ery stage. Masses of cells self-organize in a perfectly coordinated manner to form three dimensional tissues and organs with unique forms and adaptive functions. The developmental control of these processes used to be, intuitively explained, predominantly in mechanical terms. Thompson described diverse patterns of living forms as "diagrams of underlying forces", in his classic book "On growth and Form" [Thompson et al., 1942]. This approach was, however, swept away by advancements in molecular biology and by its associated focus on gene structure and activity, which remained until today the most studied aspect of developmental processes. Nevertheless, the genetic aspects do not suffice to provide a full explanation of morphogenesis [Müller and Newman, 2003], which can only emerge from precisely coordinated interaction of genetic and physical mechanisms.

In the last decade, the availability of image acquisition technologies with high spatial and temporal resolution and the development of image analysis tools, shifted scientific interest back to the mechanistic aspects of morphogenesis [Keller, 2013, Trier and Davidson, 2011]. Cells and tissues, as any other material, are subject to physical constraints: their collective behavior in a developing embryo generates mechanical forces, which play an important role in tissue morphogenesis and patterning [Mammoto and Ingber, 2010]. It is remarkable how much of developmental reshaping can be accounted for by physical properties, such as viscoelasticity, adhesion or diffusion. Some of these mechanical properties have been studied ex vivo, yet very little is known about the function of physical forces within the developing embryo [Guillot and Lecuit, 2013].

The modern, interdisciplinary approach is to monitor in vivo the mechanical forces and to connect them with molecular and biochemical processes. We do not fully understand what mechanisms drive different forces, both on cellular and tissue levels: how these forces are coordinated; or how the observed tissue rearrangements emerge from force coordination. These largely open questions motivate this thesis.

In this introductory section we discuss key aspects of cell dynamics that lead to tissue shape changes. Focusing on epithelial tissues, we describe principles of force generation by actomyosin dynamics, and how these forces are transmitted between cells and tissues. We summarize spatiotemporal control of cell and tissue morphogenesis, and also we touch on various mechanisms by which cells and tissues progress and maintain their identity and integrity.

1.1.1 Force generation on cellular level

Morphogenesis – derived from Greek, meaning "origin of shape" – is a process by which tissues establish their final shape. Tissues change as a result of changes occurring in the cells, whether it is in number, size, or shape (See Fig. 1.1). Individual cell shape changes are transmitted to neighboring cells by force transmission, which is mediated by cellular adhesion. Eventually, the local changes are translated into changes of tissue morphology (reviewed in [Heisenberg and Bellaïche, 2013]).

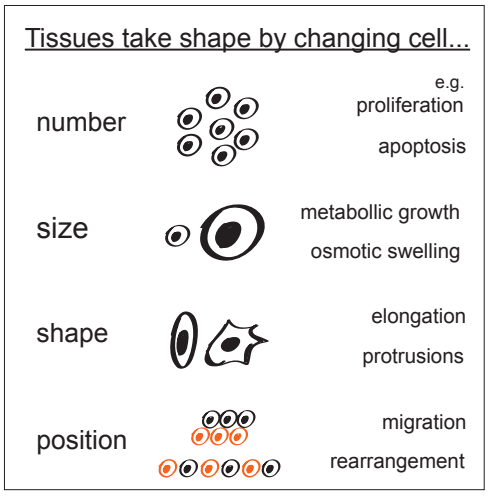

Figure 1.1: **Cellular processes which can lead to changes in tissue shape**

Several well-described single cell processes can produce tissue-level alterations: spatially controlled proliferation and patterned cell death can both directly affect tissue shape [Hopyan et al., 2011], changes in cell relative position can drive tissue rotation [Aigouy et al., 2010] [Suzanne et al., 2010], and rearrangements such as intercalation can result in tissue narrowing and elongation [Walck-Shannon and Hardin, 2014, Keller, 2006].

Cells require mechanical forces in order to restructure. Forces within a single cell are generated mainly by the cytoskeleton, a dynamic, three-dimensional structure that fills the cytoplasm. The cytoskeleton is primarily comprised of actin filaments, microtubules, and intermediate filaments [Even-Ram et al., 2007]. Microtubules are involved in intracellular transport and spindle assembly. The actin filaments, on the other hand, are interconnected with the molecular motor protein myosin, and together the two molecules generate cellular contractility. In an individual cell, actin and myosin localize at the cortical part of the cell, forming the actomyosin cortex. In epithelia, actomyosin localization is polarized to the apical portion [Howard et al., 2001, Salbreux et al., 2012].

Myosin II is a hexameric molecule made up of two heavy chains containing the motor domain, and two pairs of light chains: regulatory and essential. Myosin II is the only member of the myosin protein superfamily that can form bipolar domains with the motor domains at two sides, pointing away from each other. This type of assembly is considered essential for myosin-driven contractility. The motor domains can "walk" along actin filaments using energy from ATP hydrolysis, moving towards the barbed (+) end of the actin filament. A contractile force is generated when the motor domains on two sides of a myosin bundle try to move in opposite directions towards the barbed end, and, since they do not stretch, they pull the actin bundles closer together (Fig. 1.2A) [Pollard and Cooper, 1986].

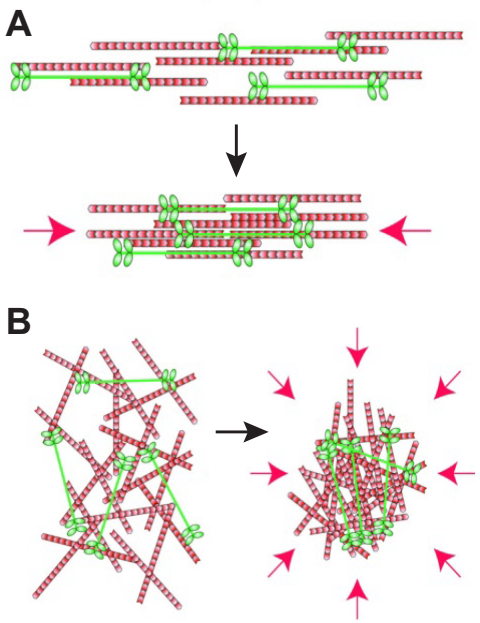

Figure 1.2: **Types of cellular actomyosin assembly.** (A) Unbranched actin filaments contract in the direction of the cable. (B) Contraction of actin filament meshwork shrinking the surface area it occupies. Actin filaments: red (barbed ends facing away). Bipolar myosin ifilaments: green, motor domains of myosin walk towards the barbed filament ends (Modified from [Martin, 2010]).

The forces generated by actomyosin depend on the organization of the cellular cortex and result in different types of contraction. In the case of stress fibers, for example, actin and myosin appear aligned in bundles called cables. In this case, myosin slides on antiparallel actin bundles bringing them towards each other, shortening the cable [Cramer et al., 1997]. As a result, a contractile force is generated in the direction of the cable, between two points or around a cell's circumference (Fig. 1.2A). Actomyosin can also be arranged in a two-dimensional meshwork, and by contracting, it decreases the surface area that the meshwork occupies (Fig. 1.2B) [Backouche et al., 2006, Bendix et al., 2008].

1.1.2 Force transmission between cells

How are local forces within individual cells orchestrated on tissue level? The contractility of actomyosin needs to be transmitted between neighboring cells in order to allow mechanical force integration. Forces can spread directly via the extracellular environment or via cell–cell and cell–matrix adhesion interactions, which are modulated by cadherins and integrins, respectively. Epithelial cells are joined primarily at apical adherens junctions made up of E-cadherins with actomyosin bundles anchored into them (see Fig. 1.3)[Gates and Peifer, 2005, Halbleib and Nelson, 2006]. Mature epithelia form a continuous band of E-cadherin around the cell circumference, which is in turn joined with an actomyosin cable; both band and cable positioned apically. In this way, epithelial cells organize into higher-level structures.

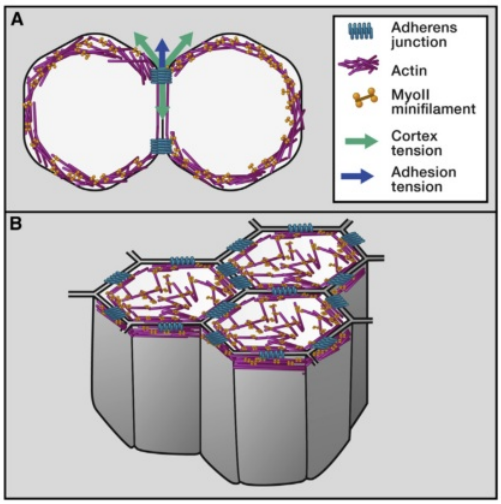

Figure 1.3: **Organization of actomyosin in mature epithelia.** Actomyosin often organizes into a continuous band around the cell apical surface, and stabilizes between neighboring cells by adherens junction, made up of E-cadherin [Heisenberg and Bellaïche, 2013].

Both force generation by actomyosin contractility and force transmission by cadherin-mediated cell adhesion are two highly conserved cell properties with important repercussions in tissue mechanics and self-organization [Dickinson et al., 2011]. Such force- generating celullar mechanisms are part of a fundamental tool kit for tissue development: different actomyosin contraction and cell-cell coupling modes can be combined and used to produce more complex patterns and drive tissue morphogenesis.

How do the groups of cells know what to do (or what to stop doing) when each cell is being subjected to neighboring forces? Many models have been proposed to conceptualize the emergence of tissue behavior. A common assumption is that all forces acting on the cells sum to zero, and, as a result, tissues evolve strictly following equilibrium states. This principle is also frequently applied to epithelial morphology, where it is assumed that cells and tissues tend to minimize their energy through adhesion and cortical tension determinants – epithelial form being determined by the state of lowest energy [Steinberg, 1963, Foty et al., 1996]. The pattern of cellular junctions arises from interplay between the elasticity of the cell, its adhesion, and its cortical contractility [Lecuit et al., 2011].

The general principle described above is mathematically expressed in the so-called vertex model, which is extensively used to describe cellular mechanisms and force balance in epithelial mechanics (reviewed in reviewed in [Fletcher et al., 2014, Farhadifar et al., 2007]. The vertex model has been applied to epithelia in various systems such as wing disc size regulation [Aegerter-Wilmsen et al., 2007, Schilling et al., 2011] and germband extension in *Drosophila* [Honda et al., 2008, Bertet et al., 2004], convergent extension in Xenopus notochord [Weliky et al., 1991], and cell migration in mouse endoderm [Trichas et al., 2012]. Vertex model ideas stem from to inorganic structures such as soap bubbles [Marder, 1987], where each cell membrane is described as a polygon. The way cells are connected to each other in tissues depends on their dimensions: surface, area, and volume. Based on these vertex model rules are estab-

lished on how to connect individual polygons into a tissue-like structure [Fletcher et al., 2014]. Thus, the vertex model provides a theoretical framework for understanding how groups of cells self-organize.

1.1.3 Force generation on tissue level

The analysis of actomyosin dynamics on a cellular level provides a direct evidence for how forces are generated within a tissue. Local forces are absolutely required to be integrated on a global tissue level in order to have an influence on tissue dynamics and shape. Apical constriction is a great example of how coordinated changes at single cell level can add up and pattern entire epithelial sheets. During apical constriction, as the name suggests, cells constrict only their apical, actomyosin enriched, domain; and if they form part of a columnar epithelium, the cells convert into a cone shape that will eventually enable tissue bending and folding (See Fig.1.4) [Odell et al., 1981].

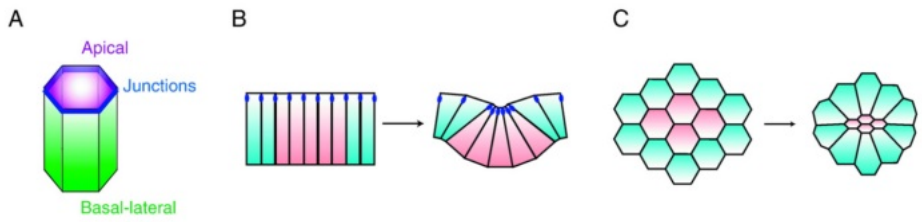

Figure 1.4: **Examples of apical constriction.** Apical actomyosin activity can lead to epithelial bending (B) or rosette formation (C), by decreasing cell apical surface [Martin, 2010].

In systems such as the neural tube closure in vertebrates or the mesoderm invagination in *Drosophila*, apical constriction is used to generate folds, rosettes, pits, and tubes [Colas and Schoenwolf, 2001] [Costa et al., 1994].

A second example of tissue-level force generation has been described during germ band extension in *Drosophila*. Here, extrinsic forces have been proposed to promote individual cell elongation along anteroposterior axis, and this in turn contributes to global tissue elongation [Butler et al., 2009]. Tissue convergence and extension, as in this case, can be driven by cell-cell intercalations, or by oriented cell migration, or by division; all translating into changes on tissue level [Martin, 2010].

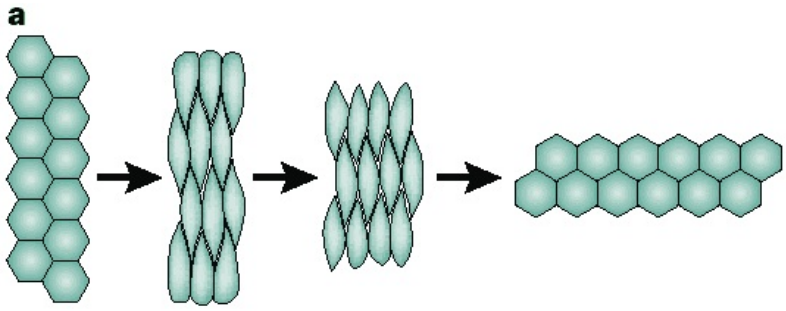

Figure 1.5: **Cell rearrangements in convergent extension.** Cells first converge towards the center, then change positions and rearrange their interfaces, which leads to an extension perpendicular to the direction of convergence (modified from [Tepass et al., 2000]).

Understanding how collective cell behavior is controlled at the scale of the tissue is crucial in deciphering the principles of morphogenesis. This is no easy task, however. Recently, additional insights on cellular dynamics came from advances in our understanding of planar cell polarization and mechanotransduction studies in tissues (see, for example [Heisenberg and Bellaïche, 2013]).

1.1.4 Tissue polarization

Almost all cell types and tissues exhibit some level of polarization, which is often fundamental for proper development and organ function. Epithelia are ubiquitously polarized along the apico-basal axis and often have a polarization in the plane of the tissue, known as planar cell polarity (PCP). The main genetic factors involved in the establishment of PCP are evolutionarily conserved and are required for vertebrate homeostasis and development. This condition makes PCP a leading topic in developmental biology [Simons and Mlodzik, 2008]. How is this polarity translated into mechanical cues? Components of the PCP pathway can be polarized at the apical junctions of cells, and through Rho-kinase activity establish polarized accumulation of myosin. In chick neural plate folding, for instance, such myosin accumulation in turn constricts the dorsoventral junctions and drives a cell intercalation [Hildebrand, 2005, Nishimura and Takeichi, 2008].

The Fat/ Dachsous (Ds) pathway is required in *Drosophila* epithelial morphogenesis; where by establishing a gradient within a tissue, it is able to generate polarized myosin distribution [Bosveld et al., 2012]. Another important molecular player is Crumbs, a highly conserved transmembrane protein that determines apical polarity in *Drosophila* [Pocha and Knust, 2013]. Anisotropic distribution of Crumbs during the formation of the tubular salivary glands has been shown to determine the subcellular localization of myosin. This organization of myosin-enriched interfaces is believed to play a role in the process of salivary gland placode invagination [Röper, 2012]. Thus both tissue and cellular level observations of polarized behavior, as well as the molecular components involved in its regulation suggest a tight link between polarization and force generation.

1.1.5 Supracellular cables

Myosin-enriched interfaces described above are thought to cooperate on a tissue level by forming supracellular cable-like structures, which have been shown to control large-scale tissue rearrangements. Throughout this work, we will report various examples of actomyosin cables involved in epithelial progression, discussed in detail in results section: chapters 3 and A.

During several developmental processes actomyosin with apical junctional, and apicomedial localization forms a chain between neighboring cells. This alignment connects cell interfaces forming supracellular actomyosin cables [Röper, 2013]. Junctions linked by actomyosin cables have been reported to be under higher tension than single, myosin enriched boundaries [Fernandez-Gonzalez et al., 2009]. One possibility is that myosin enriched vertices can recruit more myosin by sensing higher tension from their neighboring, linked cells; thus increasing the tension [Lye and Sanson, 2011]. We will discuss similar processes in the section on mechanotransduction below.

We do not fully understand the mechanism behind cable formation. Is there a common process activating cable assembly? How is it coordinated between neighboring cells? And what are the exact molecular players involved? Some upstream pathways and molecular anisotropies involved in cable localization have been identified. These include PCP components [Lienkamp et al., 2012, de Matos Simões et al., 2010]; apical cell polarity proteins such as Crumbs, E-Cadherin and Bazooka [Röper, 2012]; the Notch signaling pathway [Major and Irvine, 2006]; and the wingless/ hedgehog-signaling pathway [Monier et al., 2010].

Cables were first described in a study on wound healing response [Martin and Lewis, 1992], where the cables were observed to assemble in cells facing the wound providing a driving force for the closure. Recently, cables acting in different ways have been documented in *Drosophila* and

in vertebrate embryos. We can divide the cables into three groups based on certain similarities (summarized in Fig. 1.6).

A first group would include cables identified in wound healing, termed "actin purse-strings" (Fig. 1.6A-C); as well as additional circumferential cables that contract along the circumference of an opening, exerting a centripetal tension on the tissue. This kind of centripetal tension has been shown to be important, for example, in driving wound closure [Abbott and Lengyel, 1991, Wood et al., 2002] or in closing an epithelial gap during *Drosophila* dorsal closure, where a cable forms at the leading edge of two converging epidermises [Jacinto et al., 2002] [Hutson et al., 2003]. Circumferential cables have also been reported as being able to pull on epithelial sheet by combining tensile forces with embryonic geometry.

In another example, known as epiboly, a continuous purse-string actomyosin cable is involved in force generating mechanism. Contractile cable encircles the yolk at the margin of moving blastoderm during zebrafish gastrulation. Over the course of epiboly the cable increases in intensity and contracts; and, as a result of interplay between the circumferential tension in the cable and the spherical geometry of the embryo, the cable progresses in the direction of maximally decreasing radius, once it has passed the embryo equator [Warga and Kimmel, 1990]. Recently, it has been shown that this cable works not only by constriction mechanism, by also by incorporating a flow-friction mechanism [Behrndt et al., 2012]. Contractile ring sliding over a cylindrical geometry – has been proposed to regulate proper cytokinesis in fission yeast, suggesting a simple, global mechanism that can function both on cellular, and tissue levels [Mishra et al., 2012].

Although all cables are under tension, some are more static, and do not progressively constrict (See Fig. 1.6D-F). Instead, they work as mechanical boundaries between embryonic compartments, preventing cells from different partitions to mix. Compartment boundaries are observed in

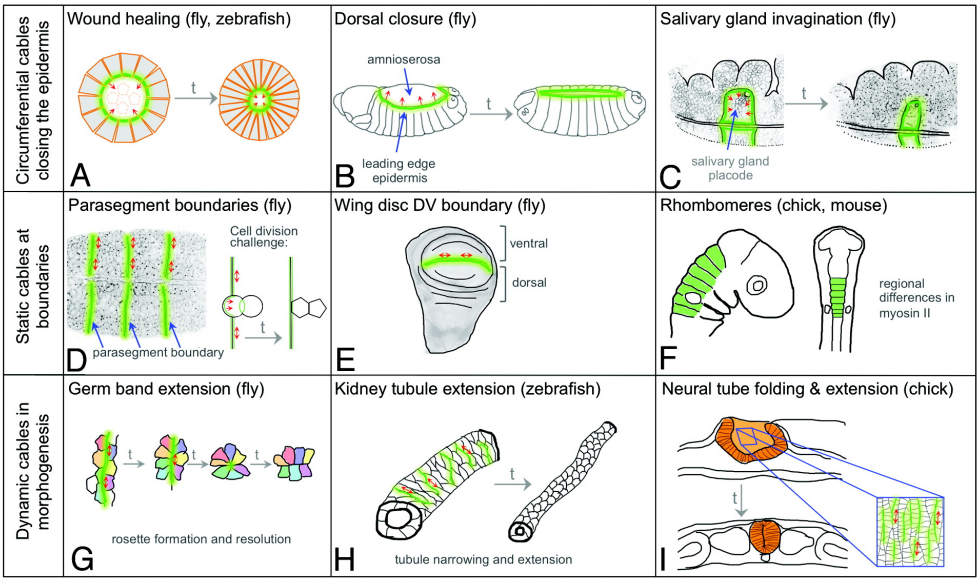

Figure 1.6: **Three main classes of supracellular actomyosin cables.** (A-C) Purse-string cables involved in wound healing, epithelial gap closure, driven by circumferential tension. (D-F) Static cables forming at compartment boundaries. (G-I) Short, dynamic cables regulating numerous cellular rearrangements (from [Röper, 2013]).

many tissues. For example, during *Drosophila* embryonic development, myosin cables coincide with an interface separating the spatial pattern of expression of the genes wingless and engrailed [Monier et al., 2010]. These genes are well characterized as molecular determinants of insect segmental units with lineage restrictions (discussed in greater detail in section 1.2.6.

Further evidence for the importance of tensile boundaries in tissues comes from *Drosophila* wing disc, where enrichment of actin and myosin has been reported both at the AP and the DV cell interfaces [Landsberg et al., 2009, Major and Irvine, 2006]. In vertebrates, compartments are also clearly separated during brain development. Cables, formed

in the apical portions of neuroepithelial cells keep rhombomeric cells segregated [Calzolari et al., 2014]. We can also distinguish a group of short and very dynamic cables, often observed during morphogenetic cell rearrangements. These cables drive formation of rosettes by shrinking multiple cell interfaces [Blankenship et al., 2006], by rearranging cell interfaces during germ band extension [Bertet et al., 2004], and by aiding in the bending of neural tubes in chick embryos [Nishimura et al., 2012].

The multiple examples and varying dynamic behaviors of actomyosin cables implicates their role as a basic piece of machinery that organizes cell behavior on a tissue level. As we will show in the results section (chapter 3 and A), cables are the main force generators in epithelial progression and segment positioning during *Drosophila* HI.

1.1.6 Mechanotransduction

One of the possible explanations for actomyosin cable formation and maintenance is the recruitment of tension-driven myosin. Cable-linked interfaces are believed to pull on each other generating tension, and this is translated into a signal for additional myosin recruitment. In turn, the increment of myosin levels increases the overall tension of the cable creating a reciprocal activation mechanism. Additionally, myosin could trigger further myosin accumulation by stabilizing its link with actin [Kovács et al., 2007, Kee and Robinson, 2008]. In support of this, linked cell interfaces enriched with myosin exhibit a more abundant and stable pool of myosin than similarly enriched, but individual interfaces [Fernandez-Gonzalez et al., 2009]. Such mechanical feedback, in which cable contraction promotes cable formation, is an example of a group of processes defined as mechanotransduction: the communication of mechanical stimuli by neighboring cells and tissues that sense their physical environment and stresses they are submitted to.

We can list several examples of instances where mechanotransduction has been shown as an important mechanism during embryo development. For example, it has been shown that the mechanical pulling of embryonic ectoderm can induce the recruitment of myosin to the cell cortex [Fernandez-Gonzalez and Zallen, 2009]. In a second example, two waves of myosin driven constriction were shown to lead to tissue invagination during *Drosophila* gastrulation. The first wave is regulated by the transcription factor Snail, and the second one by Twist. Snail mutants are defective in both waves of constriction, but, interestingly, the phenotype can be rescued by artificial, mechanical deformation; which in turn activates the second wave of contraction [Pouille et al., 2009].

Overall, the examples described above evidence the relevance of mechanosensing mechanisms for tissue adaptation and self-organization, especially in response to perturbations. The recent establishment of tools to measure and manipulate mechanical forces enables an unprecedented level of interrogation of the in vivo response to mechanical stresses. However, the usual biological model systems are rarely well suited for the in vivo study of mechanotransduction during complete developmental processes. Thus, there is a need for a wider range of biological settings [Eyckmans et al., 2011].

In the results section below (chapter 3), we describe an epithelial tissue which we consider to be a plausible system for studying in vivo mechanical interaction and sensing on tissue level.

1.1.7 Tissue spreading and collective migration

Supracellular cables can also play a role in tissue spreading. At the core of our results is a description of a novel mechanism of tissue spreading, involving multiple supracellular cables. Therefore we would like to summarize other, well-described processes in which tissues progress, and contrast them later on with our findings.

We have described cable driven tissue spreading during wound healing and DC, and in chapters 3 and A we will present novel examples in which tissue progression is driven by multiple actomyosin cables. Cable formation is just one mechanism that could contribute to tissue extension; others include pulling by another tissue, active migration, and collective cell migration [Martin, 2010].

Collective cell migration drives formation of many tissues and organs during embryogenesis, and can also be a mechanism in which a two-dimensional sheet migrates across a tissue surface. Other categories of collective migration have been described: groups of cells can move across three-dimensional space either in streams, by branching, or by adopting a slug-like progression [Friedl and Gilmour, 2009]. Cells migrate to vascularize tissues, patch up wounds, and to invade surrounding tissue as in the case of migratory tumor cells [Rørth, 2009]. Collective cell migration is a process separate from tissue invagination, tissue intercalation, or expansive growth; and it is characterized by maintaining: 1) tissue integrity, i.e. preserving cell-cell junctions during movement, and 2) supracellular cytoskeleton organization. The latter resulting in shared cell dynamics. Additionally, during collective cell migration, the presence of protrusions, which provide migrational force (traction), is often observed; as are as the structural modifications to the migrating tissues – e.g., ECM modifications such as basement membrane deposition [Friedl and Gilmour, 2009].

Collective migration could elaborate cellular networks via the sprouting or branching mechanisms, seen in fly trachea development and vasculature formation in vertebrates. The *Drosophila* tubular network is an interesting system, since there are no cell divisions during its development, and cells migrate towards a source of fibroblast growth factor (FGF). The cell located closest to the morphogen source adapts a tip cell fate, and by assembling protrusions such as filipodia and pseudopodia forms primary branches of the tracheal network [Casanova, 2007]. In addition to their role in development, branching movements are important in physiology and disease, for example during tissue neovascularization

[Gimbrone et al., 1972].

Zebrafish lateral line has become another popular model for collective cell migration, mostly because of its availability for in vivo imaging [Ghysen and Dambly-Chaudière, 2007]. The primordium of the lateral line is more than one hundred migrating cells that deposit multicellular sensory structures at regular intervals as they move. The mass of cells in the primordium is tightly associated and polarized; front cells exhibit intrinsic polarity and form protrusions, which allow it to perform precisely directed migration (reviewed in [Rørth, 2009]). FGF and Wnt signaling dictate the overall polarity of the structure and it moves in a slug- like motion along the morphogen- set path [Aman and Piotrowski, 2008].

Here, we have introduced the principles of the mechanical aspects of morphogenesis. We consider this important, as this is an open area of research, which still lacks a centralized source of information. Additionally, a description of the main force generating processes as presented above, is fundamental to the concrete presentation of the findings of this project. In what follows we will focus on *Drosophila*, which is the model system used throughout this work. Specifically, we introduce fly embryogenesis, with an emphasis on head involution, a process at the core of this thesis.

1.2 *Drosophila* head involution as the model system

Drosophila embryogenesis is an ideal system to study morphogenesis in vivo. It is a very low-maintenance model system, with a short life cycle, and for which a multitude of genetic lines and tools are available. Moreover, the *Drosophila* embryo is transparent, which allows appliance of in vivo confocal imaging. Recently, many biomechanical tools have been developed, such as laser nanosurgery, which is a powerful tool to study force communication in embryonic epithelia [Colombelli and Solon, 2013].

At the end of fly embryogenesis, all the organ systems and tissues are already developed, and we can follow their dynamics and morphogenetic rearrangements. As our model, we chose a process that marks the end of embryogenesis - the process of head involution (HI). Even though HI is both temporally and spatially related to the very well described process of dorsal closure (DC), HI is still virtually undescribed. This makes it both a challenging and fascinating research model. HI involves dramatic rearrangements of the embryonic head and epidermal spreading. It represents a novel biological setting and, based on the experience of this project, we consider it to be a great novel experimental system to explore many morphogenetic processes.

1.2.1 Head involution

At the end of embryogenesis, the *Drosophila* embryo, just like that of other cyclorraphous dipteran insects, becomes an acephalic larva. It is not, however, a headless larva as the name suggests; most of its head structures are located inside of the body cavity and will remain there until metamorphosis. The internalization of head structures comprises a complex pattern of movements, called head involution (HI). In the course of this unique morphogenetic process all six cephalognathal segments of the embryonic head rearrange and ingress. Simultaneously, the dorso lateral epidermis moves over them and completely covers the head, leaving only a small part outside: the so-called pseudocephalon. Internalized tissues come together to form the adult head, which, during metamorphosis, is pushed out of the body cavity and forms the most anterior part of the adult animal [Campos-Ortega and Hartenstein, 1997].

HI is a process about which very little is known- however early embryonic patterning is evidently important for the process: erroneous specification of head tissues leads to abnormal head morphogenesis. Mutations in one of the homeotic genes, or in genes coding for proteins involved in key signaling pathways such as Dpp or EGF disrupt early patterning of

the head [Merrill et al., 1989, Chang et al., 2003] and result in abnormal head morphology. The mutant phenotypes also points towards morphogenetic connections between HI and dorsal closure, which occurs at the same time [VanHook and Letsou, 2008]. We do not understand how the process of HI is accomplished: the morphogenetic rearrangements must be coordinated between tissues of completely different origins and fates.

The aim of this section is to summarize what is known about head involution, starting from the anatomy of the embryonic head and concluding with the phenotypes and the malformations documented so far.

1.2.2 Head segments

Unlike tissue progression in dorsal closure, where epidermis moves over (relatively) static amnioserosa tissue, HI involves epidermal progression over head segments that simultaneously move inward. The internalization of head segments does not occur all at once, nor do the segments ingress as a single unit: the process cannot be described similar to a turtle hiding its head inside of a shell. Instead, we could imagine a sock being turned inside out each part at a time, producing a reverse anteroposterior order. For example: the most anterior head primordia (Fig. 1.7: lr) moves inwards and gives rise to the most posterior tissue after involution [VanHook and Letsou, 2008].

The head just prior to HI, at stage 12, is composed of six segments and the acron, often called the seventh head segment. Individual segments are commonly divided into the compounded segments: procephalon (preoral segments, see Fig. 1.7A:P) and gnathal (postoral – Fig. 1.7A:GS) [Campos-Ortega and Hartenstein, 1997].

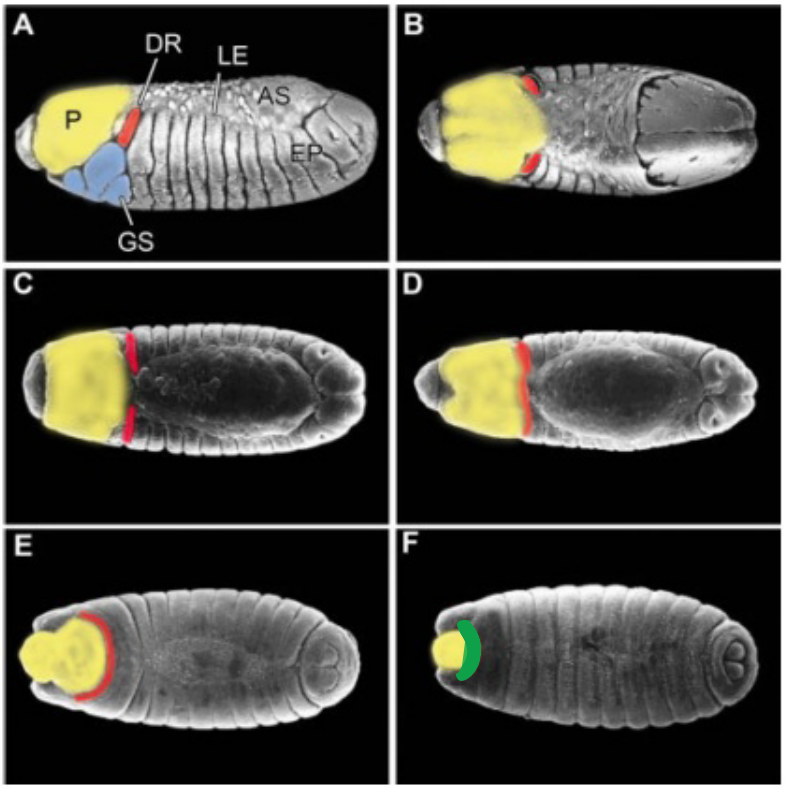

Figure 1.7: **Overview of head involution.** The gnathal segments (GS, blue) fuse dorsally into dorsal ridge (DR, red), and together progress over the procephalon (P, yellow), which simultaneously moves inside of the embryo. (A-B) lateral and dorsal view of stage 12 embryos. (C-F) dorsal views of embryos stage 13- 15. (F) DR rolls under during the initial progression, and is replaced by more posterior epidermis at the leading front (green band) (modified from [VanHook and Letsou, 2008]).

Figure 1.7 shows a schematic representation of the head segments. In the course of HI 1) the dorsal portion of procephalon will ingress towards the posterior of the embryo, and 2) the gnathal segments will progress anteromedially, where they will turn inward and partially involute. As the

procephalon moves towards the posterior on the dorsal side, it will bring its most ventral portions to the anterior tip, where they will also partially involute through the opening called stomodeum. The gnathal segments can be further subdivided into dorsal, lateral, and ventral regions. Continuing with the course of HI, 3) the dorsal region of gnathal segments will form the dorsal ridge (Fig. 1.7A:DR, red) - i.e., the initial leading edge of progressing epidermis. Note, the DR is not at the front of the progressing tissue throughout the movement; it actually rolls under the tissue originally posterior to it will take over as the leading edge (See Fig. 1.7F). We will discuss this rolling progression in chapter 3. The lateral parts will grow into segmental appendages, i.e., the fly sense organs; and together with the ventral parts will eventually form the larval mouth and foregut [Campos-Ortega and Hartenstein, 1997].

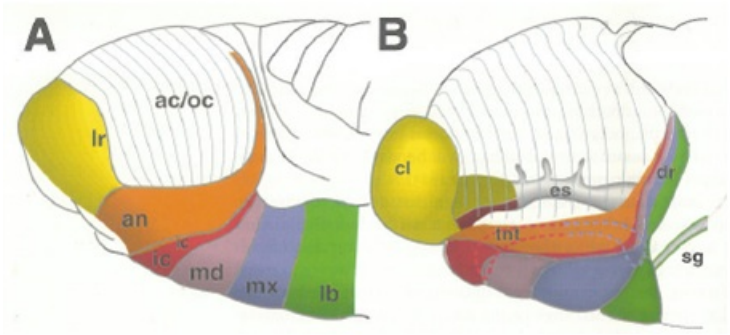

Figure 1.8: **Schematic drawings of the head segments prior to HI.** (A) Stage 11, (B) 12. Segments are shown in different colors. (B) Depicts more medial view of the head, showing the esophagus (es) Anterior is to the left and dorsal on top (from [Campos-Ortega and Hartenstein, 1997]).

The procephalon, which is the most anterior part of arthropods head, is composed of labrum (lr), antennal segment (an), intercalary segment (ic), and the acron (ac) (Fig 1.8). It is not straightforward to distinguish such structural organization in vivo, and only clypeolabrum (cl) has an easily detectable morphology consisting of a regular, cylindrical epithelium. As

such, it can be clearly separated from the procephalic cells surrounding the clypeolabrum.

The organization of the gnathal segments is similar to that of the thoracic and abdominal segments, with some differences associated with the head formation. The gnathal segments can be divided into mandible (md), maxilla (mx), and labium (lb) (see Fig. 1.8). The most anterior opening of the foregut formed at the end of HI is called the atrium; this abuts onto the pharynx, and together these two structures secrete the cephalopharyngeal skeleton (CPS). The CPS is a chitinous structure, which supports the larval head, making the architecture for the feeding muscles of the larval mouth and foregut [Campos-Ortega and Hartenstein, 1997].

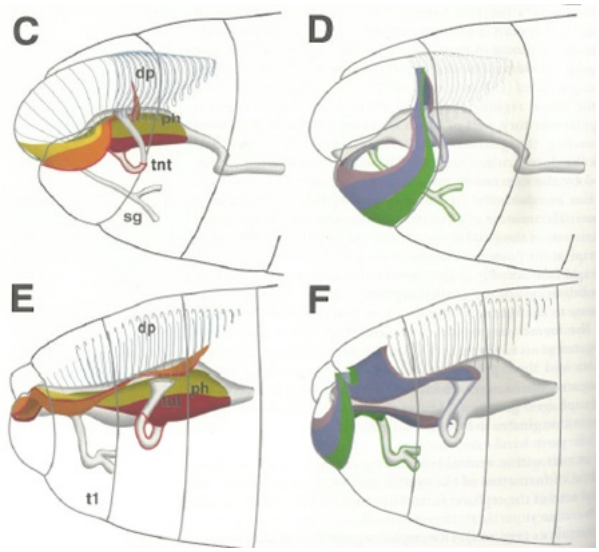

Figure 1.9: **Involution of head segments.** Procephalon (C-E) and gnathal segments (D-F) are shown separately. (C-D) Stage 15, during HI. (E-F) Stage 17, HI is complete (from [Campos-Ortega and Hartenstein, 1997]).

The atrium is formed from the head ectoderm cells that move inside through an opening called stomodeum, which is a pore at the anterior

tip. The order of segments is reversed, such that the ventral part of procephalon (labral segment) will move inside the embryo and form the roof of the pharynx. The invagination of the labrum and the intercalary segment pulls the gnathal segments towards the anterior, until the labium- the most posteriorly located segment – fuses at the tip and involutes through the stomodeum [Rogers and Kaufman, 1996].

1.2.3 Central Nervous System

Simultaneous to the process summarized above, the central brain, which dorsally is the procephalic lobe, begins to displace posteriorly. This movement is at the core of results we present in chapter 2. Our objective was to describe this process in detail, and based on time-lapse imaging, present the principles of the brain dynamics.

Just prior to HI, the brain consists of groups of neuroblasts, which segregate and delaminate from the procephalic neuroectoderm [Campos-Ortega and Hartenstein, 1997]. These tissues undergo a rotational movement and are internalized, resulting in an increased curvature of the neuraxis i.e., the axis that denotes the direction of the central nervous system. The neuraxis is shown in Figure 1.10 as a red line; during HI it bends towards dorsoposterior. The order of the neuroblast groups is reversed in a similar manner to that which we have described for the cephalognathal segments. Specifically, the neuroblasts undergo a shift such that those located anteroventrally (Fig. 1.10, green) move towards the posterior and medial part of the brain. Dorso-posterior neuroblasts (Fig. 1.9, red) move to occupy a more ventral position (Fig. 1.10) [Reichert and Boyan, 1997].

This rotational movement is accompanied by massive delamination and invagination during which the dorsomedial neuroblasts from the procephalon are integrated into the brain hemispheres as neurons or glial cells [Abbott and Lengyel, 1991], [Rogers and Kaufman, 1996]

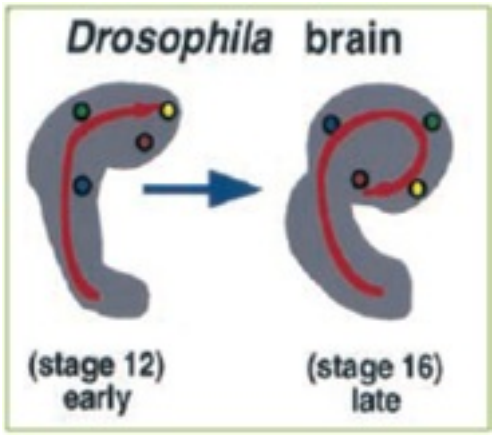

Figure 1.10: **Rotationally moving neuroblast groups in the developing *Drosophila* brain.** Red arrow indicates the neuraxis, which, over the course of HI, increases its curvature. The brain is displaced dorsoposteriorly, in the direction of the arrow (from [Reichert and Boyan, 1997]).

[Campos-Ortega and Hartenstein, 1997]. This delamination is accompanied by massive cell death; as evidenced by the presence of macrophages surrounding the dorsomedial domain of the head clearing it from cellular debris [Campos-Ortega and Hartenstein, 1997].

Figure 1.11 shows the ingression of the brain on the scale of the embryo. The central brain (Fig. 1.11, CenBr) s one part of central nervous system (CNS), which is also composed of the ventral nerve cord (VNC). The VNC goes under a process of condensation simultaneous with HI, and reduces to about 70% of its original AP length. Although VNC condensation is still a very obscure process, we know that it depends on the presence of intact glia, the neuronal cytoskeleton, and embryonic hemocytes; and on the occurrence of apoptosis [Olofsson and Page, 2005]. Almost half of the cells in the posterior part of the cord undergo apoptosis, which is also important in separating the cord from the ventral epidermis; it is known that preventing apoptosis inhibits VNC shortening [Page and Olofsson, 2008].

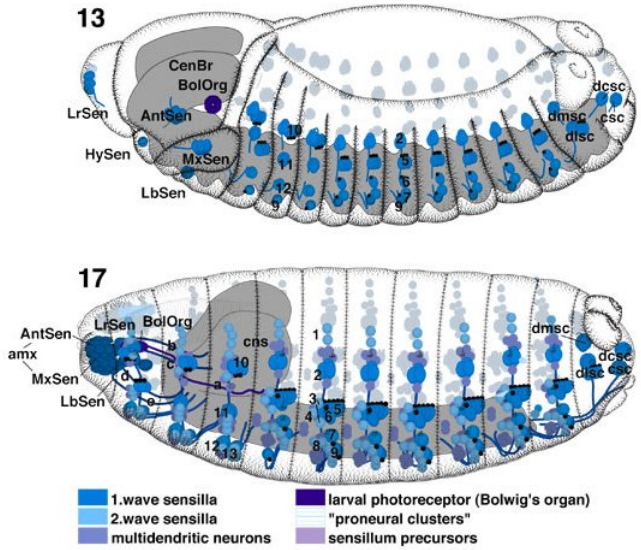

Figure 1.11: **Central brain and peripheral nervous system during HI.** The central brain is displaced dorsoposteriorly, and the ventral nerve cord (VNC) undergoes condensation. Multiple sensilla move to the anterior tip while forming neuronal connections with the brain ([Campos-Ortega and Hartenstein, 1997]).

1.2.4 Apoptosis and hemocytes in the embryonic head

Apoptosis is crucial in many morphogenetic events, and it has been reported as one of the key processes required for proper HI [Grether et al., 1995, White et al., 1994, Abbott and Lengyel, 1991] [Nassif et al., 1998]. In the embryonic head, cell death is already prominent during stage 11, and it shows a different pattern of occurrence to that seen in the trunk of the embryo, where cells undergoing apoptosis are isolated and dispersed. During HI, apoptosis is strictly patterned and occurs in noticeable groups of cells, specifically in regions where we observe massive morphogenetic rearrangements.

In this section 2.5 we describe the apoptotic pattern as seen in the head on time-lapse images. We show the cells that activate the caspase pathway, their localization, and we follow up with a detailed description of hemocyte patternings in the head.

Apoptosis is critical in progression of HI, especially during the following events: the shrinking of the head ectoderm, delamination of neuroblasts, invagination of the optic lobe, and the fusion of lateral gnathal lobes [Nassif et al., 1998]. Furthermore, it is known that mutations in proapoptotic genes (grim, hid and reaper) result in defects in HI (Fig. 1.12). For example, in these mutants the head segments fail to migrate inside the embryo and instead become crowded and exposed at the anterior tip [Nassif et al., 1998].

Additionally, the CPS is secreted but mispositioned and foreshortened, which results in malformations of the mouth structures. Interestingly, the earlier events (earlier both in embryogenesis and evolution) do not seem to be affected when apoptosis is blocked, but proceed normally. On the other hand, later events during head involution – from the retraction of the clypeolabrum to the formation of the dorsal pouch - absolutely require cell death to progress [Nassif et al., 1998].

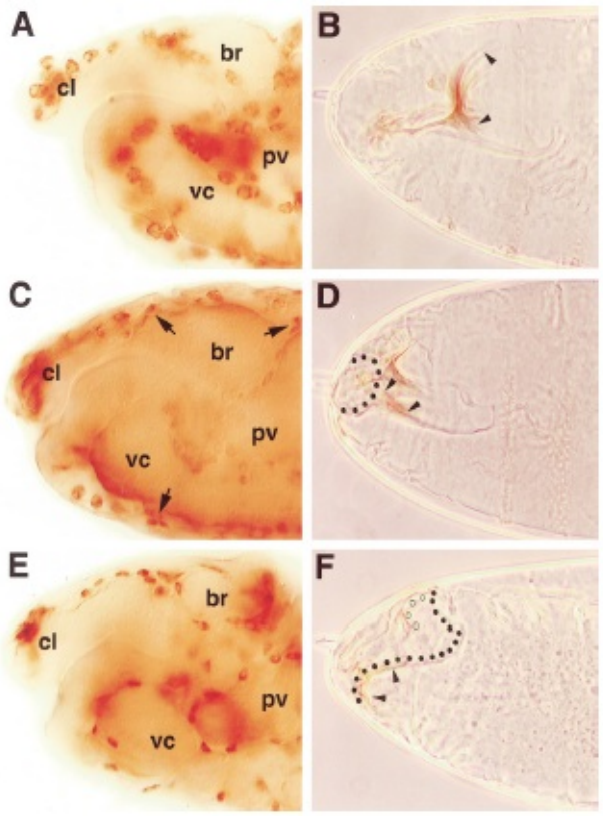

Figure 1.12: **Apoptosis and head morphogenetic defects.** (A-E) Embryos labeled with peroxidasin antibody expressed in hemocytes. (B-F) Cuticle preparations. (A-B) WT embryos; all hemocytes are large and have phagocytized cells (exhibit a granular interior). The CPS has been secreted inside of the body, covered with epidermis (arrowheads in B). (C-D) Df(3L25) embryos show partially blocked apoptosis. Only some hemocytes contain phagocytized cellular debris, head segments fail to involute and CPS secretion is shifted towards the anterior, where some parts of the head remain exposed to the exterior (dotted line). (E-F) Df (3LH99) embryos with blocked apoptosis. Hemocytes remain small, circular, and "empty". The entire head is exposed and the CPS develops only partially [Nassif et al., 1998].

Embryonic hemocytes follow a specific apoptotic pattern: they track specific routes within the head, and along the ventral nerve cord, where vast cell death has also been reported [Page and Olofsson, 2008]. After

completion of HI, hemocytes disperse and occupy random positions in the embryonic trunk (Fig. 1.13). The role of hemocytes in morphogenesis seems to be that of generating gaps in the tissue by localized removal of cells and by clearing up excess cells that, for example, fail to integrate into the brain hemispheres.

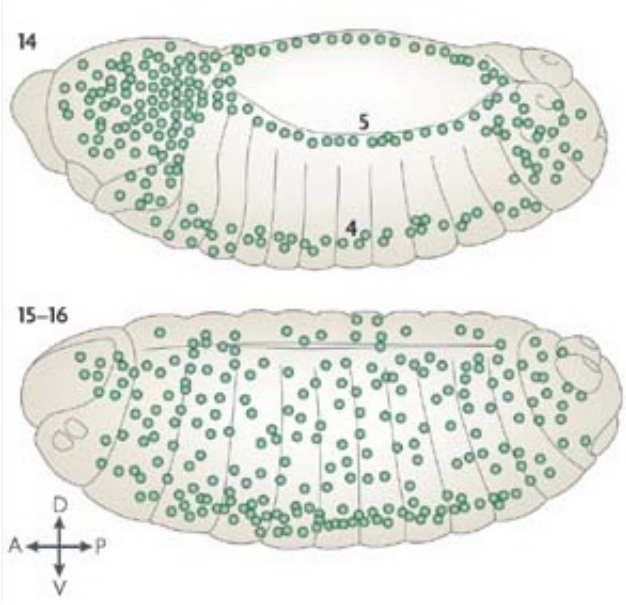

Figure 1.13: **Embryonic hemocytes.** Prior to HI hemocytes are concentrated in specific loci within the head, along the VNC and dorsal opening. Towards the end of embryogenesis, they disperse and move randomly within the embryo [Wood and Jacinto, 2007].

1.2.5 Dorsal epidermis progression

In coordination with the potential remodeling of the brain structure by apoptosis, the dorsal epidermis will migrate to cover the head tissue. The dorsal ridge (DR) is the leading structure in the initial progression of the dorsal epidermis during HI. This structure becomes visible during early

stage 12, originating from the labial bud on both sides. This structure folds over the tissue immediately anterior to it forming the so-called dorsal fold (DF). The mechanism of DF formation is at the core of chapter 3 of results. We show that the folding of the DR and forming the DF is an example of a novel tissue spreading mechanism, powered by multiple actomyosin cable.

The DF slides over the procephalon while simultaneously advancing towards the medial and rostral directions. As a result, a kind of pocket, named the dorsal pouch, is formed. The dorsal head segments get both incorporated into the pouch and covered with epidermis [Campos-Ortega and Hartenstein, 1997]. The pouch is a structure, which is preserved until the emergence of the adult fly from the pupa. A sac-like structure (ptilinium) grows inside the pouch, and numerous temporary muscles attach to it. During eclosion of the animal (emergence from pupa), the ptilinium is inflated with hemolymph, and breaks the pupa open [Sink, 2006].

The lateral portions of the gnathal segments are not drawn into the stomodeum. They end up at the rostral part of the head, where they will form part of the antennomaxillary complex (AMC). At stage 14, a fold appears on both sides of the clypeolabrum, located between its columnar epithelium and the neighboring antennal complexes. The fold deepens while the labrum is retracting towards the inside of the embryo, bringing the AMC from both sides medially close to each other and pointing anteriorly.

As it moves over the head structures, the DF is believed to recruit cells from the surrounding tissues and to enlarge. It is not at all clear, however, what is the mechanism and cellular basis of both the involution of the head structures and the displacement of epidermis over them. Certain cellular events associated with the whole process are known, including delamination, invagination, intercalation, and disruption and reformation of contacts among epithelial sheets. Other mechanisms are speculated

such as elongation, formation of cellular protrusions, and growth of epidermal cells [Campos-Ortega and Hartenstein, 1997]. In chapter 3 we propose an alternative mechanism behind epidermal movement and identify novel main force generators in the process.

1.2.6 Dorsal epidermis patterning

The epidermis that progresses over the head exhibits a repetitive, segmented pattern. This pattern, and segment size are maintained during the process of HI. One of the objectives of our work is to establish the mechanism behind such a spatially controlled tissue progression. In order to answer this, we looked in detail into the regulation of segment formation, and applied tools to interfere with segmental patterning (see methods in chapter 5).

During *Drosophila* embryogenesis, a cascade of maternal, gap, pair rule, and segment polarity genes organize the embryo into repeating, segmental stripes. Upon completion of cellularization, the embryo is divided into 14 stripes, which will later become embryonic segments dividing the epidermis [Sanson, 2001]. The major segment identity genes are wingless (wg) and hedgehog (hh), which are secreted by engrailed (en) expressing cells. The expression pattern on hh/wg constitutes a bipartite signaling organizer: it establishes a parasegment boundary (PS) with cell patterning on both sides. The PS is visible as a shallow groove during stage 11 between the wg/en-hh stripes. Importantly, an actomyosin cable forms along the PS groove and acts as a cell-mixing boundary, maintaining the expression domains [Monier et al., 2010]. During stage 12, the PS boundary is no longer distinguishable and a segment boundary is formed posterior to the en/wg stripe. This boundary forms as a deep groove that becomes evident in the larval stages between the epidermal segments. Although wg and hh are expressed in narrow stripes, they maintain each other expression by reciprocal signaling; mutation in either gene is known to disrupt the global segmental pattern [Tabata et al., 1992]. Although the for-

mation of the segmental pattern in ventral epidermis is well established, descriptions of the distribution of signaling molecules in the dorsal epidermis are scarce. Wg and hh act in two exclusive domains in the dorsal epidermis, and both are required for cell patterning across the segment [Bokor and DiNardo, 1996].

1.2.7 Head involution defective phenotypes

Mutations in apoptotic genes are among the best-characterized perturbations resulting in deficient HI. For example, mutations in the gene coding for Dpp, a signaling protein believed to regulate the apoptotic pathway, resemble a weak hid mutant phenotype [Kozlova and Thummel, 2003]. On the other hand, a phenotype associated with over proliferation of head tissues (anterior open-aop) leaves the brain exposed and impairs proper secretion of the CPS or cuticle. This evidence again points to the regulation of the size of the involuting head as a crucial aspect of HI. The epidermal progression over the ingressing head is fundamental, since only the epidermal cells can secrete the cuticle, which is required for the proper functioning of the animal throughout the life cycle. Abnormal epidermal spreading over the head results in anterior holes in the cuticle, which often seems to be correlated with oversized head structures.

Additional genetic requirements for proper completion of HI have been difficult to distinguish. HI occurs very late in embryogenesis, and defects in the process usually occur together with malformations in DC, or with incomplete germ band retraction – it is thus not clear whether a HI defective phenotype is a direct consequence of a given mutation, or a secondary effect due to malformations in other structures, such as the gut or epidermis. Nevertheless, there is partial evidence for a certain degree of genetic link between HI and DC. For instance, both the myosin heavy chain and armadillo, a component of apical adherens junctions, are examples of shared requirements for the proper progression of both DC and HI; and are necessary for epithelial sheet integrity [Ntwasa et al., 2001,

Tateno et al., 2000]. Aside from structural and adhesive components of tissues, signaling from JNK, and Rho-family GTPases is important, and perturbations in any of their components have been shown to result in incomplete DC and/or the generation of anterior holes and a disorganized CPS [Harden et al., 1999, Jacinto et al., 2002]. Nevertheless, many of the components proposed to be necessary for the two processes are also involved in other morphogenetic processes. It is thus difficult to disentangle their function and pin it to HI only.

1.2.8 Summary

The embryo goes through a great deal of dramatic morphogenetic rearrangement during the whole process of HI. The intimate relationship between head involution and other developmental processes cannot be undervalued. For example, the onset of HI is concurrent with the beginning of foregut development, the condensation of the VNC is temporally coordinated with the involution of procephalic lobes, and the unfolding of dorsal closure seems to be causally linked to HI. Nevertheless, overlooking the details, head involution, as described above is essentially a morphogenetic process, involving an unconventional tissue movement in which the head bends inwards, and an epithelial sheet covers it. It can be easily followed and recorded in vivo, both in wild type and perturbed conditions. With that in mind, this project aims to elucidate the force generating mechanisms driving the process, and subsequently to propose simple models able to explain its biomechanics.

RESULTS

Chapter 2

HEAD INVOLUTION: THE INTERNALIZATION OF HEAD STRUCTURES

2.1 Objectives

Head involution, as described in the introduction, can be divided into three major parts:

1. ingression of the procephalic lobe and the brain
2. involution of the gnathal segments through the stomodeum
3. progression of epidermis over the embryonic brain

In this section, we will focus on the ingression of the procephalic lobe and the brain.

Morphogenetic processes depend on movements and shape changes occurring on developmental time-scales. Here we will investigate the morphogenetic process of head involution by talking about the movement of the involuting procephalic lobe and the brain, as well as the processes

of apoptosis and cell removal, which contribute to final shape of head structures as they move [Nassif et al., 1998].

Previous descriptions of HI were based on analysis of fixed images [Abbott and Lengyel, 1991, Rogers and Kaufman, 1996]. Here we show, for the first time, image data of head tissues acquired in vivo using state of the art confocal microscopy techniques. Our approach was to gather time-lapse images from different planes of the anterior part of the embryo, and to show the head tissues in motion. The current chapter is meant to provide insight into the dynamics of HI and to describe in greater detail the involuting tissues and the spatio-temporal relation of their movement. We believe that this part of our work will contribute to the understanding of insect head morphology and its developmental dynamics.

2.2 Main structures of the embryonic head

We will begin this section by showing confocal images of two distinct views of the embryonic head. Figure 2.1 is meant to be a guide and a reference for head structures discussed later on in this section. Since brain involution is a process which takes place (mainly) on the dorsal side of the embryo, Figure 2.1A is a projection of images from the dorsal view. From this image we can clearly see that the head has a bilateral symmetry to it; accordingly, the next plane of our interest is sagittal plane (see Fig. 2.1B). Throughout the rest of this work, we will mostly refer to these two planes; anterior side will be kept on the left, dorsal on top.

2.2.1 Dorsal view of the head

Figure 2.1 shows the anterior tip of an embryo at stage 13, just prior to HI. It is depicting the head and anterior part of amnioserosa tissue, which is located directly posterior to the head. The embryos in Figure 2.1 are ex-

pressing a microtubule-associated protein, Jupiter, tagged with GFP. Because of the high density of microtubules in embryonic and larval head, particularly in the nervous and sensory system [Karpova et al., 2006], we obtained beautiful images of embryonic brain using this marker. The central brain hemispheres, connected by brain commissure, are the main components of the procephalic lobe. We can distinguish the clypeolabrum to the anterior, given that it is composed of columnar epithelium, a tissue that is quite distinct from the brain hemispheres. Dorsolateral portions of epidermis are shown fused into dorsal ridge (DR), located between the procephalic lobe and amnioserosa. The yolk sac, which is a foregut projection, is located on a deeper plane of the embryo, anterior to the DR.

2.2.2 Midsagittal view of the head

We were able to obtain good resolution images from the midsagittal plane of the head using a double photon confocal microscope (Fig. 2.1B). Here, the DR resembles a bud between amnioserosa and procephalic lobe. This plane cuts right through the DR, the clypeolabrum, and the brain commissure; showing only one of the brain hemispheres. The ventral nerve cord (VNC) is positioned ventrally of the central brain, and it extends all the way to the posterior tip of the embryo. The nerve cord is composed of segments called neuromeres - in Fig. 2.1B they appear prominently as a chain- like structure. The invagination at the front is the stomodeum, through which some of the gnathal segments will move (not discussed in this work). Stomodeum lies at the entry of the pharynx, a structure continuous with the oesophagus and the midgut.

Note, the following figures will show single frames from time-lapse videos. The majority of figures have a corresponding movie, as indicated in the figure legend.

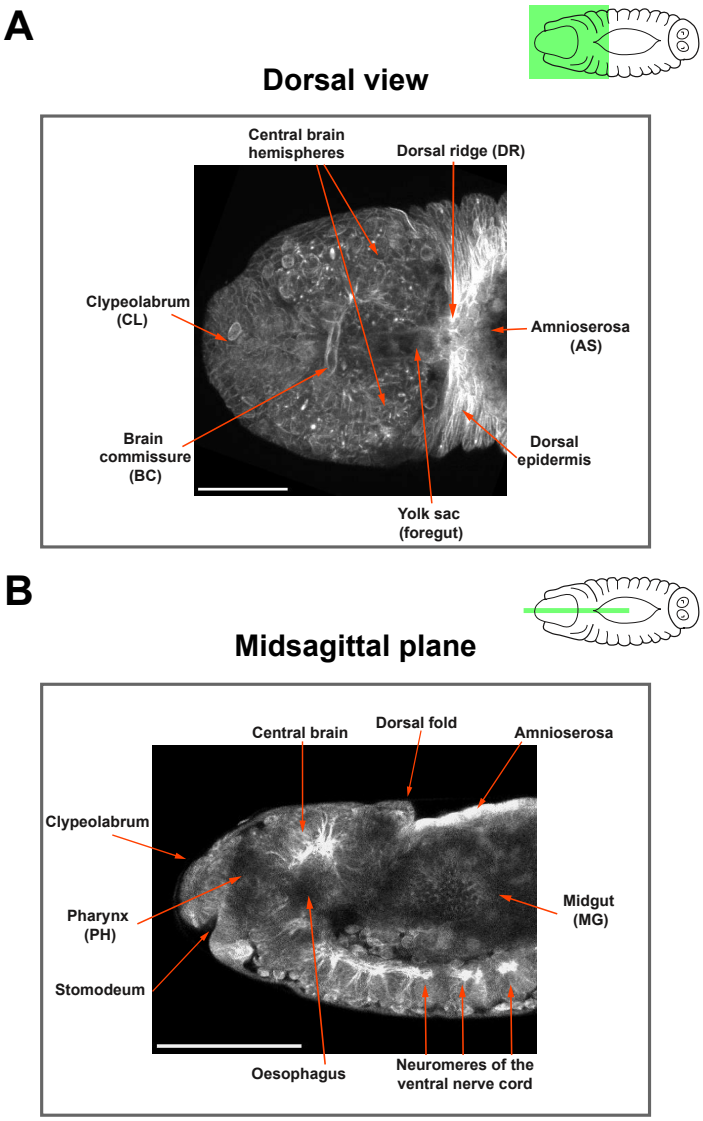

Figure 2.1: **You are here: a fluorescent guide to head structures.** Throughout this section, we will mostly refer to two planes: dorsal and midsagittal. Confocal images of Jupiter GFP embryos at the onset of HI (early stage 13). (A) Dorsal view, max projection of a section 35μm thick. (B) Midsagittal plane. Scale bars: (A) 100μm, (B) 50μm.

2.3 Ingression of Central Nervous System

2.3.1 Early stages of HI

When we look at the procephalic lobe dorsally, we can distinguish the brain hemispheres and the clypeolabrum moving towards the interior of the embryo and progressing under the DR and amnioserosa (see Fig. 2.2, asterisk). This constitutes the beginning of the procephalic lobe involution: displacement of the brain hemispheres from the most anterior tip of the embryo. Two hemispheres are joined along the mediolateral axis with brain commissure (Fig. 2.2, dashed line), which is a good landmark for following the brain's progression. The clypeolabrum (Fig. 2.2, cl) moves from anterior and ventral side onto the most dorsal plane of the embryo. It is easy to distinguish the clypeolabrum from surrounding brain tissues, because of its columnar epithelium morphology.

As the brain lobes move inside, they also change their shape and size, through a combination of mass delamination and invagination [Campos-Ortega and Hartenstein, 1997, Abbott and Lengyel, 1991] [Rogers and Kaufman, 1996]. The brain at this stage is still partially made up of neuroblasts, which delaminate from the procephalic neuroectoderm and become incorporated in the brain hemispheres as neurons and glial cells. This delamination is accompanied by massive cell death and loss of volume [Campos-Ortega and Hartenstein, 1997]. In the dorsal plane, we can see numerous hemocytes as they circle the embryonic head and move along the clypeolabrum clearing up cellular debris (Fig. 2.2, yellow arrows, movie 2.2). We will further discuss apoptotic and hemocyte pattern in section 2.6.

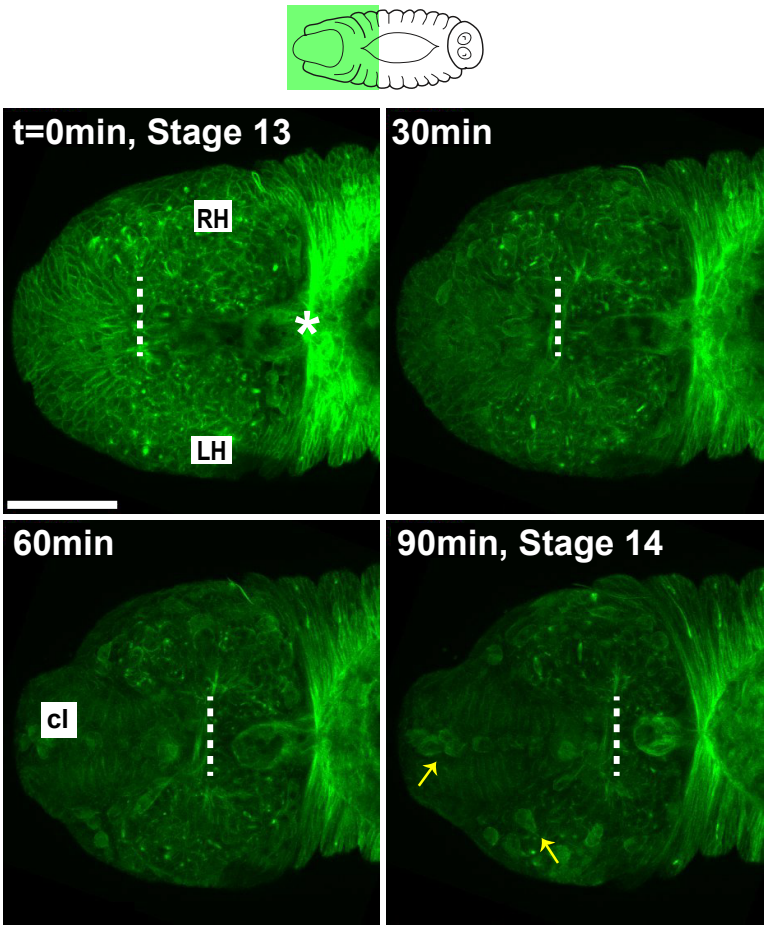

Figure 2.2: **Involution of the procephalic lobe: dorsal view.** Over the course of 90 min, the procephalic lobes move towards the posterior, as indicated by the progression of the brain commissure (dashed line) towards the dorsal ridge (asterisk). Yellow arrows: macrophages. CL- clypeolabrum. Confocal images of Jupiter GFP, max projection of 35μm in 35 planes. Scale bar: 50μm. See movie 2.2.

2.3.2 Final positioning of the brain lobes, later stages of HI

The brain continues moving inwards until the end of embryogenesis, including moments after it has been covered with epidermal tissue. In order to extract the precise shape of the brain and its final position, we imaged it using UAS-GAL4 system [Duffy, 2002]. UAS GFP was expressed under GAL4 driver expressed with ELAV, a RNA binding protein promoter (Embryonic Lethal, Abnormal Vision). ELAV regulated expression has been shown to accumulate within the CNS, both in neuroblasts and glial cells, and is required for correct differentiation and maintenance of the nervous system [Berger et al., 2007]. We can appreciate the final positioning of the brain on the scale of the embryo in Figure 2.3, where the brain reaches a position located one-third between the anterior and posterior pole of the embryo. The shape of the brain changes between stage 15 and 17, from a slightly elongated into a more circular shape (Fig. 2.3). As the brain ingresses, the sensory organs, such as the antennomaxillary complex (AMC), which derives from lateral epidermis, displaces towards the anterior (see Fig. 2.3: asterisk). Two parts of AMC travel along the sides of clypeolabrum (not labeled) and come close at the anterior tip, where they will meet and form the most anterior mouth apparatus of the larva.

2.3.3 CNS ingression: lateral view

As the embryonic head has bilateral symmetry, it is sufficient to image one lateral half of the embryo in order to visualize all the head structures. Because of the thickness of such sample (90μm), we had to make use of a double photon confocal microscope, which has a higher focal depth compared to a standard, single photon confocal microscope. With this technique we were able to get images of the entire half of the embryo. We again took advantage of Jupiter GFP expression, in order to visualize all the head structures.

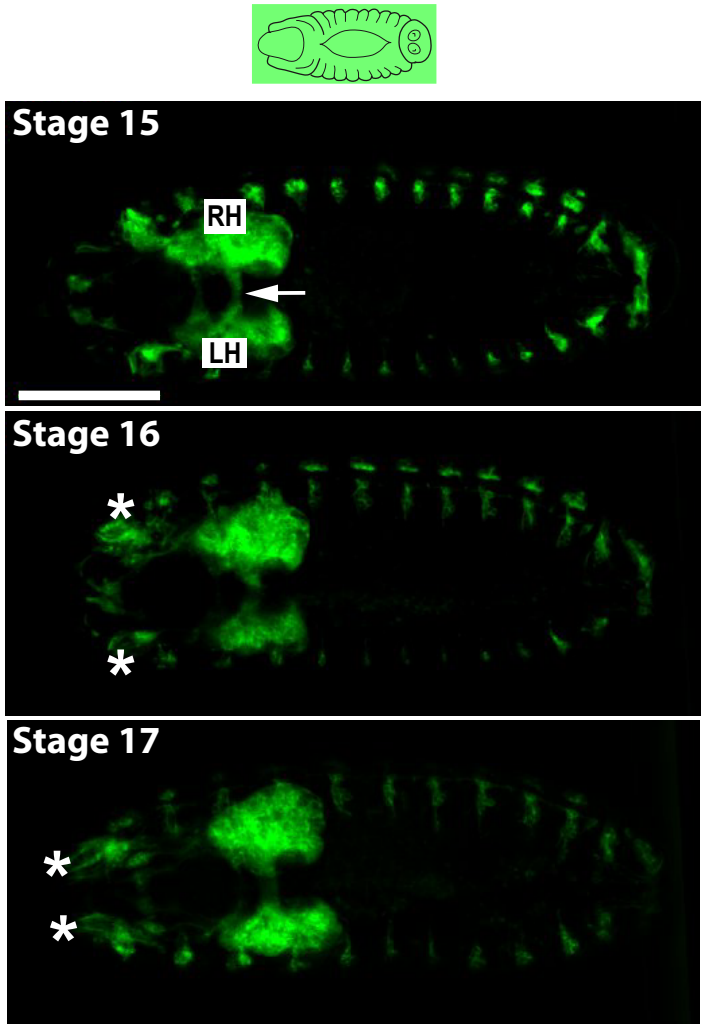

Figure 2.3: **Final positioning of embryonic brain.** The brain has partially involuted, the arrow is pointing to the cerebral commissure, which at stage 15 has already moved away from the anterior pole of the embryo. Asterisks depict dorsal sensory organ (AMC) as it moves anteriorly on both sides of the clypeolabrum (not labeled), coming together during the last stage. Confocal images of ELAV-GFP, max projection of 28μm in 14 planes. Scale bar: 100μm. See movie 2.3.

On the most lateral plane of such images we observe the epidermis (the gnathal segments) and epidermal structures such as the AMC (see Fig. 2.4B, asterisks). Epidermis and its derivatives will move over the CNS in the course of HI. Arrows point to the long sensory neurons called the intersegmental nerves coming out from the VNC perpendicularly to the embryonic anteroposterior AP axis. These nerves are also located in the lateral epidermis and will be displaced towards the anterior, as the epidermis moves over the head.

When we look at the brain on the medial plane (Fig. 2.4C), we see it as a "C" shaped structure, where the lower part incorporates into the VNC, which continues all the way to the posterior pole of the embryo. The two hemispheres, clearly distinguishable on the dorsal view (Fig. 2.2), can be further divided along the dorsoventral (DV) axis into supra-, and suboesophageal ganglion (Fig. 2.4C, white and yellow arrow). Two brain ganglions and the VNC are connected via longitudinal commissures, which run along the DV axis, and are mostly made up of glia cells [Therianos et al., 1995, Berger et al., 2007].

In order to follow the inward movement of the brain, we focused on a single, medial plane (Fig. 2.4C). During HI, the brain lobes move ventroposteriorly, increasing the curvature of the neuraxis, which is the main axis of CNS. The supraoesophageal ganglion moves further than the suboesphageal, towards the posterior, and ventrally towards the VNC (Fig. 2.4C). As a result, the shape of the CNS changes, and it bends towards the inside.

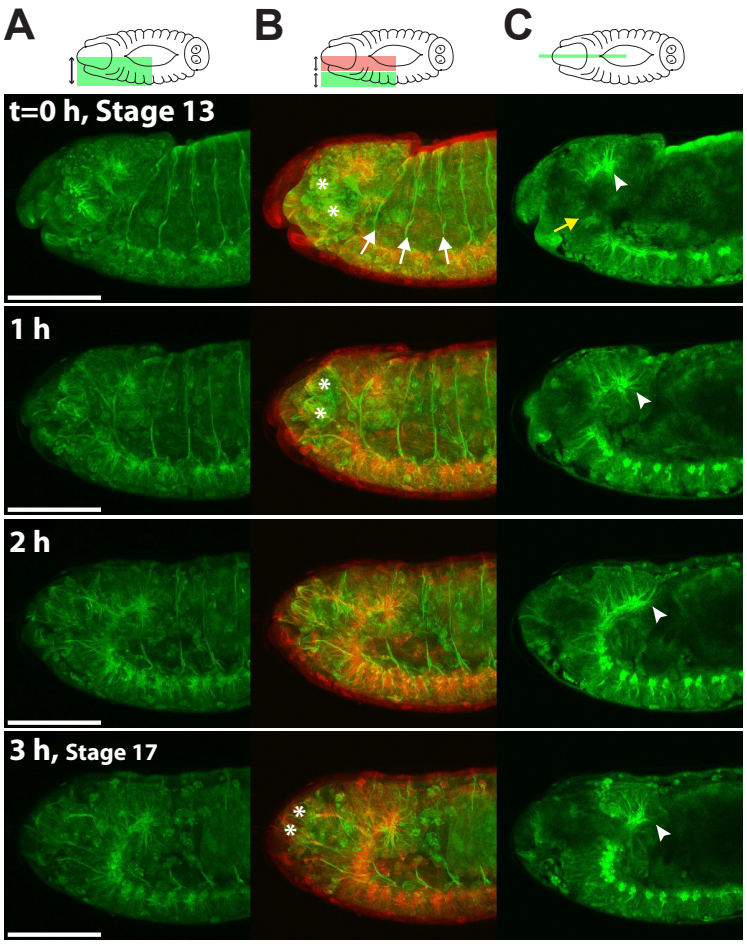

Figure 2.4: **Involution of the procephalic lobe: lateral view.** The last 3 hours of embryonic development, showing the entire process of HI. On different focal planes we can appreciate the reorganization of all the head structures (A-C): Double photon confocal images of the same embryo, Jupiter GFP. (A, B): Maximum projection of 84μm in 28 planes. (B) Color code represents the Z position of projected volume, red: Z planes between the midsagittal and midlateral plane, green: planes between the midlateral, and left lateral plane. (C) Midsagittal plane. Asterisks: AMC, arrowheads: yellow: supra-, white: suboesophageal ganglion, arrows: intersegmental nerves. Scale bar: 100μm. See movie 2.4C)

2.4 Actomyosin pattern within the CNS

So far, there have been no reported studies on the mechanics of CNS movement, or suggestions about the forces driving its ingression. The actomyosin cytoskeleton has an obvious importance for any morphogenetic rearrangements, and mutations in genes encoding cytoskeletal elements result in defects in HI. The corresponding phenotypes have been summarized in the introduction (section 1.2.7). *Drosophila* CNS has been used as a model system for studying cell shape rearrangements of developing neurons, axon growth and guidance [Hakeda-Suzuki et al., 2002, Slováková et al., 2012], or polarity establishment during asymmetric neuroblasts division [Biersmith et al., 2011, Prehoda, 2009]. It is not clear, however, what is the mechanism underlying CNS ingression, and whether there is a structure-level organization of actomyosin within the CNS. To tackle these questions, we profiled the expression of actomyosin skeleton in the CNS. In order to illuminate actomyosin, we used GFP targeted to non-muscle myosin II regulatory light chain [Karess et al., 1991] and to actin-binding region of fly moesin. For simplicity, we will refer to these proteins as myosin and actin, respectively. Moesin links the transmembrane proteins to actin cytoskeleton and is involved in cortical Actin assembly [McCartney and Fehon, 1996]. We use a construct involving moesin actin binding region–sGMCA to illuminate actin cortex [Kiehart et al., 2000].

In order to extract the exact morphology of the CNS, we obtained data for ELAV regulated expression on a midsagittal plane (Fig. 2.5A: dashed line). We describe the pattern of actomyosin within the CNS using the resultant images as a reference. Throughout the process of HI we observe a strong accumulation of actomyosin both within the supra- and the suboesophageal ganglion, and within the longitudinal commissures that connect the brain to the VNC (Fig. 2.5B, 2.5C). We also see actomyosin accumulate within individual neuromeres of the VNC - in what seems to be mostly glia cells (Fig. 2.5B, C: asterisks). The actomyosin pattern follows the organization of the CNS itself: a ladder-like structure

with bilateral symmetry, connected with commissures in transversal and longitudinal direction. Actomyosin, although present all along the CNS, seems to be preferentially localized on the inner or the dorsal portion of the CNS. In the discussion, we speculate on how contracting only the inner part of the CNS could change the curvature of neuraxis supporting the involution of the brain (see below).

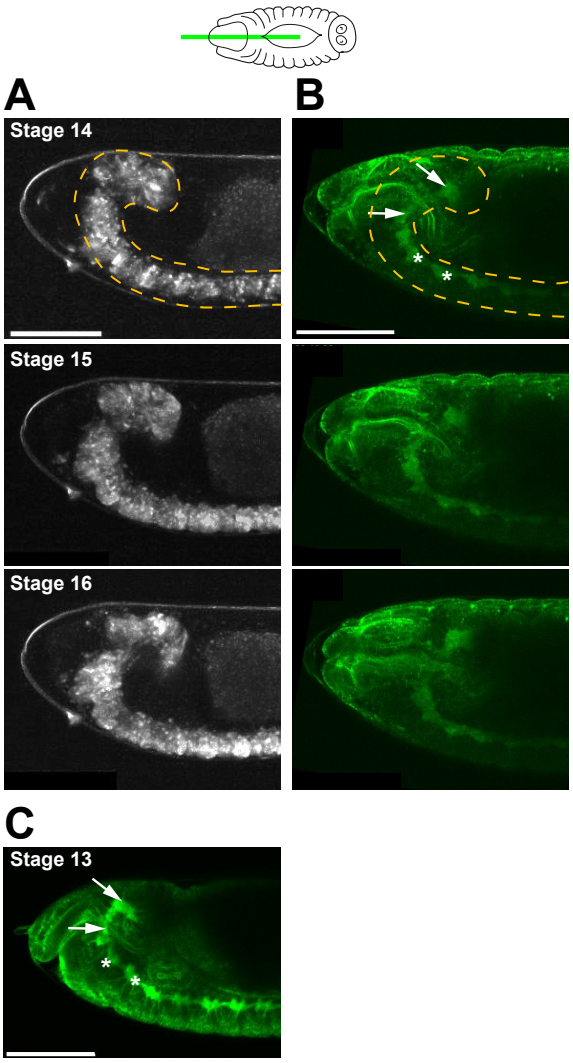

Figure 2.5: **Actomyosin accumulation within the CNS.** Outline of the involuting CNS and distribution of actomyosin within it. (A) Confocal image of midsagittal plane, ELAV>GFP. Dashed line is representing an outline of the procephalic lobe and VNC. (B, C) Double-photon confocal images, midsagittal plane, myosin and actin GFP, respectively. Arrows: myosin/ actin accumulation within the brain. Upper arrow: supra-, lower: suboesophageal ganglion. Asterisks: myosin/ actin pattern within VNC. Scale bars: 50μm.

2.5 CNS-gut relation

2.5.1 Movements of the brain and the gut are coordinated

Cephalogenesis in *Drosophila* is closely related to the development of the gut, both spatially and temporally. Previous work has demonstrated accumulation of cell adhesion molecules between the foregut and commissures in the CNS [Reichert and Boyan, 1997]. We have referred again to the midsagittal plane in order to describe the relation between the foregut and the CNS in vivo. The foregut goes under significant changes during stages 13-16: from a straight- to an S-shaped round tube (Fig. 2.6B). The midgut also transforms: it closes a double, yolk-flanking layer into a continuous lumen, which is afterwards divided into four chambers (Fig. 2.6B, stage 15). Additionally, these reorganizations result in the internalization of the gut – it becomes more centered within the embryonic body, and more compact [Campos-Ortega and Hartenstein, 1997].

All these gut rearrangements occur at the same time as HI unfolds. In order to test a possible mechanical relationship between these two systems, we examined the ingression of the CNS in parallel with gut rearrangements (Fig. 2.6A). Interestingly, we found a close correlation between the inward movement of the gut and that of the CNS: the bending of CNS follows the ventral movement of the gut. During stage 15, the CNS straightens slightly its curvature; the supraoesophageal ganglion moves dorsally, transforming minimally the “C” shape into a “L”. The straightening of the foregut tube in the anteroposterior axis and the slight dorsal progression of the brain likewise occur simultaneously (Fig. 2.6B, stage 15).

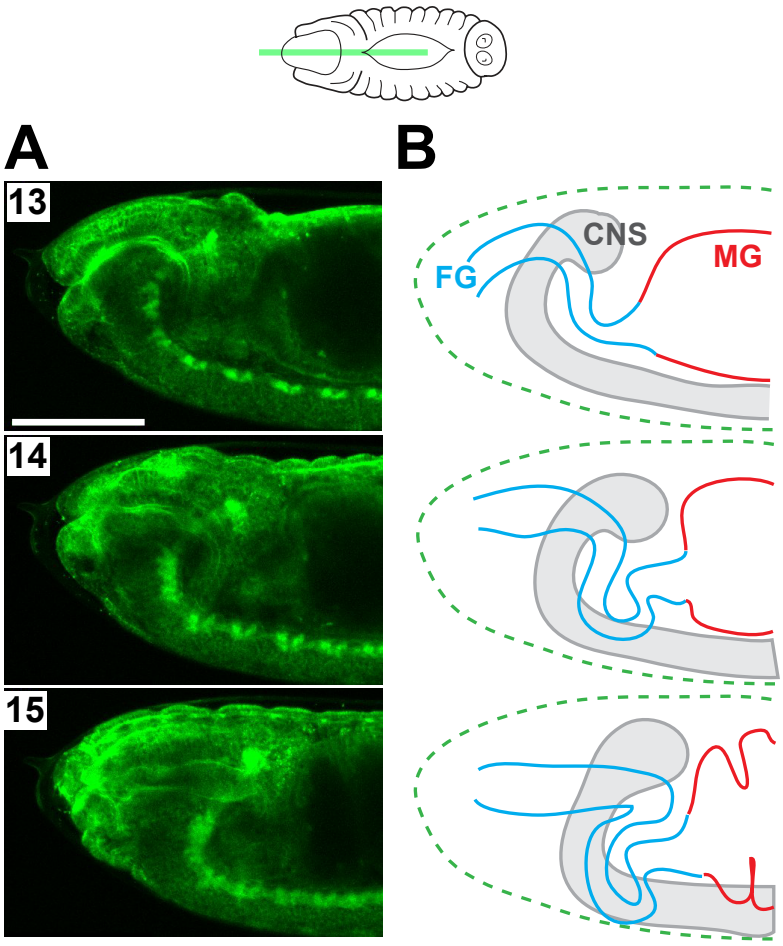

Figure 2.6: **Coordination of CNS and gut movements.** Comparing the progression of CNS and the rearrangements of the gut during HI. (A) Double photon confocal images, midsagittal plane, myosin GFP. (B) Cartoon made by drawing outlines of CNS, foregut (FG), and midgut (MG) from (A). Green dotted line represents the outline of the embryo. Scale bar 100μm. See movie 2.6.

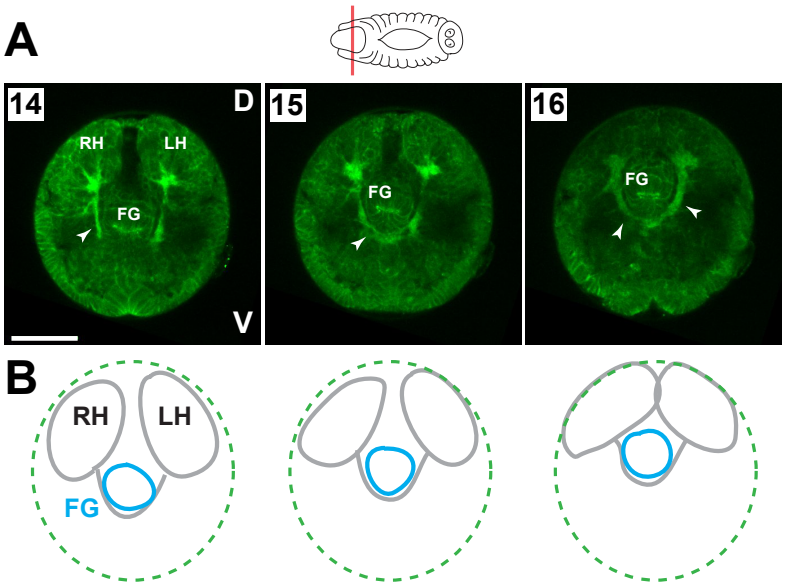

Figure 2.7: **Coordination of CNS and gut movements - transversal plane.** When we examine the transversal plane, we observe coordinated movement of the gut and the brain towards the dorsal. Brain hemispheres change shape, and come closer as they move. (A) Double photon confocal images , myosin GFP. Strong accumulation of myosin within the commissures surrounding the foregut (arrowhead). (B) Sketch made by drawing outlines of left and right hemisphere (LH, RH) and foregut (FG) from images in (A). Green dotted line represents the outline of the embryo. Scale bar 50μm.

Subsequently we asked whether there is a correlation in foregut and CNS movement in the DV axis. In order to get horizontal sections of the head, we used a double photon inverted confocal microscope, in addition to a novel way of mounting the sample. Specifically, we put the embryos vertically in a thick bed of agarose, and by placing the objective directly on top of the anterior pole of the embryo we scanned it on a transversal plane. Imaging starts at the most anterior tip and continues posteriorly for about 130μm inwards, a thickness which can only be imaged using a dou-

ble photon microscope. The tight spatial relation between the CNS and the gut is clearly visible (Fig. 2.7A, arrowhead), and the two structures move in unison on the transversal plane. At first, we observe the dorsal progression of both CNS and the gut, next they move towards the inside of the embryo. On this plane, we can also observe the change in shape and relative position of the brain lobes.

2.5.2 Laser dissection shows mechanical coupling between the brain and the gut

The movements of the CNS and the gut seem to be closely correlated. In order to investigate whether the gut inward movement is exerting a pulling force on the CNS, or vice versa (i.e., the CNS is pulling on the foregut), we performed a laser ablation experiment in order to separate these two structures. Specifically, we cut the proventriculus, a part of the foregut located between the DR and the brain, and which is clearly visible at this stage. The proventriculus is located between the pharynx, the esophagus, and the midgut. It has been shown previously that there is a strong accumulation of adhesion molecules where the foregut encounters the CNS commissures [Hummel et al., 1999]. Right before the cut, we can trace the coordinated movement of brain commissure and the proventriculus towards the posterior of the embryo (see Fig. 2.8A). Immediately after the cut, the brain hemisphere retracts towards the anterior (Fig. 2.8C, red arrows). The brain hemispheres move slightly towards the midline (black arrows). This result shows that we were able to separate the brain and the gut, and suggests their mechanical coupling.

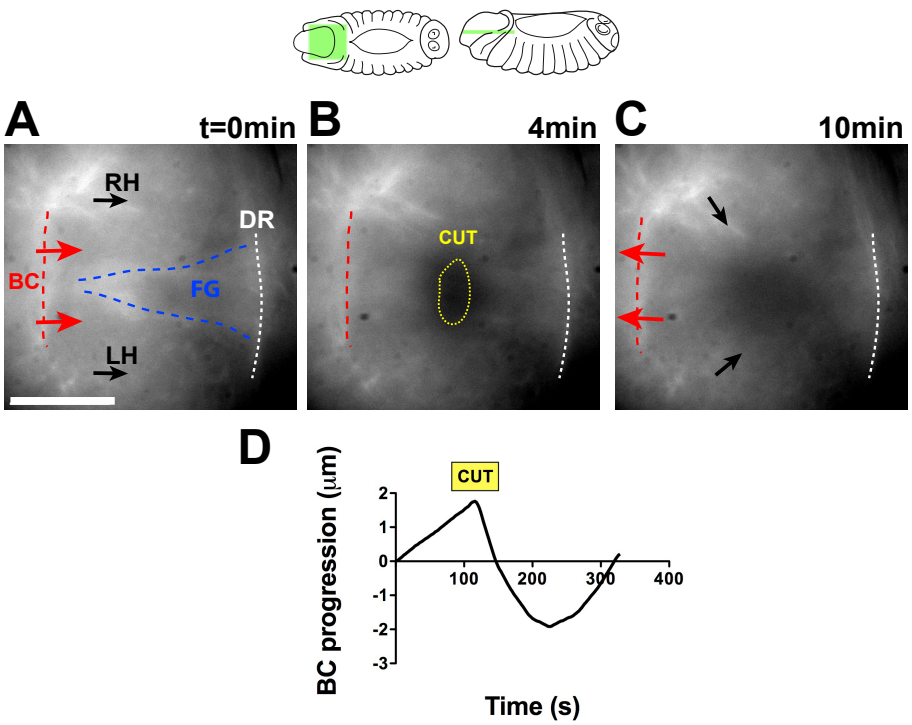

Figure 2.8: **Foregut laser ablation.** After a laser ablation of the foregut, we observe a retraction of the brain hemispheres in the direction opposite to their normal progression. (A-C) Images from a laser-ablation time lapse, horizontal plane, myosin GFP. (A) Red dashed line: brain commissure (BC), red arrows: progression of the commissure. Black arrows: movement of the brain hemispheres (left and right brain hemisphere - LH, RH). White dashed line: position of the dorsal ridge, blue dashed line: outline of the foregut protrusion (FG). (B) Yellow dashed circle: wound from the laser cut. (C) Retraction of BC towards the anterior, slight movement of the hemispheres towards the midline (black arrows). (D) Progression of the BC tracked on a kymograph drawn across the BC, parallel to the movement. 0μm/s position/time when we start tracking the BC. Scale bar 20μm.

2.6 Apoptosis and cell removal during HI

Apart from movements and displacements, modifications of size and shape are crucial for all morphogenetic processes. Morphogenetic cell death often occurs in highly reproducible spatiotemporal patterns, and can also be directly implied in specific tissue shape changes [Teng and Toyama, 2011, Page and Olofsson, 2008, Monier et al., 2015]. It has been reported to play an important role during *Drosophila* HI [Grether et al., 1995, White et al., 1994, Abbott and Lengyel, 1991] [Nassif et al., 1998]. In the embryonic head, cell death occurs in prominent groups of cells, in regions of vast morphogenetic movements. When we block apoptosis, embryos fail to undergo the process of HI: the procephalic lobe does not involute and dorsal head is exposed at surface [Nassif et al., 1998].

2.6.1 Apoptosis in the head during HI

To study further the pattern of apoptosis within the head, we used an apoptotic marker for live imaging. Apoliner 5 is a fluorescent reporter of caspase activity and marks in vivo cells that activate caspase pathway [Bardet et al., 2008]. Upon activation of the apoptotic pathway (by cleavage of drosophila inhibitor of apoptosis - DIAP1) the GFP translocates to the nucleus. We observed caspase activity in the procephalic lobes and clypeolabrum (Fig. 2.9B, C, arrowheads). We observed very little, or no caspase activity within the dorsal fold (Fig. 2.9A, dashed line) or the most dorsal tissue (Fig. 2.9A). The sketches on the left in Figure 2.9A show approximate depth of the plane depicted on the right. As we move deeper inside of the embryo, we detect more apoptotic cells within the procephalic lobe (Fig. 2.9B,C). On this plane, we can also observe many macrophages, which are easily spotted because of the large vacuoles with cellular debris inside.

2.6.2 Hemocyte pattern in the head

Based on these observations we strived to look for a more detailed pattern of hemocytes movement within the head during HI. It has been reported previously that hemocytes move in specific loci inside the head, as compared to a dispersed pattern in the rest of embryonic body [Guillot and Lecuit, 2013, Walck-Shannon and Hardin, 2014]. In order to image the hemocytes and head structures simultaneously, we created a fly line ubiquitously expressing actin GFP, and GAL4 driver expressed in Serpent promoter. Serpent is a promoter traditionally used to follow embryonic hemocytes [Rehorn et al., 1996, Fossett et al., 2003]. We observed a very specific pattern of hemocytes migration within the head. All the hemocytes either: (1) circulate around the brain hemispheres, or (2) travel along the anteroposterior axis on top of the clypeolabrum (Fig. 2.10A). The majority of hemocytes occupy deeper sections of the head, similar to the pattern of cells that activate caspase pathway (see Fig. 2.9). During stage 16, when almost all head structures are internalized, hemocytes continue circulating the brain lobes (Fig. 2.10C). This result further confirms the importance of apoptosis and cell removal in morphogenetic rearrangements of the involuting brain.

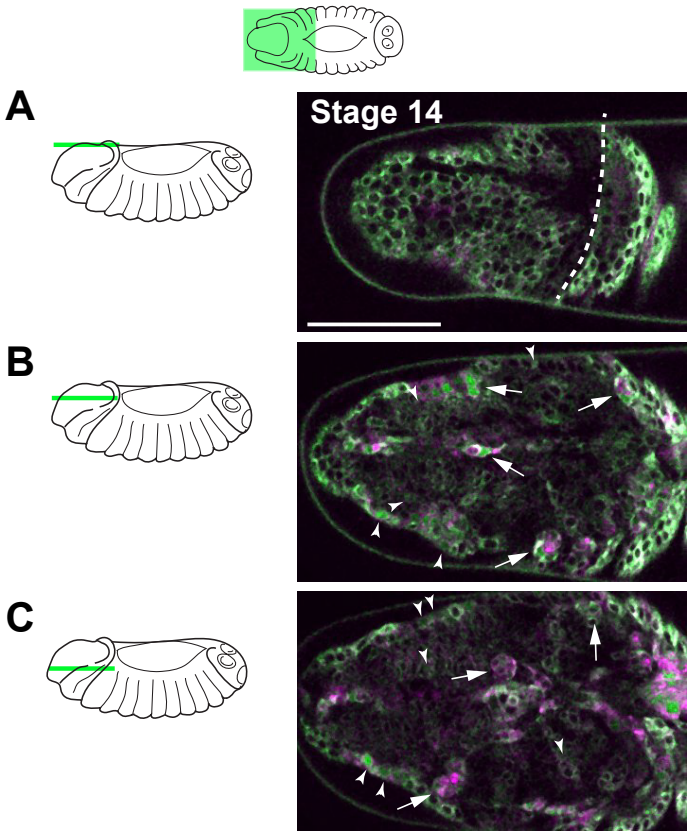

Figure 2.9: **Apoptosis pattern in the head.** Activation of apoptotic pathway in the embryonic head. We observe more apoptotic cells on the deeper planes of embryonic head, surrounding the brain lobes. In parallel to cells activating their caspase pathway, we observe many hemocytes, characterized by multiple vacuoles of phagocytized cells. Sketches on the left panel show the depth of imaged plane. Right panel: single planes from Apoliner 5 expressing embryos. Dashed line: DR, arrowheads: cells with active caspase pathway-GFP signal translocates inside the nucleus (see methods section 5.1). Arrows: hemocytes with phagocytized cells inside. Scale bar: 50μm.

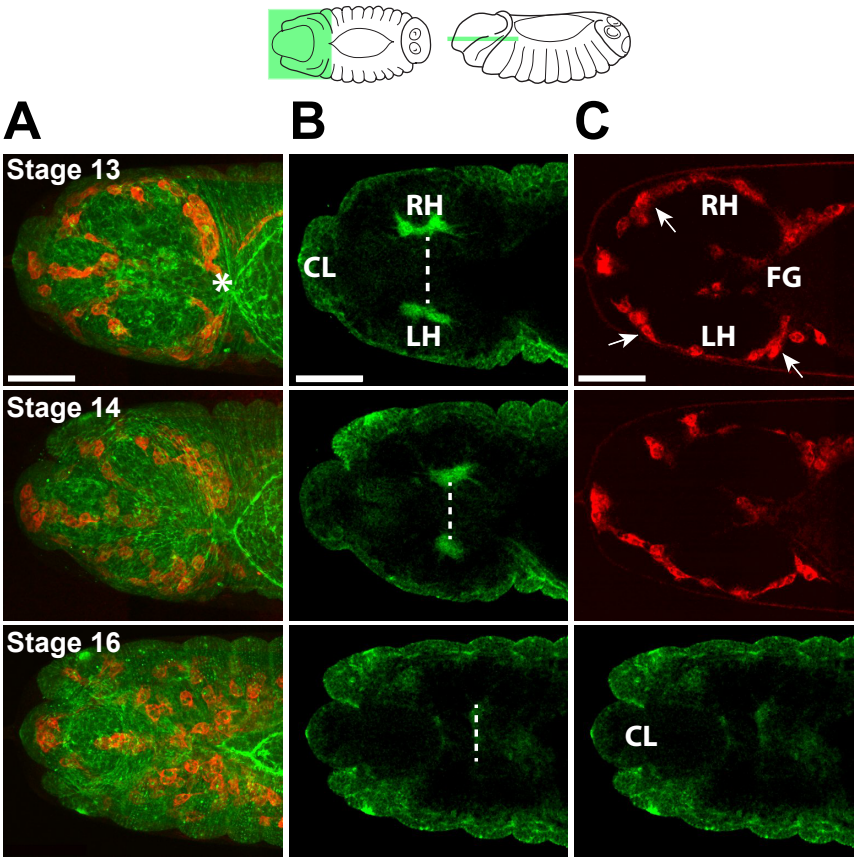

Figure 2.10: **Hemocyte pattern during HI.** The brain lobes are surrounded by hemocytes throughout the entire process of brain involution. Confocal images of dorsal view of an embryo expressing custom designed line: myosin GFP, hemocytes mcherry (sGMCA GFP, SRP GAL4>UAS mcherry CAAX, see methods section for details). (A) Merge of two channels, max projection of 36μm in 18 planes. (B-C) Single plane at 34μm depth from the most dorsal surface. The brain lobes are marked (RH, LH); the brain commissure is the dashed line. (B) Actin GFP (C): mcherry CAAX is expressed under the SRP promoter, showing the embryonic hemocytes (C: arrows). FG: foregut, CL: clypeolabrum. Scale bar: 50μm. See movie 2.10.

2.7 Discussion

The results presented in this section provide a novel, detailed description of the process of HI. State-of-the-art confocal and multiphoton microscopy allowed us to obtain high-resolution data from medial or transversal planes of the embryo. By contrasting these two planes with the dorsal view, we obtain a better understanding of the HI dynamics.

We focused on the involution of the CNS, particularly the brain lobes. We showed the inward progression of the brain lobes in motion, related to bending of the entire CNS. The CNS is a three dimensional structure with interconnected compartments: the brain ganglions and the VNC composed of neuromeres. During HI, the entire CNS undergoes condensation, the brain bends towards dorsoposterior, and the VNC condenses in anteroposterior length. We profiled the distribution of actomyosin within the CNS, finding that it follows an interesting pattern: it localizes only on the dorsal portion of the CNS. In what follows, we speculate on a mechanism potentially driving CNS ingression, reminiscent of the functioning of a bimetal strip.

We interpret the CNS as a network of subunits, which moves in a coordinated, cooperative fashion. Since only the inner/dorsal portion of the CNS is expressing contractile molecules, it results in a network with a double layer structure: (1) a highly contractile inner/dorsal layer (Fig. 2.11, 1 - green stripe), and (2) an outer layer with low contractility (Fig. 2.11, 1 - grey stripe). As a consequence of such supracellular distribution, only the inner layer will shrink significantly (Fig. 2.11, 1 - black arrows), causing the entire structure to bend and to curve inwards.

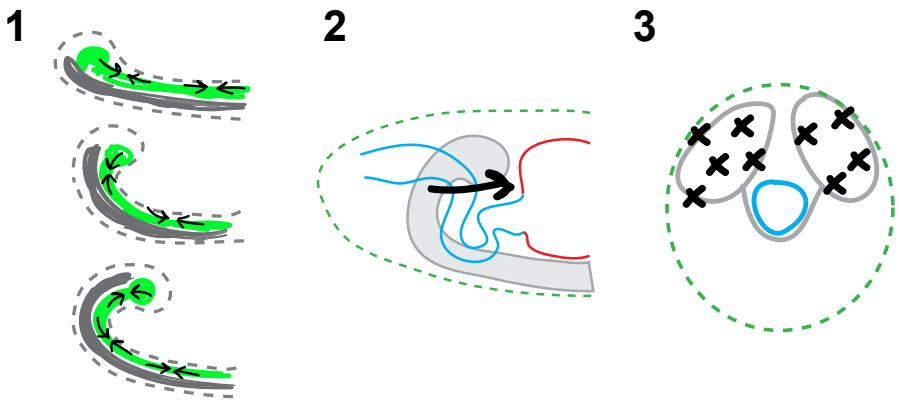

Figure 2.11: **Three-step mechanism of CNS internalization.** (1) Internalization of the brain initiated by contraction of inner, dorsal layer of the CNS. (2) The gut exerts a pulling force towards the inside of the embryo. (3) Throughout the movement, brain is reshaped by apoptosis and cell removal.

There are few examples of biologically engineered double layer structures, which are internally heterogeneous and can bend in a specific direction. An example is a bigel strip, made out of two types of modulated polymer gels. When one of its layers shrinks in response to temperature change, the entire strip bends [Hu et al., 1998]. A structure mimicking a lipid bilayer, i.e. two layers of droplets with different osmolarities, also curves up and forms a circle when flow of water causes one layer of droplets to shrink [Villar et al., 2013].

We would like to propose, here, that a supracellular actomyosin structure, which spans the length of the CNS, generates the mechanical force for the initial CNS bending. Further experiments showing actomyosin localization in between the subunits of CNS would be of great interest, in order to study a tissue- level contractile structure pattern. Next step would be a genetic and mechanical interference with such actomyosin band contractility and continuity, respectively. Actomyosin can be, depending on the tissue and UAS- GAL4 availability, easily targeted, and expression of

cytoskeleton regulating proteins within the CNS could drive e.g. decrease in myosin contractility.

Mechanical ablation of the actomyosin band, perpendicularly to the neuraxis direction, could give additional information on the distribution and magnitude of tensile forces within the CNS. Such experiment would also confirm the importance of continuity and integrity of the CNS in the process of bending. It would be interesting to observe how, after severing the CNS in two pieces, each structure would behave, and whether we could still observe any contractility in the separated pieces.

CNS and gut are spatially connected (gut tube goes through the brain commissures, see section 2.4) and sealed with adhesion molecules on the interface [Reichert and Boyan 1997]. We have observed simultaneous motion of the brain towards dorsoposterior (the described straightening of "C" shape) with the midgut condensation and shape rearrangement of the foregut (Fig. 2.11, 2). We have shown that the CNS and the foregut are mechanically linked, and we were able to separate them by laser ablation. We thus propose a further bending of the CNS driven by gut condensation and shape change. In order to further separate the dynamics of these two structures, we could impair the process of gut condensation, preferably at the late stage (14-15).

Finally, we have shown patterns of apoptosis and cell removal in the embryonic head. The apoptotic cells are located mainly in the procephalic lobe, which is surrounded by hemocytes throughout HI. This result confirms the previously proposed importance of apoptosis and immediate cell removal by hemocytes during HI. In particular, it is an example of a morphogenetic process involving spatial movement and reshaping of a tissue at the same time. Nassif et al. showed in their work that even partially blocking apoptosis results in the anterior-hole phenotype [Nassif et al. 1998, Toyama et al. 2008]. Such embryos fail to properly involute the head, which is exposed to the surface, or to form a functioning mouth apparatus.

The VNC condensation is also shown to be controlled by apoptosis and hemocytes, which is decreasing the size of the structure [Olofsson and Page 2005; Page and Olofsson 2008]. A large part of the VNC undergoes apoptosis and cell removal, required for condensation. Additionally, hemocytes have an important role in detaching the CNS from surrounding epidermis, and laying out ECM around the dynamically changing tissues. We propose that programmed cell death is required for size control of the ingressing brain; phenotypes resulting from blocked cell death are characterized by oversized brain (Fig.2.11, 3), which fails to move inward. As a consequence, epidermis cannot progress over the head and secrete the cuticle necessary for the rest of larval stages. An experiment to follow our results would involve blocking 1) apoptosis in the CNS by expressing mutated pro apoptotic genes, 2) hemocytes migration and 3) monitoring of affected head structures dynamics on time lapse images.

In summary, we consider that our results provide an interesting contribution to Drosophila late embryogenesis and we propose a three-step mechanism involved in the ingression of procephalic lobe and the brain (Fig. 2.11). CNS ingression is initiated by actomyosin driven contraction on the structure level, and further reinforced by its connection with the foregut, which moves towards posterior bringing the CNS along. Throughout the entire process, the ingressing brain is reshaped and gets smaller, so that it fits in the enveloping epidermis.

Chapter 3

FORMATION OF THE DORSAL POUCH: AN ALTERNATIVE MIGRATORY MECHANISM

3.1 Objectives

Out of the many processes involved in Head Involution we believe one deserves a particular highlight: the formation of the epidermal dorsal fold (DF) and its initial progression over the embryonic head. This process is a curious example of tissue movement, mainly because the DF moves by rolling over itself. The idea of an epithelial layer rolling is known in developmental biology, yet associated only with gastrulating embryos [Keller et al., 2003]. Here we show a process in which a mature epithelium folds and rolls over itself, covering the head structures with a double-layer of epidermis.

At the developmental stage in question (early 13), all but the head and dorsal portion of the embryo are covered with epidermis. We observe a fusion of dorsal portions of epidermal segments on the border be-

tween amnioserosa and procephalic lobe. The fused bit of tissue is called the dorsal ridge (DR) [Campos-Ortega and Hartenstein, 1997]. From this moment on, epidermis begins covering the exposed parts of the embryo. The DR moves towards the anterior tip covering the procephalic lobe, and just posterior to it, in the process of dorsal closure, lateral epidermis begins migrating dorsally and fuses over amnioserosa cells.

The process of epidermal progression over the embryonic head comprises three consecutive steps:

1. **the dorsal ridge bends and folds over itself creating a dorsal fold;**
2. **the dorsal fold progresses in a rolling motion, forming a pouch; and**
3. the dorsal fold stretches and slides over the head tissues.

In this chapter, we will focus on the initial progression of epidermis over the head. In Appendix A, we will discuss in greater detail the last step (3) of the process, when the dorsal fold stretches and slides over the head.

3.2 The dorsal ridge folds over itself

The DR forms a band of epidermis on the most dorsal portion of the embryo. If we were to look at the transversal section, and think of it as a clock, the DR would extend between hours 10 and 2. On a medial plane it resembles a small bud (see Fig. 3.1A and Fig. 3.2B, pink dot), which shortly after its formation grows in the dorsal direction (Fig. 3.1B). As more epidermis is zipped at the back, DR starts bending towards the anterior. It most likely remains attached to the underlying tissue (head ectoderm) by what we call the anchoring point. As a result, when lateral epidermis is sealed dorsally during DC, the DR continues bending

towards the anterior and touches the head ectoderm anterior to it, creating the so-called dorsal fold (DF) (Fig. 3.1B, yellow arrowhead).

Although a picture of zipped epidermis "pushing" on the DR from the back seems like a plausible bending mechanism, we also observe a strong accumulation of myosin within the fold (Fig. 3.1C). Dynamic accumulation patterns of non-muscle myosin II have been proposed as the basis of a molecular mechanism driving tissue bending and folding, given that they correlate with shape changes during invagination [Sherrard et al., 2010]. Based on the previous background, we looked for actomyosin patterns in DR bending. Figure 3.1C shows that, indeed, as the DR tilts towards the anterior, there is an accumulation of myosin within the fold (red dashed box). We measured the intensity of myosin discovering that it gradually increases as the DF formation progresses (Fig. 3.1D). Based on these observations we speculate on possible mechanisms of epithelial bending, discussed later in this section.

3.3 Let's roll! Formation of the dorsal pouch

Folding of the DR is merely the beginning stage of epidermal progression over the head. The fold then rolls inward, and progresses in a tank-like motion. The cartoon in Figure 3.2 is based on SPIM images of the fold; it shows the involution of the DR and dorsal epidermis. Cells (groups of cells - not to scale) are represented by dots in different colors. As the rolling motion starts, all of the initial DR tissue is placed directly on top of the head ectoderm. The dorsal pouch will form in between these two tissues (head ectoderm and epidermis) (Fig. 3.2, yellow arrowheads). The pouch is a structure preserved until the end of the larval cycle, when an adult fly emerges from the pupa [Sink, 2006].

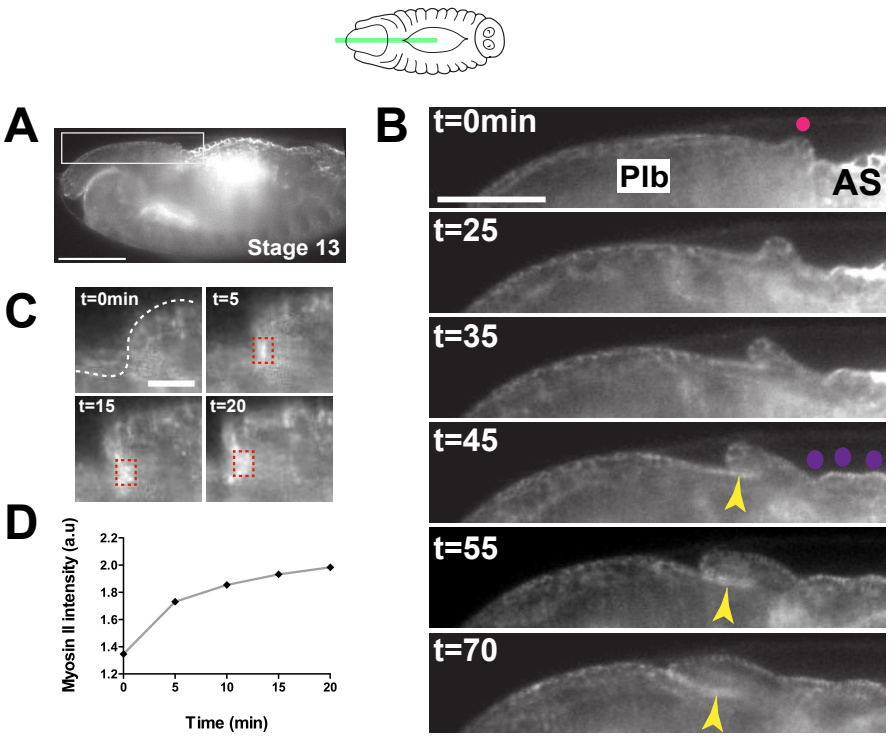

Figure 3.1: **Formation of the dorsal fold.** DR (B: pink dot) bends, and folds over itself becoming DF. The fold progresses towards the anterior forming a pouch (yellow arrowhead). Epidermis coming from the posterior becomes the most dorsal (B: purple dots). We observe increasing myosin accumulation on the side of DR bending. (A-C) SPIM images, medial plane of: (A-B) E-Cadh, (C) myosin. (A) Early stage 13 embryo, DR localization on the scale of embryonic head. White box: zoomed-in region shown in B. Scale bar 50μm. (B) Formation of the DF; Plb: procephalic lobe, AS: amnioserosa. Scale bar 25μm. (C) Close view of the bending DR, the red square depicts a region in which we quantified myosin accumulation. 10μm. (D) Myosin intensity measured in a region $10x10pxl$, normalized by the average intensity of the picture. See movie 3.1.

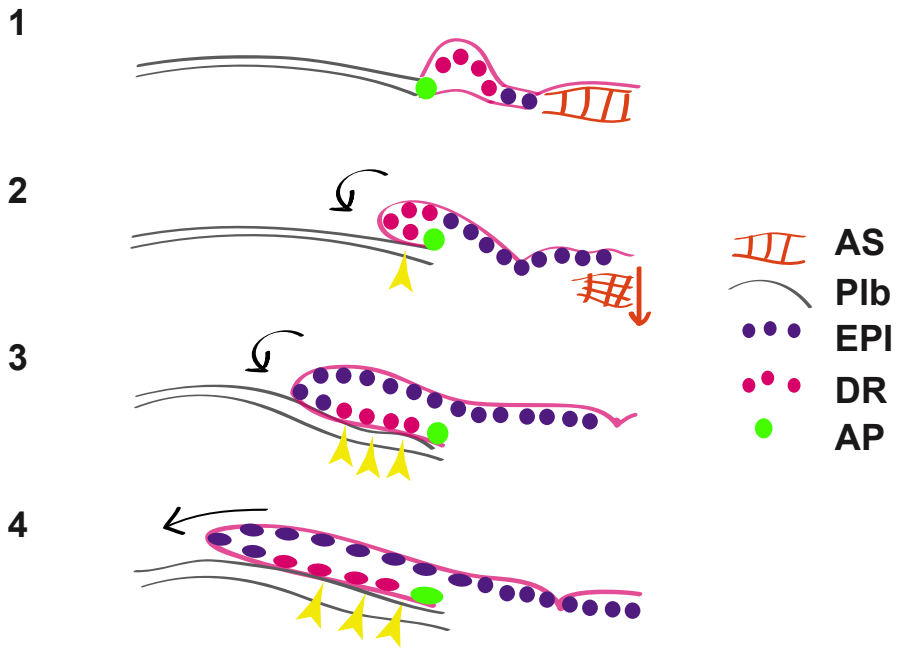

Figure 3.2: **Let's roll!.** Sketch based on SPIM images (see Fig. 3.1). AS cells are delaminating towards the ventral (orange arrow), and are covered with zipped epidermis. Dots represent epidermal cells. DR (pink): cells forming the dorsal ridge. The anterior cell of DR is shown in green and represents the anchoring point of fold formation (AP). EPI (purple): cells which have been zipped over AS. Note, cell number and size are not to scale.

The rolling continues for about one hour: more tissue comes from the posterior and is rolled under. Because the tissue continues progressing forward in tank-like motion, with a steady attachment point, a double epithelial layer is placed over the head. Given that more tissue comes in contact with the head ectoderm and the original anchoring point does not shift forward, the dorsal pouch enlarges (Fig. 3.2, green dot). During early stage 15, we observe a transition from rolling to stretching of both epithelial layers (Fig. 3.2, part 4).

3.4 Behavior of actomyosin within the DF

Myosin accumulation (described above) is not the only pattern we observe during the process of fold progression. When we examine SPIM images of a close-up view of the progressing DF, we observe punctual accumulations of myosin across the dorsal epidermis (Fig. 3.3A, arrowheads). The expression pattern is not composed of mere punctae – it only appears so on the sagittal view. The dots in Figure 3.3A are really cross-sections of long, supracellular cables running along the lateral axis perpendicularly to the direction of fold movement. The cables are clearly distinguishable on the dorsal view (Fig. 3.3B, arrowheads).

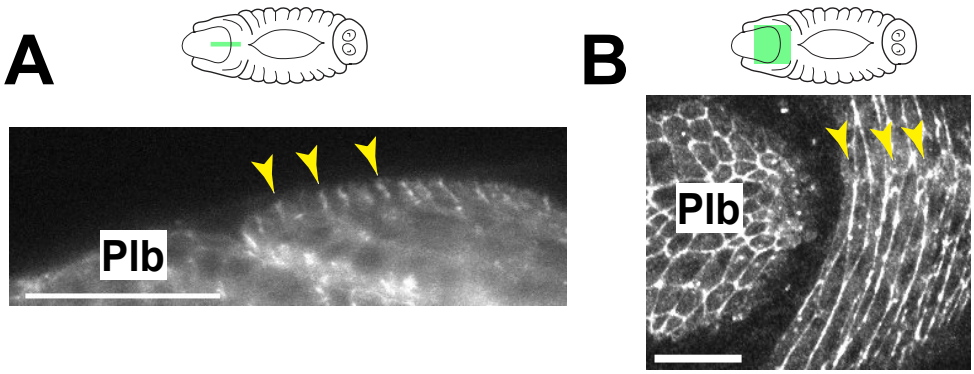

Figure 3.3: **Myosin pattern within the dorsal fold** What seems like punctae on a sagittal view are cross sections of long, supracellular myosin cables (arrowheads). (A) SPIM image, medial plane. Scale bars 20μm. (B) Confocal image, dorsal view. Scale bars 10μm. Plb: procephalic lobe.

Supracellular cables are formed when cells in a regularly arranged tissue polarize the enrichment of subcellular actomyosin to specific cell boundaries. These boundaries are frequently found linked to one another [Fernandez-Gonzalez et al., 2009]; as a result, we observe chains of connected cell interfaces. Myosin is discerned in the apical portions of anterioposterior cell boundaries along the whole width of the dorsal epidermis within the DF (Fig. 3.3B). In contrast, apical myosin is distributed in all cell boundaries within the procephalic lobe (Fig. 3.3, Plb). We can thus distinguish round cells in the Plb, whereas we only see cell rows, not individual cells, in the DF. Consequently, the myosin network in the dorsal epidermis is organized in multiple, parallel, supracellular cables. Figure 3.4 shows the exact view of epidermis presented in Figure 3.3 – here captured in the process of rolling and stretching. Myosin enrichment in cables is maintained throughout the process of DF progression. Both on the sagittal and dorsal view, we observe individual accumulations at the front as they are rolled under. Subsequently, the next cable in line progresses to the front and disappears under the dorsal layer (Fig. 3.4).

The DF rolls for about 30 min (5-7 cell rows), and then begins stretching (both of epidermal layers) and sliding over the underlying procephalic lobe (Fig. 3.4). When tissue starts stretching, however, a single leading edge myosin dot/cable persists throughout the rest of the movement. We will discuss the sliding and leading edge (LE) cable in greater detail in Appendix A. Previous work has demonstrated a crucial role for supracellular cables in morphogenesis [Fernandez-Gonzalez et al., 2009, Monier et al., 2011, Franke et al., 2005], summarized in the introduction (seen section 1.1.5. Here we report a previously undescribed morphogenetic process in which such actomyosin structures are involved.

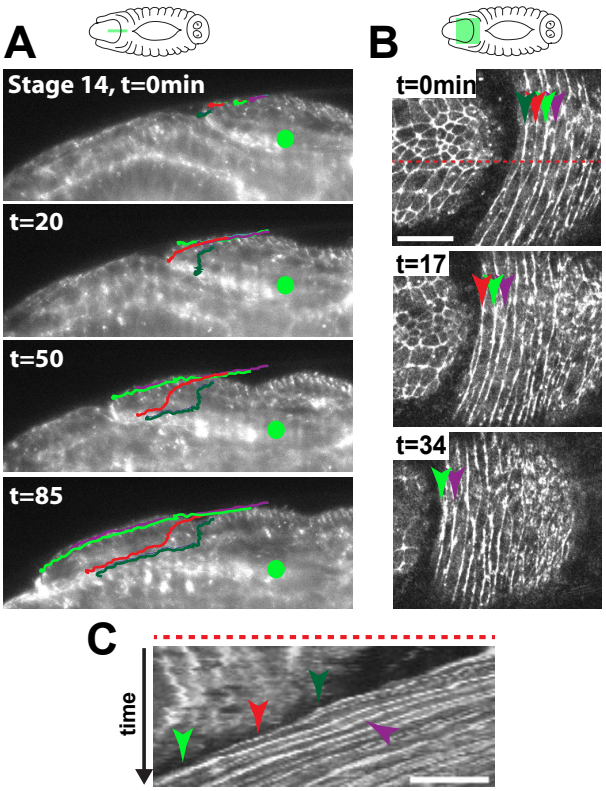

Figure 3.4: **Multiple actomyosin cables in the process of rolling.** Frames from time-lapse movies showing two phases in pouch formation: rolling and sliding. Continuation of Figure 3.3 (same images, time lapse). Punctual accumulations (medial plane) and cables of myosin (dorsal view) can be followed throughout the movement of the DF. When the tissue stops rolling, one point/ cable remains at the front. (A) Lines correspond to tracked myosin accumulation (FIJI, manual tracking), as they roll (dark green and red), and slide (light green and purple). Green dot: anchoring point. (B) Transversal actomyosin cables in the DF. Arrowheads point to individual cables, which are rolled under (dark green, red) or lead the sliding phase (light green and purple). (C) Kymograph showing rolling cables. Red dashed line in (A) shows where the kymograph was taken. Scale bars: A: 20μm, B, C: 10μm. See movie 3.4.

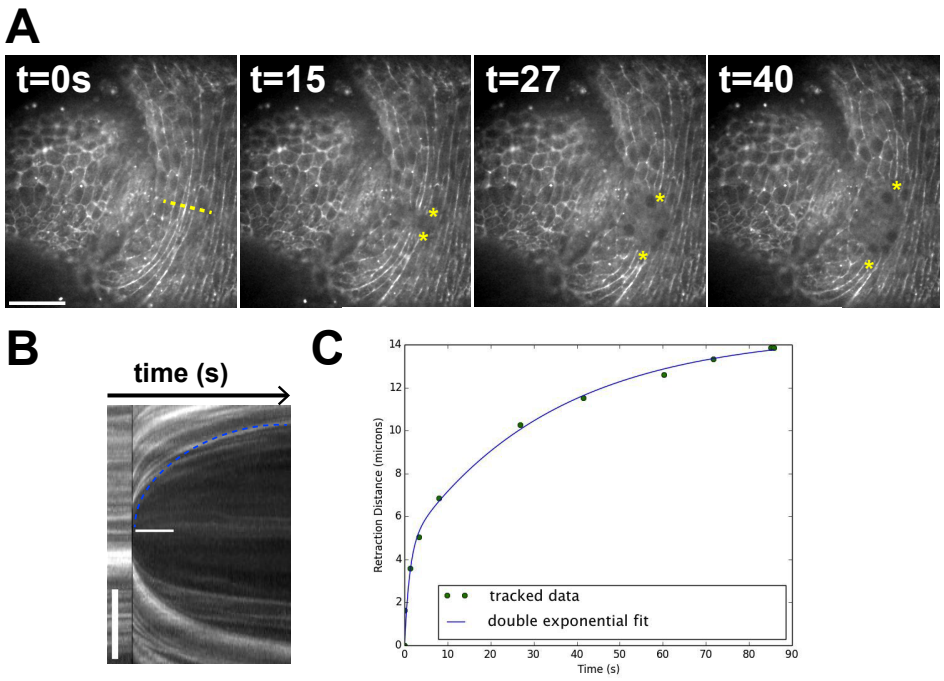

Figure 3.5: **DF actomyosin cables are under tension.** (A) Confocal images, myosin. Yellow dashed line shows the laser cut, about 3 cables wide. Asterisks show tissue retraction. (B) Kymograph from images in (B), taken on a line 30pxl wide, in the direction of the cut. The blue line represents tissue retraction. (C) A typical fit to data obtained in (B), from which we extract the initial retraction velocity. Scale bar: A: 20μm, B vertical: 10μm, horizontal shows time: 20s. For more details of laser ablation experiments and data analysis, please see materials and methods (chapter 5). See movie 3.5.

3.5 Tensile properties of the cable network

Supracellular actomyosin cables can work as local force generators [Röper, 2013]. Myosin-enriched interfaces, which are at the core of cable formation, have been reported to be under higher tension than single interfaces with similar, localized, myosin enrichment [Fernandez-Gonzalez et al., 2009]. In order to assess whether the DF cables are under tension, we performed laser ablation experiments and measured the speed of recoil. The latter is used to estimate the tension stored in the cables. We have found that the cables involved in rolling are under high tension (multiple cables cut: 5μm/s, Fig. 3.6) compared to ablation experiments done on the epidermis leading edge cable during DC (2-6μm/s, personal communication).

To study further the interplay between the parallel actomyosin cables in the DF, we performed an experiment in which we cut only the first two cables, and observed the response in the cables posterior to the cut. We noticed an interesting response: when we cut the first cables (2 cables), we see an immediate response in the cables located posteriorly: they contract, decrease the anteroposterior distance between individual cables and increase myosin concentration (Fig.3.6, black dotted-line box). Under such conditions, the tissue movement is not arrested and the posterior cables become leading cell rows. Next we ablated the "wound response" cables and found that they are also under high tension (3.2μm/s) – although lower than the primary leading cables.

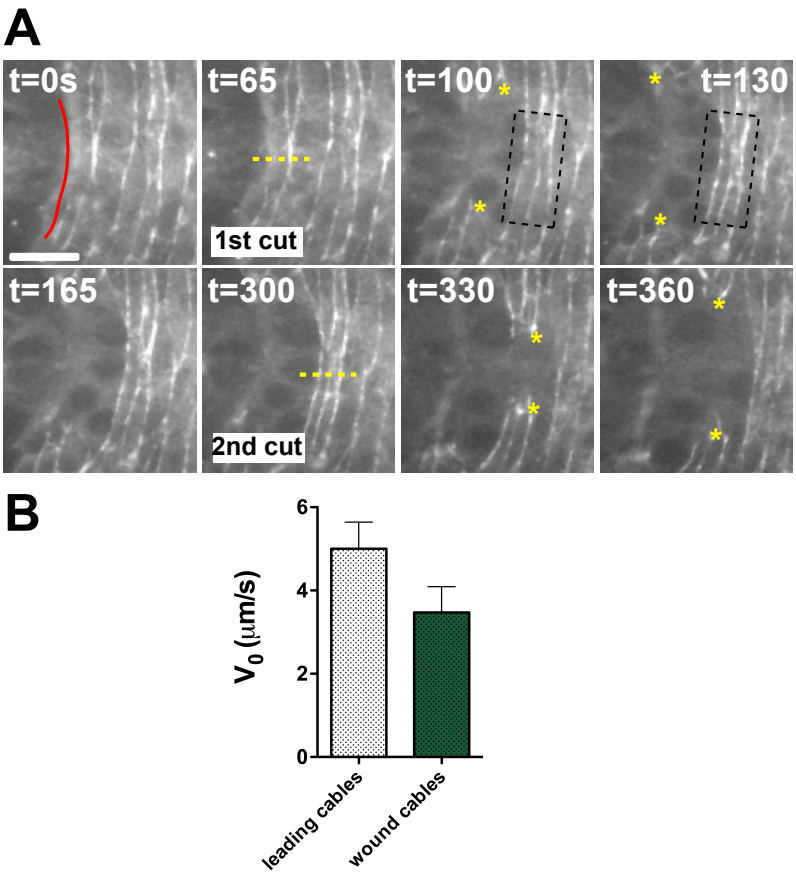

Figure 3.6: **Laser ablation of front row cables results in myosin increase in cables posterior to the cut.** (A) Laser ablation of leading edge cables (red line: LE). Yellow dashed line indicates the cut, asterisks tissue retraction. After the first cut, posterior cables depicted inside of the black dashed box, decrease their A-P distance and increase myosin intensity. The second cut is made on the exposed, posterior cables. (B) Initial retraction velocity for few cables (2) at the leading edge and the wound cables. Scale bar: 10μm. See movie 3.6.

3.6 Leading edge cable

At a certain moment during DF progression (1 hour) we observe a transition from rolling to simultaneous stretching of two epidermal layers, a process we call "sliding" (see Fig. 3.2, 4). One leading edge (LE) cable persists throughout the process of sliding (see Fig. 3.4A) and, in contrast to the earlier phase, does not roll under. It seems that the LE cable is pre-established during rolling, i.e. sliding begins as soon as a specific cable arrives to the front of the tissue.

Dorsally, when we trace this leading edge cable back to when the tissue is rolling; we cannot spot anything unusual about it. In Figure 3.7A we show a slightly more lateral view of the head. The leading edge cable of the sliding phase is clearly visible as a continuous cable located at the most dorsal portion of the gnathal epidermis (Fig. 3.7A, asterisk). If we look carefully, we can observe that this cable undergoes a shape transformation, what seems to be zipping and shortening from the lateral side. The cables located just anterior to it will roll under (Fig. 3.7B, arrows). When the main cable zips from the side and becomes a more circular structure, (Fig. 3.7B, 55min) it arrives at the front of the dorsal epidermis and takes over as the LE cable.

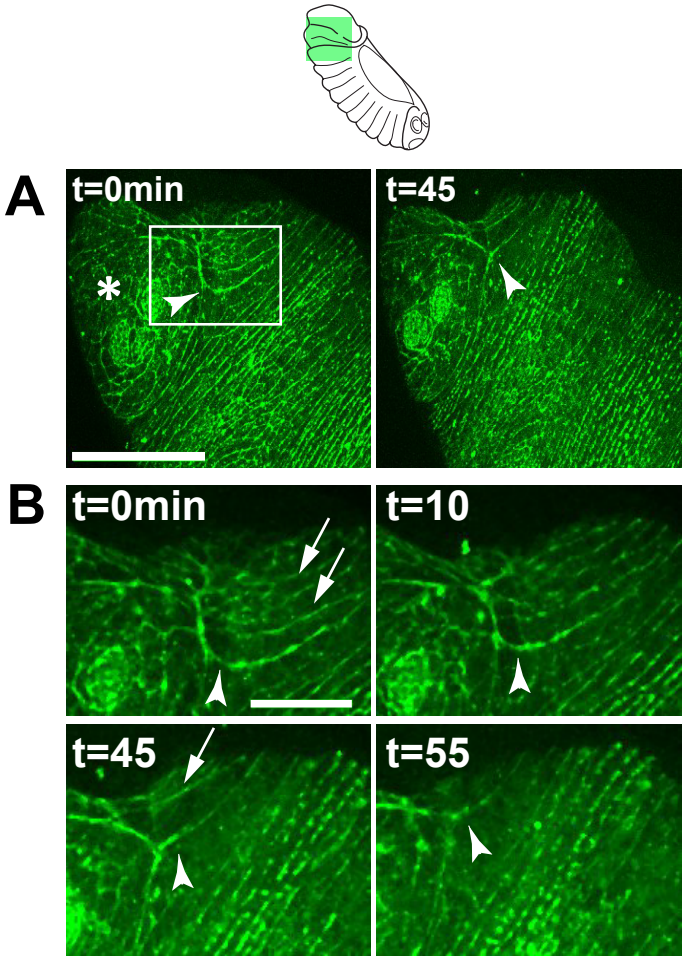

Figure 3.7: **Formation of the LE cable.** It seems to be predetermined which cable is the leading cable during sliding (arrowhead). It undergoes zipping and rounds up as the cables in front roll under themselves. Once it is located at the most anterior tip of the fold, epidermis will begin to slide over the head. Confocal images, lateral view myosin. Scale bar A: 50μm, B: 20μm. See movie 3.7.

3.7 Discussion

3.7.1 Tissue bending

Epithelial folding is a very common morphogenetic process that drives the formation of three-dimensional structures, both in vertebrates and invertebrates [Davidson, 2012]. Folding highly relies on apical cell constriction driven by either the redistribution of myosin [Martin et al., 2010, Sherrard et al., 2010, Roh-Johnson et al., 2012] or by a shift in adherens junction [Wang et al., 2012]. In introduction section 1.1.5 we also mentioned the role of short actomyosin cables observed in neural tubes in chick embryos, just prior to bending [Nishimura et al., 2012]. Recently, a mechanism has been proposed in which cells undergoing apoptosis in a specific pattern exert a pulling force on the tissue. This delamination is combined with appearance of dynamic myosin cables, and ultimately folds the epithelia [Monier et al., 2015].

We have described a novel setting of tissue folding in mature embryonic epithelia: the formation of the DF. We have observed some of the above-mentioned mechanisms, which tissues adapt to fold:

1. increased accumulation of myosin within the fold (Fig. 3.1C)

2. appearance of short myosin cables in the ectoderm located anterior to the folding tissue. See movie 3.8.

3. apoptotic pattern within the procephalic lobe – which corresponds to the area in which we have also observed the short myosin cables. See movie 3.8.

Overall, the interplay of these individual mechanisms, which are commonly studied in isolation, could provide an explanation for the global mechanism of DR bending.

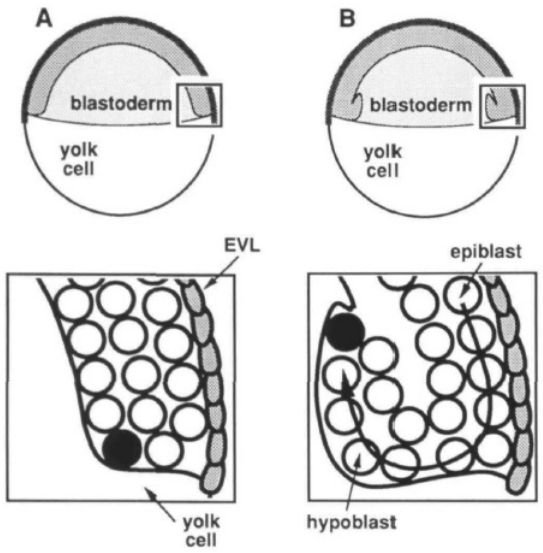

Figure 3.8: **Diagram of blastoderm involution.** (A) Onset of gastrulation. (B) 20min later, blastoderm initiates inward involution. Side views. DEL (deep epithelial layer) located at the blastoderm margin (black) is the first out of involuting cells [Warga and Kimmel, 1990].

The mechanism of tissue rolling is, however, not a very well characterized process of tissue progression. The idea of an epithelial layer rolling inward to form an underlying second layer is well known in developmental biology, but associated only with gastrulating embryos [Keller and Shook, 2011]. Zebrafish or Xenopus embryos are two examples where blastoderm rolls under itself and begins migrating towards the animal pole of the embryo. The mechanism thought to be driving such involution is pushing the cells forward with aid from cell proliferation or by active migration inward [Warga and Kimmel, 1990, Keller, 2006].

The rolling of the DF we describe in this section is a first account of such process in a fully developed epithelium. What makes it particularly interesting is that, in contrast with previously described cases, at the developmental stage of interest there is no cell division in the dorsal

epidermis [Foe and Alberts, 1983], nor cellular protrusions at the leading edge of the rolling tissue (Fig. 3.9).

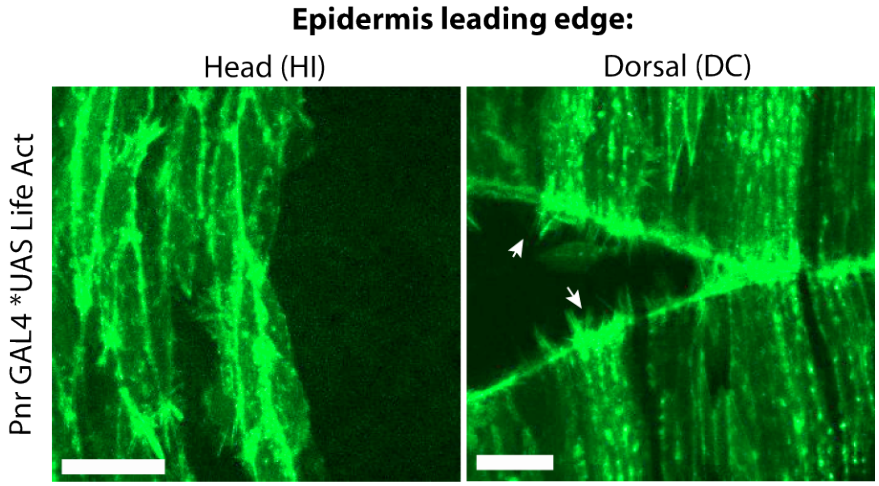

Figure 3.9: **Epidermal LE protrusions are not present during HI.** Comparison of dorsal epidermis progressing over the head (HI), and zipping in the process of DC. Arrows point to actin protrusions, filipodia in two epithelial layers flanking the dorsal opening. Note that actin is also organized in prominent cable like structures in the DF. Confocal images of embryonic epidermis expressing actin GFP. Scale bars 10μm.

The finding that these well characterized, force generating cellular processes are missing in the case of DF suggests that there is an additional mechanism propelling the tissue forward during rolling. We hypothesize that the dynamical assembly of multiple tensile myosin cables in the DF uncovered here underlies a force generating mechanism potentially driving the process.

3.7.2 Rolling with multiple cables: Makisu mechanism

In this work we discovered a very peculiar pattern of actomyosin cables in the DF. This is, to the best of our knowledge, the first case of a tissue with such a multiple, highly organized, assemblage of parallel cables which seem to be involved in one process. The direction of cables perpendicular to the long movement axis, as well as the high tensile properties suggests a mechanical role in fold progression. Cables are formed in the antero-posterior cell junctions, enriching each cell row.

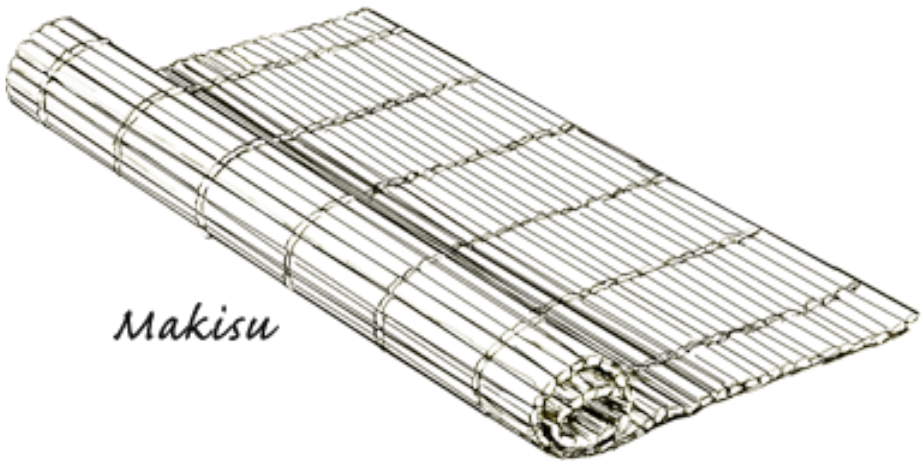

Figure 3.10: **The original Makisu mat.** Bamboo sticks are arranged in parallel, and held by cotton strings (http://www.eastsidesushifilm.com).

One possible interpretation of such organization is that multiple, parallel actomyosin cables play a role in the proper rolling of individual cell rows. In support of this, static cables have been previously shown to maintain boundaries between cellular compartments [Major and Irvine, 2006], add stiffness to tissue and prevent cells from mixing [Monier et al., 2010]. One of the potential explanations for the presence of cables in the DF is that by increasing the stiffness of AP boundaries, cables aid to maintain

cell row size, shape, and prevent cells from mixing. We would like to propose the "Makisu mechanism" of rolling. *Makisu* is a mat woven from parallel bamboo sticks in a sheet held together on the sides by a cotton string. It is commonly used in Japanese cooking, in particular to make rolled sushi: makizushi (Wikipedia).

The bamboo sticks in makisu are arranged in parallel rows, and when the mat is rolled over food, one bamboo stick rolls at a time. In the case of DF, we could imagine that, in order to prevent cell bulging, mispositioning or squeezing, each cell row is enhanced with a cable-and like bamboo sticks, rolls only one at a time. We could speculate that this additional rigidity, organized in cables perpendicular to the movement, could work as a mechanism that controls proper rolling of individual cell rows.

Another important observation is that the DR is anchored to the underlying head, and as more epidermis is zipped at the back in the process of DC, it does not push the entire DF towards the anterior. Instead, the cells which have zipped promote the process, by forcing cells at the front to roll under,resulting in an increase of the AP length of the DF (see Fig. 3.2, steps 2 and 3). This rolling motion lasts until the main; LE cable arrives at the most anterior tip of the progressing tissue, and initiates the sliding phase. LE cable is already pre-established, and it needs to arrive to the LE as a continuous cable. Here is when the Mikasu mechanism could be really useful: controlled rolling, row by row, reassures the correct position and integrity of the LE cable.

3.7.3 Parallel, multiple cables are a novel biological setting for mechanotransduction studies.

The feedback between the cables is a very interesting example of how such actomyosin polarization can govern morphogenesis on a tissue scale. The increase in myosin intensity that we observe after cutting the front cables is different than that observed during a regular wound healing re-

sponse. Myosin recruitment to a wound site is a fairly common process observed in embryogenesis, and it involves immediate myosin enrichment, including assembly of a cable in cells facing the wound [Bement et al., 1999]. However, in the present case we do not observe such directional myosin recruitment. Instead, the cables located behind the cut contract and increase myosin levels in a process that better fits a model of tension response than that of wound healing. The cables posterior to the cut are under high tension; they become the leading edge of the movement taking over the function of the cables that have been ablated.

Given the results presented so far, we speculate that multiple actomyosin cables can function as a network, which provides a support system to the progressing tissue. It is only the self-organized behavior of the whole cable system with ultimately provides the robustness and plasticity to the tissue necessary to complete the morphogenetic process. Multiple cables could only enhance the function of one cable, and operate on tissue scale. The response to laser ablation shows how much strength is added to the system when a structure is repeated throughout the tissue.

We consider that this section contributes to the field by presenting a novel, interesting example of tissue progression and its association with actomyosin organization. Supracellular cables are relatively novel in developmental biology, and many questions as to the molecular events leading to cable formation remain open.

CONCLUSIONS

Chapter 4

CONCLUSIONS

In this thesis we focused on the study of Drosophila head involution, (HI), a virtually unstudied morphogenetic process. Overall, we present five main contributions to the field of developmental biomechanics. 1) We present a detailed description of the morphogenetic processes constituting HI. 2) We report a newly discovered actomyosin structure spanning the length of the whole CNS, and propose a mechanism in which its contraction drives the bending and involution of the brain. 3) We describe a novel mode of rolling progression of the epidermal tissue driven in part by multiple, parallel contractile cables, and refer to it as the "Makisu mechanism". 4) We propose a novel force generating mechanism driving tissue spreading, in which several contractile cables evenly distributed in the epidermis both regulate epithelial progression and establish precise segment size and positioning. Finally, 5) we report a mechanical pattern displayed by the cells in the dorsal epidermis and relate it with the expression of the segment polarity gene hedgehog (hh).

In what follows we briefly summarize the main results supporting these contributions.

The process of HI

We report, for the first time, in vivo imaging data, revealing the dynamic tissue rearrangements during HI. HI consists of dramatic rearrangements of the head during the last stages of embryogenesis (stage 13-17), involving coordinated, simultaneous changes in tissues of different origins. The involution, defined as the ingrowth or inward curling of a group of cells, involves the following steps: 1) the inward movement of the embryonic brain and the procephalic lobe, 2) the partial involution of the head segments through an opening at the anterior pole, and 3) the progression of epidermis over all of the aforementioned structures. As a result of the whole process, the brain and head structures are internalized and become completely covered with epidermis at the end of embryogenesis.

The epidermis is segmented into a repeated pattern of stripes which highly correlates with very well-established genetic expression patterns. Every epidermal segment carries imaginal discs that, throughout the larval stages, grow into specific appendages and organs of the adult fly. The final positioning and size of epidermal compartments is thus very important in establishing the phenotype, as it provides such segmental identity. Based on conclusions from observations of the process under both wildtype as well as mechanically and genetically perturbed conditions, we propose various mechanisms driving the individual steps of HI.

Supracellular actomyosin structure

Throughout the process of HI, we described the dynamics of the brain and the procephalic lobe involution, analyzed the spatiotemporal relation of the brain and surrounding tissues (i.e. the gut), and reported in vivo tissue remodeling by means of apoptosis and cell removal. In these studies, we discovered an actomyosin structure spanning the length of the CNS (the brain and ventral nerve cord). We propose that the contraction of such structure drives the bending and involution of the brain. The process of brain involution, in turn, may be aided by the condensation of the gut towards the center of the embryo via mechanical coupling of the brain

and the gut. Importantly, we found that the brain needs to decrease in size and remodel its shape in order to involute properly. Additionally, the results of these studies provide further support for the argument that morphogenetic cell death is required throughout the entire process of HI. Specifically, by patterning in vivo the apoptotic cells within the head, and by showing precise hemocyte routes in the head, we show that that seems to be the case.

The "Makisu mechanism"

By focusing on the progression of epidermis over the head we show that epidermal progression occurs in two phases. In the first phase, a thin stripe of epidermis on the most dorsal side of the embryo begins moving by first folding over itself, and subsequently rolling in a tank-like motion, forming the dorsal fold and a pouch underneath. In the second phase, the epidermis stretches and slides towards the anterior pole of the embryo continuously until the head is completely covered. This second phase, the sliding process, results in the regular positioning of the epidermal segments along the AP axis of the embryo.

The mode of rolling progression of the epidermal tissue described here is a qualitatively novel mechanism of spreading, shown for the first time in mature epithelia. In the present case, the dorsal fold is attached to the underlying head ectoderm, and is continuous with the dorsal epidermis at the back; the latter is simultaneously being zipped and moving towards the fold. Because of this arrangement, the dorsal tissue coming from the back is rolled under, and the fold enlarges in AP length, as more tissue is zipped in the back. Tissue rolling was previously described in gastrulation; where it is usually powered by active cell migration, or by cell proliferation. Interestingly, these two cellular processes do not occur at the stage we describe. Instead, we observe multiple, parallel contractile cables flanking each cell row in the progressing tissue, and we propose that such structural organization has a key role in controlling the proper rolling of epidermis. To our knowledge, this is the first account of an

arrangement of multiple, parallel cables in an epithelial tissue. We call it the "Makisu mechanism", specifically referring to a model where stiff, cable enriched cell boundaries are placed one under another in a controlled manner; avoiding cell bulging, mixing, or squeezing. Makisu is a mat used in Japanese cooking to prepare sushi rolls. The parallel arrangement of bamboo sticks in the mat reminded us of the parallel actomyosin cables.

Force generation during tissue spreading

We found that the dorsal epidermis rolls under until one of the actomyosin cables arrives at the front; this cable has a peculiar geometry, and throughout the rolling phase it undergoes zipping and significant contraction at the dorsolateral side of the embryo until it reaches the front as a circumferential cable. We propose this cable contraction to be the main driving force of tissue rolling, acting by pushing the cell rows from the back. We refer to this emergent cable as the leading edge cable. We show that by combining circumferential contractility with the embryonic head geometry, the leading cable provides a force for tissue sliding. Additionally, we discovered and report here a connection between the progressing epidermis, driven by the leading edge cable, and the tissue zipping mechanism at the back occurring during dorsal closure. Specifically, we found that although the front cable exerts sufficient force to pull the epidermis, it needs to work in coordination with tissue zipping in order to avoid epidermal overstretching.

However, when we tried to simulate this scenario using a simple biophysical model including only the combination of circumferential contractility and head geometry, we were not able to reproduce the final epidermal patterning. Based on observations in vivo, we showed that, at the end of embryogenesis the epidermal segments have almost identical AP width and that, due to the ovoid geometry of the embryo, the peripheral area of individual segment decreases in a progressive manner from the most anterior segment (T1) towards the posterior (A1). We also

showed that epidermal cell boundaries have higher tension in the AP oriented boundaries relative to that in the DV oriented boundaries, suggesting that contractile forces are oriented perpendicular to the axis of tissue progression. Additionally, each epidermal segment displays a gradient of cell circularity and a gradient of tension, both increasing towards the posterior segment boundary. Such spatial heterogeneity seems to emerge due to the fact that the intersegmental boundaries, which are enhanced with actomyosin cables, display the highest tension, creating a repetitive pattern within the dorsal epidermis. This results in an actomyosin cable at the front, i.e. the leading edge cable, and intersegmental cables, which appear regularly spaced along the AP axis. Interestingly, when including these latter observations in our simple biophysical model, we were able to reproduce equal segment size and positioning. This result suggests that we have uncovered a novel force generating mechanism driving tissue spreading. In this mechanism several contractile cables evenly distributed in the epidermis both regulate epithelial progression and establish precise segment size and positioning

Coordination between morphogen signaling and mechanical patterns

We were able to relate the mechanical pattern of cells in the dorsal epidermis with the expression of a segment polarity gene hedgehog (hh). The gene hh is a morphogen, whose primary described function is to define the segmentation of an organism. For example, in Drosophila it establishes the polarity and cell fate patterning in each epidermal segment. Our results suggest that hh signaling could also be involved in the regulation of contractile forces necessary for proper segment size and positioning along the AP axis of the embryo. We showed that overexpression of hh in the dorsal epidermis results in an impaired pattern of cell circularity and tension. As a result, the tissue displays a homogenous spatial pattern of tension, which also implies a lower tension in the intersegmental boundaries in contrast to the wild-type condition. As a result of the perturbation we also observe less pronounced intersegmental grooves, and disruption in final segment AP width and positioning. These results open

many questions about the role of segment polarity genes in control of segment morphogenesis.

Concluding remarks

Taken together, the four contributions briefly presented above provide an interesting empirical account of a much more general problem in developmental biology: how the interplay between tissue mechanics and molecular signaling orchestrates tissue morphogenesis and patterning.

On the one hand, our work has revealed a novel biological setting, a process in Drosophila embryogenesis which was previously undescribed: the head involution. On the other hand, through an extensive use of state of the art time-lapse microscopy in combination with mechanical, chemical, and genetic pereturbations; we make the case that tissue morphogenesis emerges from the feedback between physical processes and molecular signaling.

Based on the overall picture brought to light with this thesis, we conclude that the arguably "simple" morphogenetic process of Drosophila head involution is a complete model for the study of tissue morphogenesis. We hope that our contributions will motivate new studies at the interphase between biophysics and developmental biology using HI as a model system.

MATERIALS AND METHODS

Chapter 5

5.1 *Drosophila* strains and maintenance

Fly stocks were raised on standard cornmeal medium at 25°C.

- The **brain and head structures** were imaged using Jupiter-GFP, and ELAV-GAL4> UAS-GFP.

- **Apoptosis** was studied using UAS-Apoliner5, which was a gift from J.P. Vincent lab. Apoliner is a fluorescent reporter of caspase activity in live imaging [Bardet et al., 2008]. When apoptotic pathway is not active, Apoliner signal colocalizes RFP and GFP to the membranes. Once the pathway is activated (cleavage of *Drosophila* inhibitor of apoptosis 1- DIAP 1), GFP relocalizes to the nucleus and can be easily distinguished from RFP signal.

- To monitor **hemocyte activity** together with embryonic tissues, the following fly strain was created: srp-GAL4/CyO; sGMCA-GFP/TM3, Ser.

- The imaging of **epidermis** was performed using sqh[Ax3]; sqh-GFP, shg-GFP, ubicadh-GFP#5, sGMCA, EN-GFP (Gift from Marta

Llimargas lab). Additional fly line was created in our lab: Resille tomato/ Ax3 sqh-sqh GFP (Angughali Sumi).

- To manipulate expression in **amnioserosa** ubicadh-GFP/ C381-GAL4>UAS Rac N17 (UAS-Rac1.N17: Bloomington #6292).

- To manipulate expression in **dorsal epidermis** in late stages of embryogenesis (stage 11 onward), pnr-GAL4/TM3ser was used [Fromental-Ramain et al., 2008].

- To affect expression of **Hh and Wg** the following lines were used:
  - * UAS wg (Bloomington #5191)
  - * UAS hh (gift from Perrimon Lab, Harvard Medical School)
  - * UAS HP1
  - * UAS Ptc$^{\Delta loop2}$ (last two were a gift from A. Cassali, IRB Barcelona [Casali and Struhl, 2004].

5.2 Image Acquisition

5.2.1 Embryo collection

Embryos were collected at 25°C using agar plates with instant yeast mixture (Bruggeman) placed in the middle. The embryos were then aged for 16-18h at 18°C, dechorionated in 50% bleach for 2 min, washed with water, and mounted on a glass bottom micro well dish (MatTek). The dish was previously coated with heptane glue. Mounted embryos were then covered with halocarbon oil and imaged at room temperature.

For imaging at the SP5 Upright Confocal microscope the embryos were mounted on a micro well dish laterally and covered with 1% agarose.

The dish was then filled with PBS solution.

For transversal plane imaging at the SP5 Upright Confocal, first a 2% agarose drop was placed inside of a micro well dish, and was let to solidify with a small piece of parafilm on top – creating a flat surface. Then vertical tunnels inside of the agarose bed were formed, and the embryos were put inside of each of the tunnels vertically (anterior pole on top) – we refer to this procedure as "carrot–like mounting". The sample was covered with an additional drop of agarose, and finally, the dish was filled with PBS and imaged using a water- immersion objective.

For SPIM imaging custom mounting plates were generated. Briefly: (1) round cover glass (5mm diameter, 1.5 thickness, Electron Microscopy Sciences) was glued to an end of a glass capillary; (2) the cover glass was then coated with heptane glue; (3) After mounting the embryos, the entire glass was covered with a drop of 1% agarose; and (4) the agarose was glued to one side of the cover glass using super glue.

5.3 Imaging

The dorsal and lateral views of the embryos were generated with either (1) Leica SP5 confocal microscope (Leica DMI 6000), lens: HCX PL APO CS 40x 1.25- 0.75 Oil, or HCX PLAN APO λ blue 63x 1.4- 0.6 Oil; (2) Andor Spinning Disk (Olympus IX81, inverted), lens U plan FLN 40x 1.3 Oil or plan S Apo 60x 1.45 Oil.

The midsagittal views were generated with a custom made SPIM, employing a Hamamatsu Orca-ER camera with a pixel-pitch of 6.45μm, a 63X water immersion objective lens for detection, and a 10X air objective for illumination (REF Huisken , Swoger). The sagittal and transversal views were generated with Leica SP5 Upright (Leica DM 6000 CFS), lens: HCX IRAPO L 25x 0.95 Water.

5.4 Image analysis

All the time-lapses were analyzed using software packages: Fiji, Matlab, Packing Analyzer [Aigouy et al., 2010], and Python.

5.4.1 Cell circularity

The apical cell surface area and perimeters were measured on embryos expressing E-cadh-GFP by manual segmentation of maximum projection using Fiji. Cell circularity, C, was calculated using the following formula:

$$C = 4\pi \left(\frac{A}{P^2} \right). \tag{5.1}$$

Cell circularity maps were generated using automatized segmentation (Packing Analyzer) and a Python script for coloring the cells based on their circularity.

5.4.2 Epidermal segment measurements

The AP length of individual segments was manually measured with Fiji on maximum projections of the dorsal view of Ecadh-GFP expressing embryos along the dorsal midline (Fig. 5.1, h). The position of the micropyle at the anterior pole of the embryo was used as a reference for defining position of the segments (i.e., 0μm).

The first thoracic segment (T1) width was measured from its most anterior tip-visible at the plane depicting the micropyle- to the intersegmental groove (IS) separating it from the T2. The widths of thoracic segments T2, T3 and A1 were measured as the distance between the corresponding IS between them.

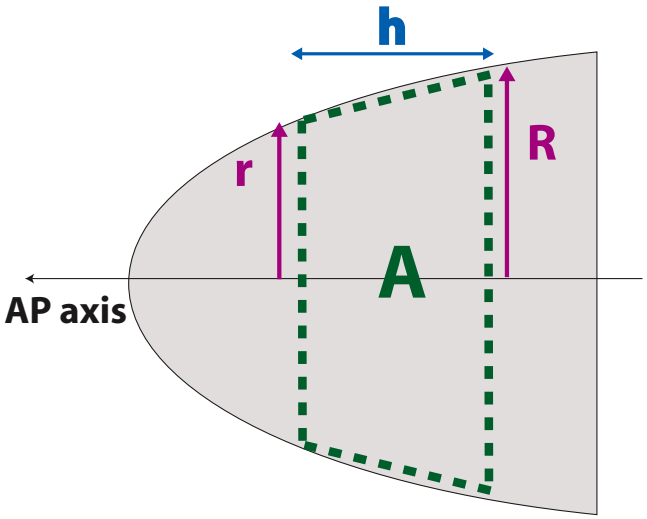

Figure 5.1: **Estimation of segment peripheral area**

Segment peripheral area for a given segment was estimated assuming the segment shape as a frustum of a right circular cone using the following relation:

$$A = \pi(r + R)\sqrt{(R - r)^2 + h^2}, \tag{5.2}$$

where h is the AP length of the segment, R and r are the radius of the embryo along the transverse axis at the posterior and anterior poles of the segment, respectively (Fig. 5.1). The measurements were done on a single plane depicting the micropyle in parallel or perpendicularly to the AP axis.

5.4.3 Quantification of tissue progression

The estimate of position of each segment during the epidermal spreading was achieved by drawing a Kymograph along the AP axis on the dorsal midline of maximum projection timelapses performed on UAS-EN GFP expressing embryos (Fig. 5.2). Each kymograph was generated along a line of 10 pixels width. The coordinates of posterior side of each EN compartment were extracted using a manual segmentation on Fiji and a custom-made routine developed in Matlab.

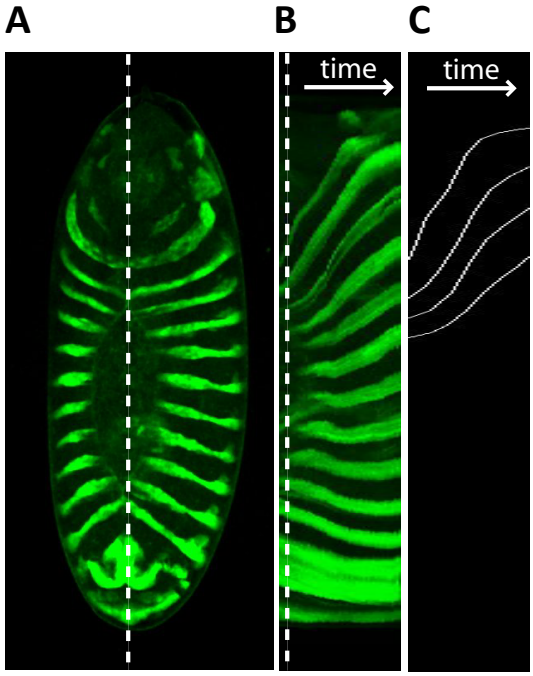

Figure 5.2: **Segment progression.** A: Dorsal view of EN: GFP embryo, stage 14. The dotted line indicates the slice used to generate the Kymograph in B. B: Maximum projection of a 10pxl wide kymograph in time. C: Manual drawing of lines in (B).

Velocity of progression was obtained from the differentiation of coordinates of each EN line and shown either for individual time points or as an average.

5.5 Embryo manipulation

5.5.1 Laser nanosurgery

The laser ablation experiments were performed with two different setups: (1) a scanned 355-nm pulsed (470 ps)-laser (JDS Uniphase, now Teem-Photonics, Grenoble-France) coupled through the epifluorescence port of an AxioVert 200M (Carl Zeiss, Germany) and focused through a Zeiss C-Apochromat 40x /1.2 W lens, and (2) a DPSL- 355/14 pulsed laser (ns) coupled to a spinning disk microscope (DSU Olympus IX81). Imaging rates were about 1-3 images/s in fluorescence. The laser-pulse energy used in the experiments was estimated to be around 200nJ per pulse – after a measurement at the objective flange and including a correction factor for the objective lens absorption at 355nm. For the dissection of the cell-cell junction and acto-myosin cables, initial recoil velocities were measured on a kymograph along the dissected structure. The profile of spatial relaxation was manually extracted from the kymograph and fitted with a single exponential using a Python script. The initial retraction velocity V_0 was calculated from the fitting function $f(t)$ as follows:

$$f(t) = A\left(1 - \exp^{\frac{-t}{\tau}}\right) \tag{5.3}$$

$$V_0 = \frac{A}{\tau} \tag{5.4}$$

Here, A is the retraction amplitude and τ the time constant of the exponential decay.

5.5.2 Pharmacological treatment

Pharmacological inhibitors were injected anteriorly into the previtelline space of embryos at stage 14-16. Rho-kinase inhibitor (Y-27632 dihydrochloride) was injected at 30 mM. Injected solutions were diluted ≈20-fold in the embryo.

5.6 Biophysical modeling

In the following, we will give details regarding the calculations and theoretical concepts presented in Appendix A. We have aimed at simplifying the three dimensional geometry of the embryonic head. When viewing cuts of the head in planes orthogonal to the AP axis, the embryonic head appears circular (see Fig. 5.3A). We have thus assumed the embryonic head to have a rotational symmetry with respect to the AP axis. When considering head geometry as appearing in a saggital plane (see Fig. 5.3B), one finds that the outline of the upper halve of the head is well described by a function of the form

$$r(x) = \sqrt{a^2(L-x)}. \tag{5.5}$$

Here x measures position along the AP axis. Kymographs show that the intersegmental boundary between segment A3 and A4 is relatively static during the course of HI (see Fig. 5.3C). We have thus assumed this boundary to be fixed and consider it as the origin of our coordinate system. In other words, x measures distance from the A3/A4 intersegmental boundary in the AP direction. The total extension of the head along the AP axis is denoted by L. The parameter a sets the height, h, at x=0. More specifically, $h = \sqrt{a^2 L}$. We will refer to r as the *radius* or *radius function*. Rotating the white curve appearing in Fig. 5.3B, generates a paraboloid approximating head geometry. Based on microscopic images, we have chosen $L = 250\mu m$ and $a^2 = 28\mu m$.

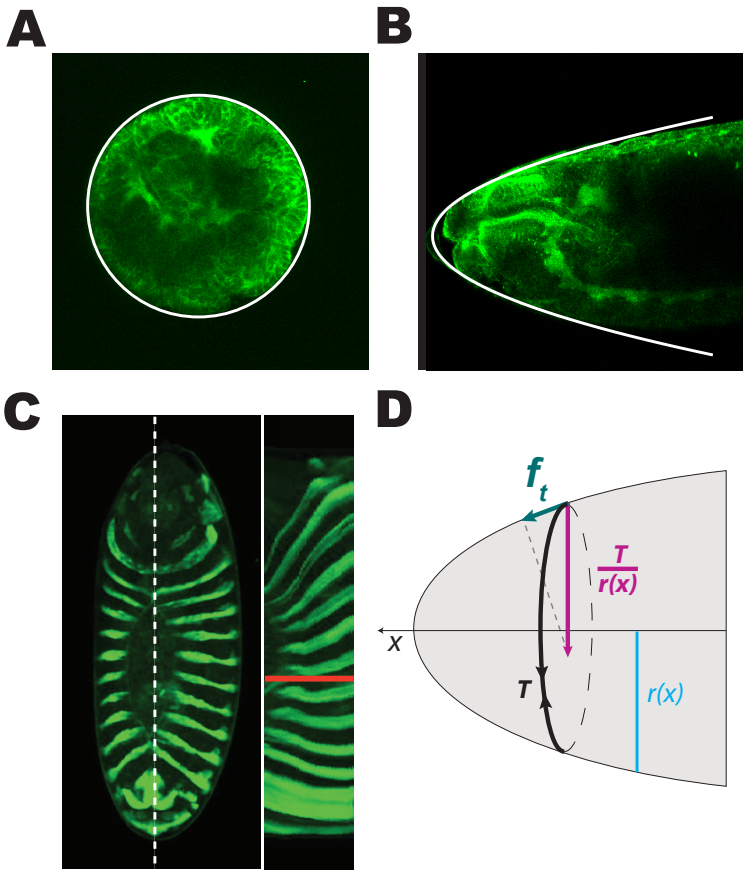

Figure 5.3: **Head geometry and circumferential cables.** (A) In a transversal view, the embryonic head appears to be circular. (B) In a saggital view, head geometry can be approximated by a parabola, whose tip is located at the tip of the head and whose axis of symmetry is parallel to the AP axis. (C) From a kymograph (right panel) taken from the midline in a dorsal view (left panel), we find that the SI between A3 and A4 is almost stationary during HI. (D) From (A) and (B) it follows that head geometry can be approximated by a paraboloid. Tension in circumferential cables (black solid and dashed line) induces an inward directed force density of magnitude T/r(x). Here x measure distance from the A3/A4 segment boundary along the AP axis. A projection of the induced force density onto the tangential direction shows that there is a non-vanishing component, $\mathbf{f_t}$, pointing anteriorly.

Note, the embryonic head appears flat close to $x = 0$. This fact is not reflected by our choice of the radius function r. While an ovoid, i.e. an ellipse rotated about the AP axis, would give a better approximation of head geometry, this choice complicates the analytical calculations presented here. The main conclusions are, however, unaffected by our choice.

A circumferential actomysion cable at a given position x can be visualized as a circle on the surface of the paraboloid, running orthogonal to the AP axis (see Fig. 5.3D). When only one of the rotated head slices is considered, it will appear as a single point on the graph of r. Reminding the reader of the assumed rotational symmetry, we will in the following consider the latter representation. A line tension, T, generated by an actomyosin mediated active contraction, will act in parallel with the cable. Due to the circular geometry, it gives rise to a force density, $\mathbf{f_a}$, acting orthogonally to the AP axis, pointing towards the interior of the embryo. According to the law of Laplace, the magnitude of this force density, f_a, is proportional to the active tension T and inversely proportional to the radius $r(x)$, i.e.

$$f_a(x) = \frac{T}{r(x)}. \tag{5.6}$$

Due to the change in r along the AP axis, $\mathbf{f_a}$ for each x has a nonzero tangential component, $\mathbf{f_t}$, with magnitude

$$f_t(x) = \frac{T}{r(x)} \frac{r'(x)}{\sqrt{1 + r'(x)^2}}. \tag{5.7}$$

Here, the prime denotes a derivative with respect to x.

In order to discuss the final width of segments when HI is complete, we consider the epidermis as an elastic material that is moved over the surface of the paraboloid used in approximating head geometry. As the height of the epidermis is small compared to the radius r, we will, more

specifically, consider it to be a two-dimensional sheet. The elastic properties of such a material are captured by two parameters, its bulk modulus, E, and its shear modulus, G. Due to frequent intercalation events occurring within the epidermis, shear stresses are likely to equilibrate on time scales much shorter than time-scales associated to epidermal movements during HI (data not shown). We have thus assumed that $G = 0$. As noted before, the intersegmental boundary between segments A2 and A3 remains almost stationary during HI. We have thus considerd only the mechanics of the segments anterior to this boundary. After all the segments up to this boundary are fused, the epidermis can be viewed as a closed hull enclosing the head. We will furthermore neglect differences in movement along the circumference of the embryo and assume that the position of epidermis is rotationally symmetric in that sense. The mechanic problem thus reduces to one dimension only. Instead of solving the full continuum problem, we have opted for a discretized approach. More specifically, we consider the epidermis as represented by a set of discrete nodes, $p_1, \ldots, p_n$, where each two nodes can be thought of as being separated by the same number of cell rows (see Fig. 5.5A). One choice is to consider these nodes to coincide with the intersegmental boundaries. In the following, we will be interested in finding the final position $x(p_i)$ of these nodes when HI is complete, i.e. when the epidermal layer has been fully pulled over the head.

After HI is complete, the nodes p_i will be distributed along the radius function in a manner such that all forces within the system equilibrate. We are considering interactions mediated by the tissue between the respective nodes to be elastic, ignoring the effect of shear stresses. This interaction thus leads to a force density, $\mathbf{f_i}$, acting on each node p_i, with magnitude

$$f_i = K\left((A_0 - A_{i-1}) - (A_0 - A_i)\right)\mathbf{t_i}. \tag{5.8}$$

Here, K can be thought of as an effective spring constant, depending on the bulk modulus, E, of the epidermis. By A_i we denote the surface area on the paraboloid, delimited by circumferential circles at the positions p_i and p_{i+1}. More precisely, we have

$$
\begin{aligned}
A_i &= 2\pi \int_{x(p_i)}^{x(p_{i+1})} r(x)\sqrt{1+r'(x)}\,dx \\
&= \frac{1}{6}a\pi\left((4L+a^2-4x(p_1))^{3/2}-(4L+a^2-4x(p_2))^{3/2}\right).
\end{aligned}
$$

The area A_0 denotes a preferred area of the piece of epidermis delimited between two points and is assumed to be the same for all sections. The vector $\mathbf{t_i}$ denotes the normalized tangential vector to the radius function at position $x(p_i)$., i.e.

$$
\mathbf{t_i} = \frac{1}{\sqrt{1+r'(x_i)^2}}\begin{pmatrix} 1 \\ r'(x_i) \end{pmatrix} \tag{5.9}
$$

In addition to elastic interactions, when considering intersegmental contractile cables, an active force density $\mathbf{f_t}$ will act on the nodes (see above). In equilibrium, all forces at each node have to sum up to zero, i.e.

$$
\mathbf{f_t}(\mathbf{x}(\mathbf{p_i})) + \mathbf{f_i} = \mathbf{0}. \tag{5.10}
$$

Let us now assume, the leading edge cable would be the only force generator in the system. We will consider the nodes p_i to denote the positions of the intersegmental boundaries between the segments A4-T1, i.e we will consider the positions of 7 nodes, p_1 to p_7. As described earlier, we assume p_1 to be static, i.e to be fixed at $x = 0$. Head involution being complete, i.e. the leading edge having arrived to the very anterior of the head, implies that $x(p_7) = L$. When plotting normalized segment surface area and average cell area as a function of segment number, one sees that they follow the same trend along the AP axis. We take this as an argument that the number of cells within each segment is the same for all segments. As a consequence, we assume that A_0, i.e. the preferred segmental area is equal, too.

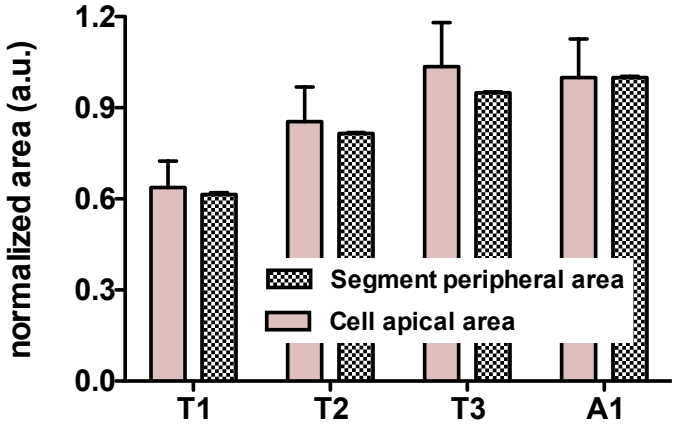

Figure 5.4: **Average cell apical and segmental peripheral area.** For the four anterior segments, A1-T1, we have quantified both the average apical cell area and the segmental peripheral area. When plotting values normalized to the average values obtained for A4, one finds that both measures vary in a similar fashion when moving anteriorly. This indicates that the number of cells is the same for each segment. We therefore assume each segment to have the same preferred area A0.

To determine the final state, we now need to solve the 5 coupled equations

$$\mathbf{f_t}(\mathbf{x}(\mathbf{p_i})) + \mathbf{f_i} = \mathbf{0}, \quad i = 2, 3, 4, 5, 6. \tag{5.11}$$

In the case, where no additional forces to the leading edge are acting within the system, this reduces to solving

$$(\mathbf{A_i} - \mathbf{A_{i-1}}) = \mathbf{0}, \quad i = 2, 3, 4, 5, 6, \tag{5.12}$$

i.e. to a situation in which all enclosed surface areas are the same (see Fig. 5.5B), independent of the value of the stiffness K. When considering the case of intersegmental boundaries being equipped with actomyosin

cables, which are under a tension T, we have to resort to solve (5.11) numerically. In order to check whether our conclusion also holds within the presence of a tension gradient, we have considered a system of interconnected nodes as discussed above, however have added 4 additional nodes between each pair of the nodes corresponding to intersegmental boundaries. Intermediate nodes are assumed to be separated by a similar number of cell rows. We have therefore, as above, chosen the value of A_0 to be the same for each resulting portion of epidermis. We have adjusted tensions in proportion to the tension values measured in laser cut experiments (see Fig. 6 in Appendix A).

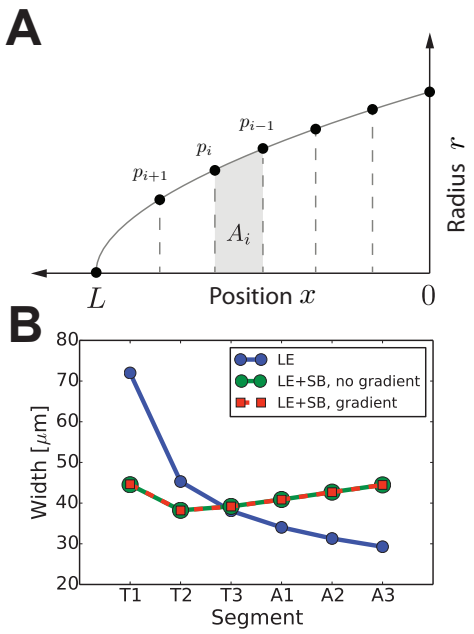

Figure 5.5: **Elastic sheet model of segment positioning.** (A) We have considered the first 6 segments of epidermis to be represented by a thin elastic sheet that is covering the embryonic head, approximated as a paraboloid. As for the rotational symmetry, only one slice of the paraboloid needs to be considered. Discretizing the mechanic problem, we consider only the positions, p_i, of nodes at the intersegmental boundaries. Interactions between these nodes is assumed to be elastic and is effectively described by a springlike interaction (K, spring constant). Note, here it is differences in segmental areas (not distances between nodes) that scale the resulting coupling force density. (B) Assuming HI to be complete, we have investigated final segment width in three cases: i) no additional forces at IS boundaries, (ii) additional cables at SI boundaries with a tension T, (iii) a tension gradient in each segment (additional nodes were added in this case), proportional to the one observed *in vivo*. While for (i), segment widths are very different, in the case of (ii) and (iii) they are almost equal. For the results in B, the following numerical parameters were used: $L = 250$, $a^2 = 28$; (LE) $n = 7$ nodes, $x(p_1) = 0$, $x(p_7) = L$; (LE+SI, nogradient) $n = 7$ nodes, $x(p_1) = 0$, $x(p_7) = L$, $K = 1.0$, $T = 220.25$ (on each node); (LE+SI, gradient) $n = 25$ nodes, $x(p_1) = 0$, $x(p_25) = L$, $K = 5.0$, $T = 25.3875, 33.85, 42.3125, 50.775, 67.7$ (repeated each 5 nodes).

Appendix A

PATTERNED CONTRACTILE FORCES PROMOTE EPIDERMAL SPREADING AND REGULATE SEGMENT POSITIONING DURING *DROSOPHILA* HEAD INVOLUTION

Patterned contractile forces promote epidermal spreading and regulate segment positioning during *Drosophila* head involution

Natalia D. Czerniak, Kai Dierkes, Arturo D'Angelo, Jim Swoger, Julien Colombelli, Jérôme Solon

CRG, Barcelona, Spain

Abstract

Control of spatial positioning of cells during epithelial rearrangement is fundamental for proper animal development. Here, we show that the spreading of the epidermis during *Drosophila* head involution is spatially controlled, resulting in evenly positioned segments along the AP axis. We show that the propelling forces are generated by a contractile actomyosin cable at the leading edge of the epidermis. In addition, we found that each individual segment displays a gradient in tensile forces along the AP axis. This gradient of tension originates from the contractile properties of the epidermis and can be modulated by hh signaling. Suppression of this gradient by overexpressing hh leads to a final mispositioning of the epidermal segments. With a physical description of the epidermis, we show that patterned tensile forces along a spreading tissue can generate propelling forces and can control the final segment position. Our study unravels a mechanism by which patterned tensile forces regulate spreading and positioning of epithelial tissues.

Keywords: *Drosophila* embryogenesis, Morphogenesis, Head involution, Supracellular cable, Biomechanical forces

Preprint in preparation for Current Biology *April 29, 2015*

1. Introduction

Epithelial spreading is a fundamental mode of tissue rearrangement occurring during animal development and wound closure. In many cases, it is associated with the collective migration of cells, inducing a reorganization of the involved tissue by pulling on their neighbors [1, 2]. An alternative-spreading mechanism is used during wound healing: in this case, a contractile ring forms at the leading edge, promoting the spreading of the epithelium [3]. More recently, it has been shown that during zebrafish gastrulation, additional actomyosin flows act as a friction based motor, providing forces for moving the enveloping cell layer over the yolk cell [4, 3].

During the process of head involution (HI), taking place in late Drosophila embryonic development, the epidermis spreads anteriorly to envelope the head tissues and fully covers the embryo [5]. Spreading occurs concurrently with the sealing of two epidermal halves on the dorsal side of the embryo during dorsal closure [6]. These two processes, tissue fusion and spreading, result in the final positioning of the epidermal segments that will give rise to the different organs of the fly [7]. Even though the mechanisms underlying the sealing of the epidermis are identified [8, 9, 10], the mechanisms driving the epidermal spreading and regulating the final segment position are still not understood.

Here, we perform a quantitative analysis of tissue spreading during head involution. We show that the spreading of the epidermis is spatially controlled along the AP axis, resulting in regularly positioned segments of equal

width. Our results indicate that similarly to zebrafish epiboly an actomyosin cable forms at the leading edge and, because of the ovoid shape of the embryo, generates a tangential force powering anterior movement of the epidermis. Additional contractile forces distributed along the epidermis are required for proper epidermal spreading and final segments positioning. Indeed, each epidermal segment shows an inhomogeneity in cell shape correlating from a gradient in tension along the AP axis. Inhibition of contractility with Rho-kinase inhibitor suppresses the gradient in tension as well as cell shape inhomogeneity within epidermal segments and blocks the progression of the epidermis and prevents correct epidermal positioning. Misregulation of tension within the epidermis and consequent impairment of spreading and final segment positioning is also observed when over expressing hedgehog signaling in the epidermis. This suggests a regulation of the tensile properties of the epidermis by hedgehog activity.

Finally, within the framework of a physical description of the process, we show that distributed tensile cables along the epidermis can generate propelling forces and promote an even segment distribution. Our study identifies a novel spreading mechanisms by which several contractile forces evenly distributed in the epidermis regulate epithelial spreading and precise segmental positioning. Our results point towards a regulation of these contractile forces by segmental polarity genes, therefore suggesting a coupling between segment organization and morphogenetic rearrangement leading to segment positioning.

2. Results

2.1. Homogeneous epidermal spreading leads to evenly distributed segments during HI

We first asked how the spatial organization of the segmented epidermis would reorganize during spreading in HI. We first show epidermal progression at the anterior pole of the embryo, combining a dorsal and lateral view, starting when the tissue is sliding with a discrete cell row at the leading edge (LE). Expressing GFP with the engrailed promoter (UAS-GFP En-Gal4), allows us to follow the progression of the LE of the tissue [11], as well as of the posterior compartment of each one of its segments (Fig. 1A, movie A.1).

The lateral imaging shows two distinct modes of spreading: (i) at first, the dorsal epidermis tilts dorsally towards the anterior while the ventral epidermis remains static, (ii) once the segments are orthogonal to the AP axis, the entire tissue progresses in this configuration towards the anterior pole of the embryo (Fig. 1A, movie A.1). We have quantified the time course of progression of individual segments by tracking posterior segments boundaries on the dorsal side of the embryo (Fig. 1B). After individual segments are fused successively due to zipping, their progression appears homogeneous with an approximately constant velocity for each individual segment, varying from 1μm/min for the LE to 0.4μm for the segment T3 (Fig. 1B and 2A).

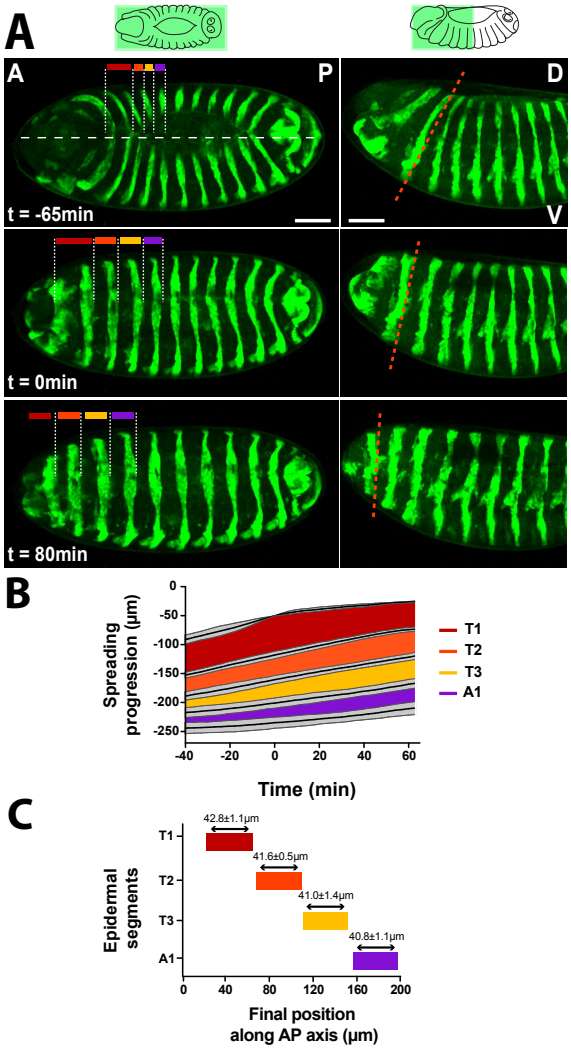

Figure 1: **Epidermal spreading during HI leads to evenly spaced segments.**

Figure 1 **Epidermal spreading during HI leads to evenly spaced segments.** (A) Time lapse showing the dorsal (left) and lateral view (right) of epidermal spreading kinetics during HI on embryos expressing EnGal4>UAS GFP. At the onset of the process ($t = -65min$), the dorsal epidermis progresses while the ventral remains immobile. After 60 min, when the segments are orthogonal to the AP axis, both dorsal and ventral epidermis progress towards the anterior pole. The colored dashed lines on the dorsal view show the posterior boundary of three thoracic segments (T1-T3) and first abdominal segment (A1). The red dashed line on the lateral view highlights the dorsoventral tilt of anterior segments occurring at the onset of the process. Scale bars: 50μm. (B) Graph showing the progression in time of each individual segments during HI (see Materials and Methods in main text). (C) Graph showing the final positioning of segments T1-A1 along the AP axis (measured on the dorsal midline) at the end of HI. The AP width of the four segments is almost equal.

During the progression, the width of individual segments is converging towards a similar value (Fig. 2A). Eventually, this progression leads to a remarkable regular segment positioning along the AP axis, and the final AP segment width is constant for all of the anterior segments (T1- A1, Fig. 2C). In the following, we investigate the mechanisms at the origin of force generation during the epidermal spreading.

2.2. Tissue spreading during HI associates with enrichment in myosin at the leading edge

We identified two sequential modes of progression: 1) the epidermal movement is initiated by a rolling of the epidermal dorsal fold over itself towards the anterior of the embryo. Analysis of cell displacement shows a succession of leading cells, in a movement similar to a caterpillar track. The epidermis continues spreading by sliding over the head tissues until complete covering of the embryo (see movie 3.4). Our analysis shows that during the latter phase of progression, the linear arrangement of cells remains constant. Neither of the two modes is associated with the appearance of cellular protrusions, such as lamelipodia or filopodia (see Fig. 3.9 in main text). This suggests that cells are not actively crawling towards the anterior pole but that the movement is powered by an alternative mechanism. The sagittal sections showed successive accumulation of myosin at the tip of the leading cells during the first transient epidermal rolling and further stable myosin enrichment during the sliding of the tissue, which corresponds to supracellular actomyosin cables.

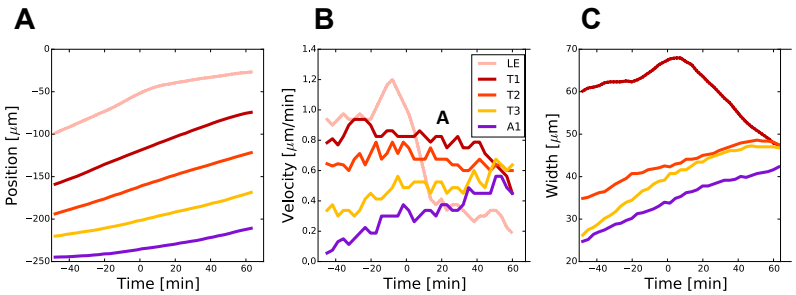

Figure 2: **Final width of segments T1-A1.** (A) Segment progression in time, obtained by following the LE (salmon) or posterior EN expressing domain. (B) Velocity of progression of T1-A1 obtained from central differences of traces shown in A. (C) The width of progressing segments in time (see Materials and Methods in main text).

2.3. The mechanical tension generated by the actomyosin cable promotes the epidermal spreading

In order to assess whether the leading cable generates contractile forces contributing to the progression of the epidermis during HI, we have used laser microsurgery to probe the tension generated by the cable. We compared the initial retraction velocity of the LE cable to epidermal cellular junctions in, parallel to the LE (see Fig. 3B-D). The measured velocity was four times higher within the LE cable than within other cell junctions in the epidermis and remains approximately constant during the entire process (see Fig. 3E). This suggests that the tension generated by the cable could be essential for the spreading of epidermis.

Theoretical considerations show that a contractile band at the LE surrounding an embryo with an ovoid shape could, in principle, promote move-

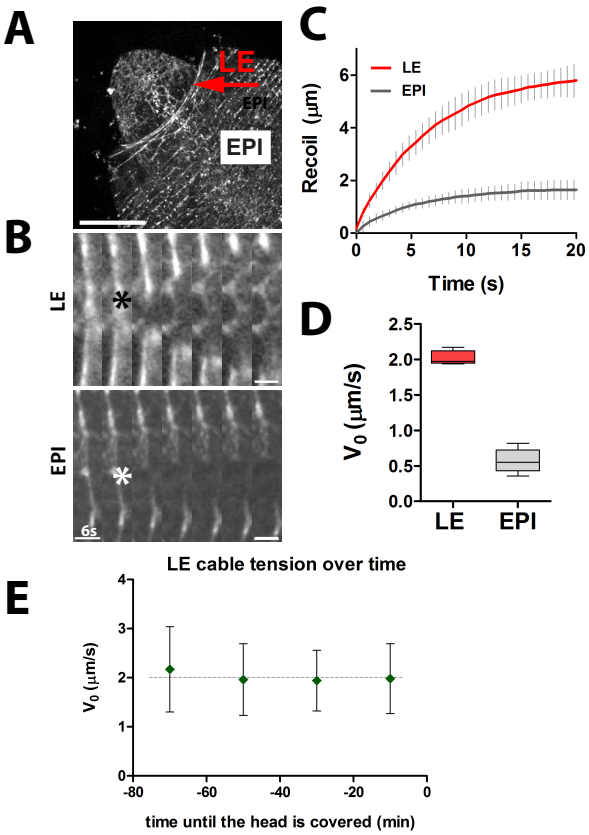

Figure 3: **Mechanical tension generated by the LE cable.** (A) Image of myosin expressing embryo, indicating where laser dissections were performed, i.e. either at the LE (leading edge cable, red arrow) or EPI (epidermal AP junctions). (B) Time lapses showing the spatial relaxation after dissection of the LE actomyosin cable (Top, LE), and a cell junction in the epidermis (Bottom, EPI). (C) Tissue recoil following the cut. (D) Average initial retraction velocity after laser dissection of the LE cable and junctions in the epidermis. (E) Average initial recoil velocity of LE measured over time.

ment in the direction of the slope of the ovoid, due to the tangential component of the contractile force [4, 12]. To test whether the cable tension was promoting the tissue progression, repeated ablations of the cable were performed on individual embryos approximately every 30 seconds, to avoid the cable recovery, over the time course of 5min. This procedure resulted in a temporal arrest of the progression of the epidermis, indicating that the contractile tension in the LE cable and its integrity are necessary for the epidermal progression (Fig. 4A).

To further probe whether the force generated by the LE is sufficient to drive movement of the epidermis, we aimed at uncoupling epidermal spreading from tissue release during DC. By a tissue specific expression of a dominant negative form of Rac (Rac-N17) in the amnioserosa (AS) tissue covering the dorsal gap, we impair DC and epidermal fusion resulting from the zipping (Fig. 4B) [13]. We observe that the epidermal spreading still proceeds, however, compared to WT embryos, the AP length of the epidermal segments increases: the fused epidermis covers the head tissues exhibiting an overstretching of T1 and T2 (Fig. 4B). This indicates that the forces generated by the LE are sufficient to pull on and spread the epidermis. All together, these results suggest the following picture: a pulling force exerted by the LE powers the process of epidermal spreading during HI in coordination with the fusion and release of tissue during DC at the back.

However, this simple picture fails to explain two experimental observations: (i) after the first segment arrives at the anterior pole (making the

LE ineffective as a force generator), the other segments are still progressing anteriorly for about 40-60 minutes. (Fig. 4B) (ii) While continuous LE cable dissection arrests LE progression, the progression of posterior SB is not affected (Fig. 4A). These two observations show the involvement of additional forces within the process.

2.4. A gradient of mechanical tension is present within individual epidermal segments

In order to determine the presence of additional forces promoting the epidermal spreading, we have performed additional time-lapse imaging of E-cadherin-GFP expressing embryos, capturing the progression in the dorsal, as well as lateral and ventral thoracic segments during the last 60 min of spreading, i.e. after the leading edge has arrived at the anterior pole. At the end of the process, the apical surface of epidermal cells shows a stereotypic pattern with elongated cells at the anterior of each segment and more squared-like cells at the posterior (Fig. 5A). We have also observed that, in general, the cells are packed in the epithelium in a highly organized manner: the AP cell boundaries are mostly oriented perpendicularly to long body axis (AP), and are all roughly parallel.

In order to check whether this spatial organization has any tensile forces distribution, we performed laser dissection of individual cell junctions, and compared those oriented in AP and DV direction. We observe a strong anisotropy of tension, with a three times higher retraction velocity of AP junctions compared to DV junctions (Fig. 5B-C). This indicates that epidermal tension is oriented orthogonally to the movement of the epidermis,

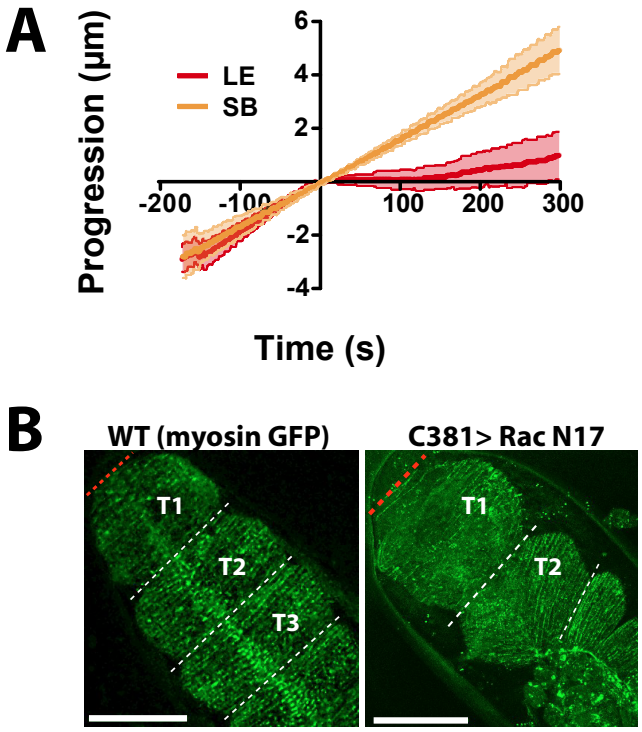

Figure 4: **LE exerts a pulling force on the epidermis.** (A) The average displacement of the LE (red) and of the most anterior intersegmental boundary (SB, orange). Successive laser ablations of the LE are performed after t=0min. The progression of the LE spreading is arrested, indicating that the contractile forces generated by the LE cable are necessary for epidermal progression. At the same time, the SB progression is not impaired by LE arrest. (B) Dorsal epidermis after tissue spreading in WT embryos expressing actin GFP, and in embryos expressing a dominant negative form of Rac in the amnioserosa tissue (C381 GAL4¿ UAS Rac N17). The T1 and T2 segments are overstretched in the embryo with blocked zipping, suggesting that forces generated by the LE cable are sufficient to pull on and stretch the epidermal layer. Scale bars: 50μm.

suggesting that, similarly to the LE cable, the epidermis could generate additional forces promoting tissue movement.

This inhomogeneity in cell shape within segments has previously been reported in the ventral epidermis, due to existence of denticle belts [14, 15]. We extracted the contour of each individual cell and calculated the circularity of the apical cell surface (Fig. 6A-C WT).The circularity gives an estimate of anisotropy in shape, and we observed a gradient in average cell circularity established along the AP axis of each thoracic segment (Fig. 5 and 6A-C). The cells located in the anterior (2nd row posterior to SB) are preferentially elongated along the dorsoventral axis (DV), with a circularity comprised between 0.1 and 0.3. In contrast, cells located in the posterior of each segment display a more isotropic shape with circularity between 0.6 and 0.8. Additionally, we measured the initial retraction velocity after dissection of AP cell-cell junctions depending on the position of the cell within each segments along the AP axis, and found a strong correlation. We observed a gradient of tension with low AP junctions tension at the anterior compartment and higher AP junctions tension in the posterior compartment of each segment (Fig. 6D).

A maximum of tension is detected in the junctions of para-, and segmental boundaries, with a retraction velocity of 0,8μm/s in average, while a minimum of tension is detected in the most elongated cells, with a retraction velocity of 0,3μm/s. The observed maximum in tension corresponds to region with local enrichment in myosin, forming supracellular cables at the

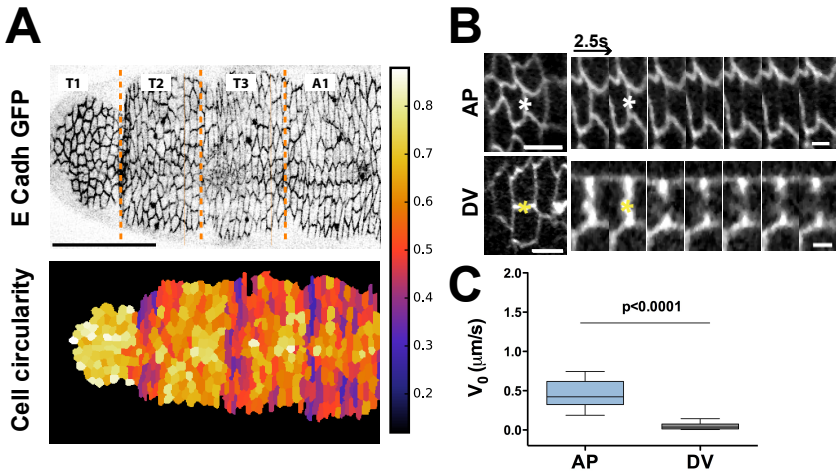

Figure 5: **Cell shape and tension in the dorsal epidermis.**(A) Dorsal epidermis (T1-A1), Ecadh-GFP (upper panel) and the corresponding segmentation of individual cells (bottom panel) colored according to cell circularity (see Materials and Methods in main text). Cells at the anterior of each segment are elongated along the transverse axis; cells at the posterior are more roundish. Additionally, a gradient of cell circularity is observed within each segment. (B) Time lapse images showing the spatial relaxation kinetics after laser dissection of an AP (top) and DV epidermal junction (bottom). (C) Initial retraction velocity of AP and DV epidermal junctions. The difference in initial velocities clearly indicates an asymmetry of tension in the epidermis, with AP junctions being under higher tension than DV junctions.

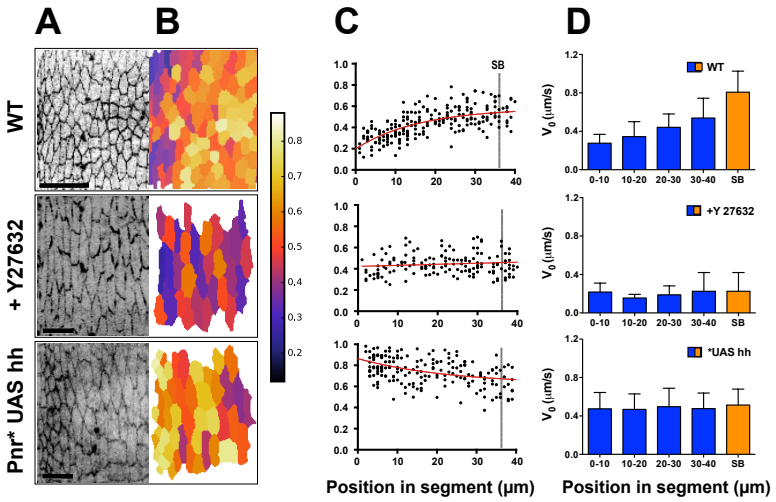

Figure 6: **Gradient of cell morphology and tension within epidermal segments.** In all panels, data is shown for WT, injected with Rho-kinase inhibitor (+Y27632), and hedgehog ectopic expression driven by pnr GAL4 (Pnr*UAS hh). (A) Images of dorsal view of T1, from A-P segment boundary, E-cadherin-GFP. Scale bars: 15μm, UAS hh: 10μm. (B) Manual segmentation of images in A, colored according to cell circularity. (C) Average cell circularity as a function of intrasegmental position along the AP length of T1-T3. Position 0 refers to the 2nd cell row in each segment. Note, due to this choice, the most anterior cell row has positions between 35-40μm. SB: segment boundary (dashed line). We see a gradient of circularity in the WT. It is abolished both in injected and hh expressing embryos. Injected embryos have lower overall circularity. Ectopic hh expression results in increased circularity, particularly evident at the anterior of the segment. (D) Initial retraction velocity of single AP boundaries along the segment, grouped in 10μm wide bins. Orange bars: junctions in cells flanking the SB. We observe a tension gradient in WT embryos, similar to the circularity gradient: anterior, elongated cells have lower tension, than the posterior, round cells. In injected embryos, tension, as well as circularity is overall much lower and homogenous. In hh overexpression, tension is homogenous. Also, in the SB flanking cells retraction velocity is overall lower than WT embryos, suggesting a lower tension.

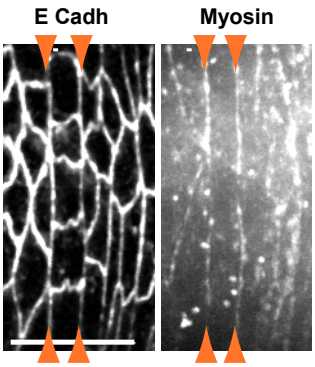

Figure 7: **Myosin cables accumulate at the SB in dorsal epidermis.** Image of SB region between T1 and T2, E-cadherin (left) and myosin (right). Arrows are pointing to the most anterior cell row (groove cell, SB: left arrow of each pair), where we observe a transition in cell morphology from round to elongated cells. Circumferential myosin cables localize on both sides of this cell row to the AP junctions, forming supracellular cables surrounding the embryo (both dorsal, lateral and ventral epidermis). Scale bar: 20μm.

segment boundaries (both para-, and segmental boundaries) (Fig. 7). Cables have been reported in *Drosophila* ventral epidermis at the parasegmental boundary, between the domains of wingless and hedgehog expression. They are believed to prevent cell mixing between neighboring compartments [16].

All together, our results indicate a pattern of mechanical properties of cells within each individual segment. A gradient of tension is present within each segment, with high AP junctional tension in the posterior cells and a much lower AP junctional tension in the cells located at the anterior of each segments.

2.5. The tension gradient within epidermal segments promotes epidermal progression

To investigate whether the observed gradient of tension results from actomyosin contractility at the apical site of the epidermal cells, we have locally injected the Rho-kinase inhibitor Y-27632 at the anterior pole of embryos expressing E-cadherin-GFP (see Materials and Methods in main text). In these conditions, we observed a major slow-down of tissue progression confirming that actomyosin contractility at the LE is required for the spreading to occur (Fig. 8). Interestingly, the progression of epidermal segment boundaries is also strongly impaired; indicating that contractility of the LE, and within the epidermis is required for the progression leading to the final segment positioning (Fig. 8).

Additionally, Rho-kinase inhibition also totally disrupts the AP pattern in apical cell surfaces within each individual segments (Fig. 6C, Y27632). We do not observe the AP gradient in cell circularity, the cells are more elongated consistently with a decrease in contractility (Fig. 6A-C, Y27632). Laser dissection experiments reveal that the junctional tension in these conditions is lower than in the WT and homogeneous along the AP axis (Fig. 6D, Y27632). All together, these results indicate that actomyosin contractility is generating the observed gradient of tension within the epidermis and promotes epidermal progression.

2.6. Modulation of tensile properties of epidermal cells by hh signaling

Epidermal segments are compartmentalized along the AP axis, and governed by expression of different signaling molecules, such as wingless or

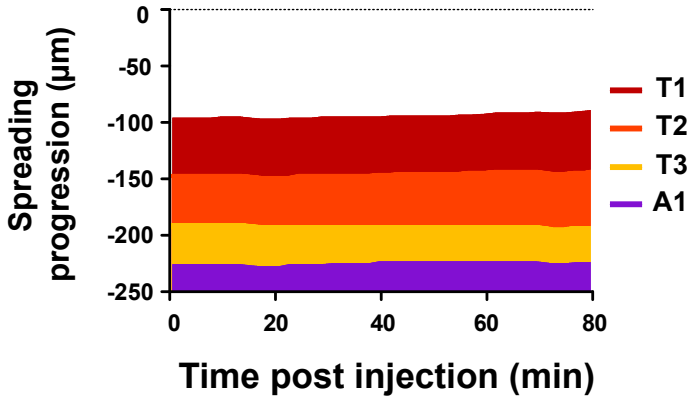

Figure 8: **Progression of epidermal segments as a function of time after injection with Rho-kinase inhibitor**Progression of epidermal segments as a function of time after injection with Rho-kinase inhibitor (see Materials and Methods in main text). The progression of segments T1-A1 is arrested and correct positioning impaired (see Fig. 1B).

hedgehog. It has been previously shown that hedgehog signaling can promote cell shape remodeling by the regulation of myosin levels [17]. Therefore, we wondered whether hh mediated signaling could affect the observed patterning in mechanical properties and the epidermal spreading. To test it, we first down-regulated hh signaling by expressing inactive form of the hh receptor patched UAS PtcΔloop2 (unable to bind hh) on the dorsal side of the epidermis with the Pnr Gal4 driver (Fig. 9C). Because Pnr is expressed only at late stage of embryogenesis (stage 13 onward), affecting hh signaling does not impair early epidermal patterning and developmental processes[18].

In such conditions, we observed a mild phenotype with epidermal cells that are slightly less elongated along the DV axis. To verify that hh could affect epidermal cell morphology, we then overexpressed hh signaling with the Pnr-Gal4 driver by two means: directly expressing hh with UAS-hh (Fig. 6, UAS hh) or expressing an active form of the receptor Ptc HP1 (Fig. 9B). In both cases, we observed the disruption of the gradient of circularity along the AP axis. Cells appear more round in average, suggesting higher apical contractility. The SB are less pronounced (Fig. 10) consistently with previous observations on the maintenance of segmental boundaries [19, 16].

Laser dissection experiments of individual cell junctions confirm that the tension is more homogenous along the AP axis, with a retraction velocity of 0.5μm/s in average (Fig. 6D). This suggests that the observed changes in circularity are a consequence of a variation in apical cell surface tension, as higher cortical tension leads to round apical surfaces. The tension of the

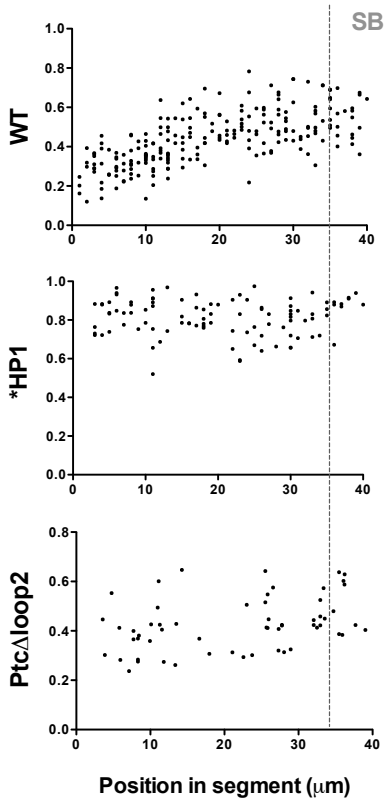

Figure 9: **Modulation of hh signaling results in altered cell circularity.** (A-C) Average cell circularity as a function of position within segments T1-T3. (A) WT (B-C) expression of UAS Hp1 and UAS Ptc Δloop2, respectively, driven with Pnr GAL4. (B) The active form of receptor Ptc-HP1 results in overall higher cell circularity, and a homogenous pattern. (C) Down regulation of hh activity with Ptc Δloop2 results in a less pronounced gradient of circularity.

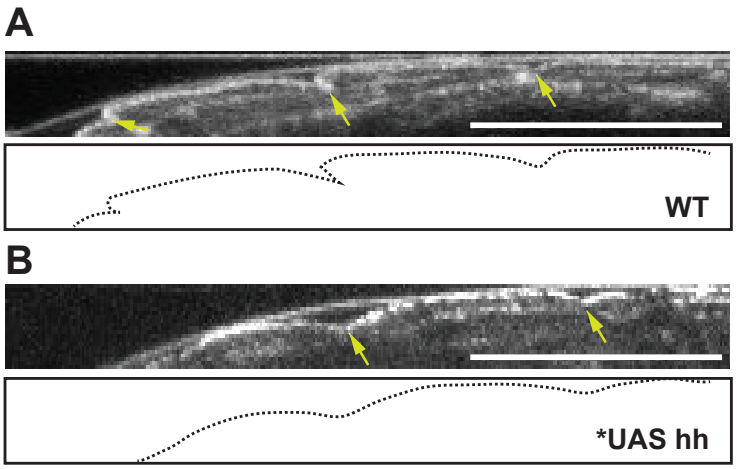

Figure 10: **Intersegmental grooves are less pronounced in hh overexpressing embryos.** (A-B) Midsagittal view of the most dorsal anterior epidermis, E-Cadh GFP (upper panel). Scale bars: 50μm. Drawing of the outline of dorsal epidermis showing the depths of intersegmental grooves (yellow arrows, lower panel) (A) Note the deep grooves in WT embryo (B) Embryo expressing UAS hh under Pnr GAL4 driver shows less pronounced grooves. Segment width and positioning along the AP axis is also inferred.

intersegmental boundaries is significantly lower than in WT (Fig. 6D). Overexpression of hh in the dorsal epidermis therefore suppresses the gradient of apical cortical cell tension and cell circularity observed within individual segments and the peak of tension at the SB.

The final width and positioning of the epidermal segments are also altered in hh overexpressing embryos. In contrast with the WT, we observe a progressive decrease in segments width, from the anterior to posterior (Fig. 11C). A geometrical estimation of the area of each segment shows that the area of

hh overexpressing embryos is now constant in the AP axis (Fig 11.D). Similar ectopic overexpression of wg, on the contrary did not show any particular phenotype in apical cell surface morphology or final segment positioning (data not shown). This indicates that wg in contrast with hh is not directly involved in the regulation of the cell mechanics in the epidermis.

All together, our results show that hh signaling modulates the mechanical properties of cells within the epidermis. Overexpression of hh signaling under pnr GAL4 driver suppresses the segment mechanical pattern and leads to less pronounced intersegmental grooves. The suppression of this pattern leads to mispositioning of the segments along the AP axis (Fig. 11).

2.7. Spreading and final epidermis positioning is reproduced in silico with patterned contractile forces

In this section, we describe in more physical terms how circumferential cables can provide driving forces for the observed tissue progression. The proposed mechanism has been discussed previously with regard to a tension based motor involved during epiboly [4] and the stabilization of the cytokinetic furrow during cell division of fission yeast [12]. We assume that the embryonic can be simplified and described by a paraboloid (Fig. 12), which means that the radius r decreases as we move towards the anterior along the AP axis. The tension stored in circumferential cables induces a force density pointing towards the interior of the embryo; the force magnitude according to the law of Laplace is given by $T/r(x)$. This combined with the embryonic shape supports a simple geometric argument, where the force density has a component $\mathbf{f_t}(\mathbf{x})$ into the tangential direction.

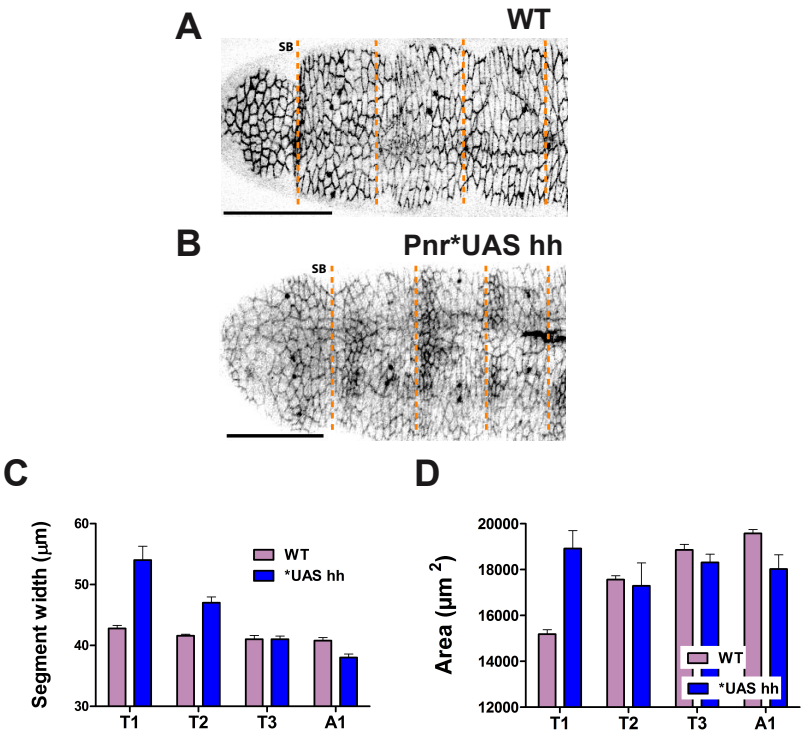

Figure 11: **Final segment width and positioning is disrupted by ectopic hh expression.** (A-B) Images of dorsal epidermis (T1-A1), E-cadherin GFP. Dashed lines: SB, scale bars: 50μm (A) Segments T1-A1 show almost equal width. (B) Overexpression of hh disrupts the segmental pattern, width varies in between the segments, quantified in C. (C) Average width of T1-A1 compared between WT and hh embryos. hh overexpression results in segments width decreasing from T1 (54μm) to A1 (38μm). (D) Average peripheral segment area compared between WT and hh embryos. hh overexpression segment area is homogenous between T1-A1, and we do not observe the increase in peripheral area typical for WT embryos (see Materials and Methods in main text) .

Note that $\mathbf{f_t}$ points anteriorly and it is precisely this tangential component, which, by acting towards the anterior tip of the embryo, can act as the driving force of tissue progression during HI. We want to stress, f_t would vanish in the case of a constant radius r. In other words, on the surface of a cylindrical embryo, circumferential contractile cables would not be effective in driving tissue progression. The described mechanism can be viewed as depending both on active tension in the cable and the geometry of the embryonic head.

In theory, a contractile LE under sufficient tension would be able to pull the entire epidermis over the embryonic head (see Fig. 4). However, we have showed that the LE cable alone does not explain the final embryonic pattern, i.e. segment size and positioning. We thus asked about the role of additional cables oriented along the transversal axis of the embryo, both within the segment, and at the SB. In the following, we will present results obtained within the framework of a simple physical description of epidermal mechanics. In particular, we show that additional force generators are needed to ensure the correct final positioning and width of the epidermal segments.

For simplicity, we consider the epidermis behaving as an elastic sheet, which can be described by bulk and shear modulus. Note, we neglect shear stress due to frequent intercalations occurring in the dorsal epidermis (personal communication). In Figure 12, we consider only the SB, represented as nodes p_i on the radius function r and we assume each segment to have the

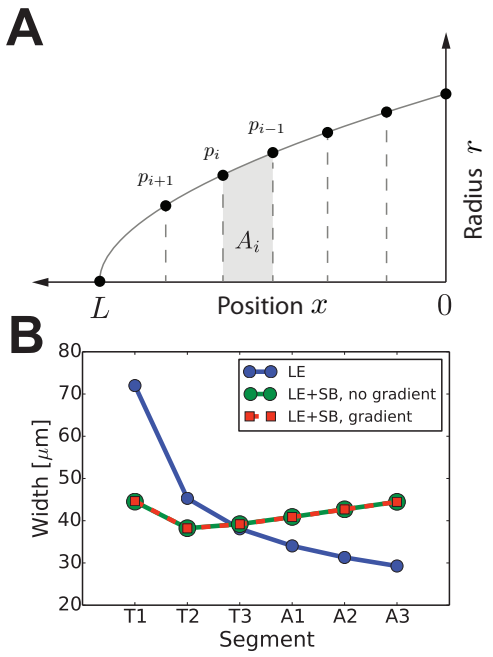

Figure 12: **Elastic sheet model of segment positioning.** (A) We have considered the first 6 segments of epidermis to be represented by a thin elastic sheet that is covering the embryonic head, approximated as a paraboloid. As for the rotational symmetry, only one slice of the paraboloid needs to be considered. Discretizing the mechanic problem, we consider only the positions, p_i, of nodes at the intersegmental boundaries. Interactions between these nodes is assumed to be elastic and is effectively described by a springlike interaction (K, spring constant). Note, here it is differences in segmental areas (not distances between nodes) that scale the resulting coupling force density. (B) Assuming HI to be complete, we have investigated final segment width in three cases: i) no additional forces at IS boundaries, (ii) additional cables at SI boundaries with a tension T, (iii) a tension gradient in each segment (additional nodes were added in this case), proportional to the one observed *in vivo*. While for (i), segment widths are very different, in the case of (ii) and (iii) they are almost equal.

same preferred area A_0. Such assumption is justified by the observation that average cell area and segment peripheral area increase in a similar fashion, i.e. cell number in each segment seems constant (see Fig. 11D and Materials and Methods in main text).Elastic interactions within epidermis lead to a force density $\mathbf{f_i}$, acting on each node p_i, with magnitude

$$f_i = K\left((A_0 - A_{i-1}) - (A_0 - A_i)\right)\mathbf{t_i}. \tag{1}$$

Here K is a stiffness related to the bulk modulus of the material and $\mathbf{t_i}$ is a normalized tangential vector at p_i. We also assume that at the end of HI all forces are balanced, i.e.

$$\mathbf{f_t}(\mathbf{x}(\mathbf{p_i})) + \mathbf{f_i} = \mathbf{0}. \tag{2}$$

If only an active LE cable is required for the proper HI progression the result would be

$$(\mathbf{A_i} - \mathbf{A_{i-1}}) = \mathbf{0}, \quad i = 2, 3, 4, 5, 6, \tag{3}$$

,

i.e. all segments would end up with identical peripheral area. If this was the case, the AP widths of all segments would have to be different, which is not the case (see Fig. 1C). This is due to the ovoid geometry of the embryonic head, where the radius decreases towards the anterior tip (see Fig. 12). On the other hand, when assuming all SB are under a tension T and adjusting T appropriately, we are able to reproduce the segment width. The same is true when we consider the gradient of tension within segments (see Fig. 6).

In summary, we believe the arguments discussed in this section give credibility to the following view on the role of circumferential tensile cables in the process of HI: 1) circumferential tension in combination with the ovoid geometry of the embryonic head provides the driving force for epidermal spreading, and 2) while a LE cable could in principle be sufficient to drive such progression, additional force generators are needed in order to achieve a correct final segment width and positioning. For more details on the biophysical model, see Materials and Methods in main text.

So far, we have only considered the final state, i.e. the position of epidermis on the embryonic head at the end of HI. It will be interesting to investigate whether our simple description can also capture the dynamics of HI as observed *in vivo*. Several issues would have to be taken under consideration. As the balance of forces is influenced by head geometry, a more correct representation of head shape is desirable. Additionally, tissue progression is likely to be influenced by the time-course of tissue fusion events during DC. Here, we have concentrated on the final stage of HI and could thus neglect this effect. When sliding over the head, the epidermis would be subject to friction with the underlying embryonic ectoderm. In order to account for HI dynamics, a proper description of friction would be necessary.

3. Discussion

In this study, we identify the mechanisms promoting epidermal spreading and regulating segment positioning during drosophila HI. We show that evenly distributed contractile forces are at the origin of the spreading and

positioning of epidermal segments during HI. Similar to zebrafish epiboly, an acto-myosin cable forms at the leading edge of the progressing epithelium and generates contractile forces that, because of the ovoid shape of the embryo, contractile forces that, combined with the ovoid geometry of the embryo, result in generate propelling forces. Additional regulation of the epidermal spreading is performed by tensile forces distributed along the epidermis.

The *Drosophila* epidermis is segmented at this stage of development; segment polarity genes are sequentially expressed along the AP axis defining the different segments boundaries. We found that contractile properties of the apical surface of the cell are is also patterned. A gradient of mechanical tension is present within each individual segment and allows positioning of the segments along the AP axis of the embryo. We have also reported that the highest mechanical tension is at the para-, and intersegmental boundaries, where cell AP junctions are enhanced with actomyosin cables.

Interestingly, affecting hh signaling impairs the pattern of mechanical tension in the epidermis. A primer role of hh is to define the segmentation of the organism [20]. However, recent works have identified that hh signaling also influences morphogenesis by acting on cell contractility. For instance, hh signaling is required for the formation of the epidermal grooves [21], for the invagination of the eye morphogenetic furrow [17] or for the maintenance of boundaries in the wing disk [19]. Our results suggest that hh signaling could also be involved in the regulation of contractile forces necessary for proper segment positioning along the AP axis of the embryo.

References

[1] P. Friedl, D. Gilmour, Collective cell migration in morphogenesis, regeneration and cancer, Nature reviews Molecular cell biology 10 (2009) 445–457.

[2] S. R. K. Vedula, A. Ravasio, C. T. Lim, B. Ladoux, Collective cell migration: a mechanistic perspective, Physiology 28 (2013) 370–379.

[3] D. P. Kiehart, Wound healing: the power of the purse string, Current biology 9 (1999) R602–R605.

[4] M. Behrndt, G. Salbreux, P. Campinho, R. Hauschild, F. Oswald, J. Roensch, S. W. Grill, C.-P. Heisenberg, Forces driving epithelial spreading in zebrafish gastrulation, Science 338 (2012) 257–260.

[5] R. Finkelstein, N. Perrimon, The molecular genetics of head development in drosophila melanogaster, Development 112 (1991) 899–912.

[6] A. VanHook, A. Letsou, Head involution in drosophila: genetic and morphogenetic connections to dorsal closure, Developmental Dynamics 237 (2008) 28–38.

[7] J. A. Campos-Ortega, V. Hartenstein, The embryonic development of drosophilae melanogaster (1997).

[8] J. D. Franke, R. A. Montague, D. P. Kiehart, Nonmuscle myosin ii generates forces that transmit tension and drive contraction in multiple tissues during dorsal closure, Current biology 15 (2005) 2208–2221.

[9] M. S. Hutson, Y. Tokutake, M.-S. Chang, J. W. Bloor, S. Venakides, D. P. Kiehart, G. S. Edwards, Forces for morphogenesis investigated with laser microsurgery and quantitative modeling, Science 300 (2003) 145–149.

[10] F. Jankovics, D. Brunner, Transiently reorganized microtubules are essential for zippering during dorsal closure in drosophila melanogaster, Developmental cell 11 (2006) 375–385.

[11] B. T. Rogers, T. C. Kaufman, Structure of the insect head as revealed by the en protein pattern in developing embryos, Development 122 (1996) 3419–3432.

[12] M. Mishra, Y. Huang, P. Srivastava, R. Srinivasan, M. Sevugan, R. Shlomovitz, N. Gov, M. Rao, M. Balasubramanian, Cylindrical cellular geometry ensures fidelity of division site placement in fission yeast, Journal of cell science 125 (2012) 3850–3857.

[13] S. Woolner, A. Jacinto, P. Martin, The small gtpase rac plays multiple roles in epithelial sheet fusiondynamic studies of drosophila dorsal closure, Developmental biology 282 (2005) 163–173.

[14] S. A. Dilks, S. DiNardo, Non-cell-autonomous control of denticle diversity in the drosophila embryo, Development 137 (2010) 1395–1404.

[15] M. H. Price, D. M. Roberts, B. M. McCartney, E. Jezuit, M. Peifer, Cytoskeletal dynamics and cell signaling during planar polarity establishment in the drosophila embryonic denticle, Journal of cell science 119 (2006) 403–415.

[16] B. Monier, A. Pélissier-Monier, A. H. Brand, B. Sanson, An actomyosin-based barrier inhibits cell mixing at compartmental boundaries in drosophila embryos, Nature cell biology 12 (2010) 60–65.

[17] D. Corrigall, R. F. Walther, L. Rodriguez, P. Fichelson, F. Pichaud, Hedgehog signaling is a principal inducer of myosin-ii-driven cell ingression in drosophila epithelia, Developmental cell 13 (2007) 730–742.

[18] A. Ducuing, B. Mollereau, J. D. Axelrod, S. Vincent, Absolute requirement of cholesterol binding for hedgehog gradient formation in drosophila, Biology open 2 (2013) 596–604.

[19] K. P. Landsberg, R. Farhadifar, J. Ranft, D. Umetsu, T. J. Widmann, T. Bittig, A. Said, F. Jülicher, C. Dahmann, Increased cell bond tension governs cell sorting at the drosophila anteroposterior compartment boundary, Current Biology 19 (2009) 1950–1955.

[20] T. Tabata, S. Eaton, T. Kornberg, The drosophila hedgehog gene is expressed specifically in posterior compartment cells and is a target of engrailed regulation, Genes and Development 6 (1992) 2635–2635.

[21] C. W. Larsen, E. Hirst, C. Alexandre, J.-P. Vincent, Segment boundary formation in drosophila embryos, Development 130 (2003) 5625–5635.

Appendix B

FIGURE: PATTERNING OF DORSAL EPIDERMIS

Patterning of dorsal epidermis at the end of embryogenesis

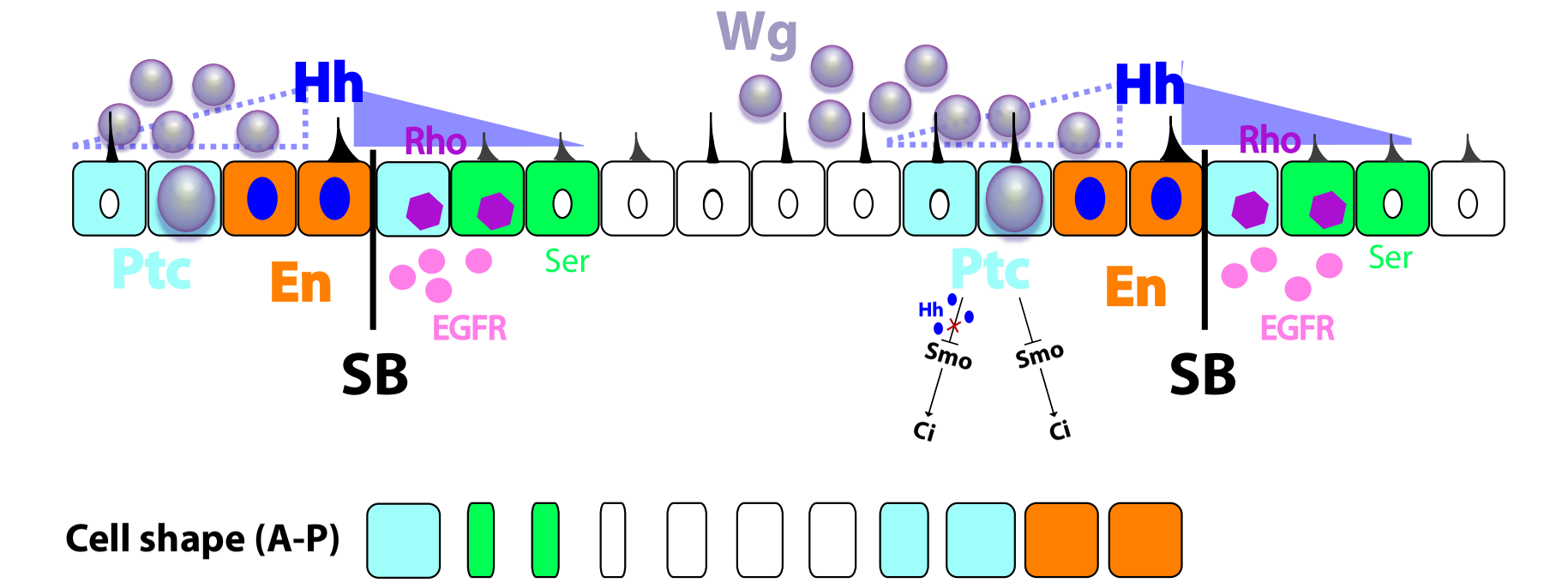

Gathered from:
Heemskerk, Dinardo 1994
Bokor, Dinardo1996
Sanson 2001
Chanut, Delalande 2006
Briscoe, Therond 2013

Appendix C

LIST OF ABBREVIATIONS

A1-A3	abdominal segments (first-third)
AMC	antenomaxillary complex
AP	anteroposterior axis
AS	amnioserosa
ATP	adenosine triphosphate
BC	brain commissure
CenBr	central brain
CL	clypeolabrum
CNS	central nervous system
CPS	cephalopharyngeal skeleton
DC	dorsal closure
DF	dorsal fold
Dpp	decapentaplegic
DR	dorsal ridge
DV	dorsoventral axis
ECM	extracellular matrix
EGF	epidermal growth factor
ELAV	embryonic lethal abnormal vision
EN	engrailed
EPI	epidermis
FG	foregut
FGF	fibroblast growth factor
GFP	green fluorescent protein
GS	gnathal segments
Hh	hedgehog
HI	head involution
LE	leading edge
LH	left hemisphere
MG	midgut
P	procephalon
PCP	planar cell polarity
PH	pharynx
PLB	procephalic lobe
Pnr	pannier
PS	parasegmental boundary
Ptc	patched
RH	right brain hemisphere
SB	segmental boundary
TI	thoracic segment (first)
VNC	ventral nerve cord
Wg	wingless

Bibliography

[Abbott and Lengyel, 1991] Abbott, M. K. and Lengyel, J. A. (1991). Embryonic head involution and rotation of male terminalia require the drosophila locus head involution defective. *Genetics*, 129(3):783–789.

[Aegerter-Wilmsen et al., 2007] Aegerter-Wilmsen, T., Aegerter, C. M., Hafen, E., and Basler, K. (2007). Model for the regulation of size in the wing imaginal disc of drosophila. *Mechanisms of development*, 124(4):318–326.

[Aigouy et al., 2010] Aigouy, B., Farhadifar, R., Staple, D. B., Sagner, A., Röper, J.-C., Jülicher, F., and Eaton, S. (2010). Cell flow reorients the axis of planar polarity in the wing epithelium of drosophila. *Cell*, 142(5):773–786.

[Aman and Piotrowski, 2008] Aman, A. and Piotrowski, T. (2008). Wnt/β-catenin and fgf signaling control collective cell migration by restricting chemokine receptor expression. *Developmental cell*, 15(5):749–761.

[Backouche et al., 2006] Backouche, F., Haviv, L., Groswasser, D., and Bernheim-Groswasser, A. (2006). Active gels: dynamics of patterning and self-organization. *Physical biology*, 3(4):264.

[Bardet et al., 2008] Bardet, P.-L., Kolahgar, G., Mynett, A., Miguel-Aliaga, I., Briscoe, J., Meier, P., and Vincent, J.-P. (2008). A fluorescent reporter of caspase activity for live imaging. *Proceedings of the National Academy of Sciences*, 105(37):13901–13905.

[Behrndt et al., 2012] Behrndt, M., Salbreux, G., Campinho, P., Hauschild, R., Oswald, F., Roensch, J., Grill, S. W., and Heisenberg, C.-P. (2012). Forces driving epithelial spreading in zebrafish gastrulation. *Science*, 338(6104):257–260.

[Bement et al., 1999] Bement, W. M., Mandato, C. A., and Kirsch, M. N. (1999). Wound-induced assembly and closure of an actomyosin purse string in xenopus oocytes. *Current biology*, 9(11):579–587.

[Bendix et al., 2008] Bendix, P. M., Koenderink, G. H., Cuvelier, D., Dogic, Z., Koeleman, B. N., Brieher, W. M., Field, C. M., Mahadevan, L., and Weitz, D. A. (2008). A quantitative analysis of contractility in active cytoskeletal protein networks. *Biophysical journal*, 94(8):3126–3136.

[Berger et al., 2007] Berger, C., Renner, S., Lüer, K., and Technau, G. M. (2007). The commonly used marker elav is transiently expressed in neuroblasts and glial cells in the drosophila embryonic cns. *Developmental dynamics*, 236(12):3562–3568.

[Bertet et al., 2004] Bertet, C., Sulak, L., and Lecuit, T. (2004). Myosin-dependent junction remodelling controls planar cell intercalation and axis elongation. *Nature*, 429(6992):667–671.

[Biersmith et al., 2011] Biersmith, B., Liu, Z., Bauman, K., and Geisbrecht, E. R. (2011). The dock protein sponge binds to elmo and functions in drosophila embryonic cns development. *PloS one*, 6(1):e16120.

[Blankenship et al., 2006] Blankenship, J. T., Backovic, S. T., Sanny, J. S., Weitz, O., and Zallen, J. A. (2006). Multicellular rosette formation links planar cell polarity to tissue morphogenesis. *Developmental cell*, 11(4):459–470.

[Bokor and DiNardo, 1996] Bokor, P. and DiNardo, S. (1996). The roles of hedgehog, wingless and lines in patterning the dorsal epidermis in drosophila. *Development*, 122(4):1083–1092.

[Bosveld et al., 2012] Bosveld, F., Bonnet, I., Guirao, B., Tlili, S., Wang, Z., Petitalot, A., Marchand, R., Bardet, P.-L., Marcq, P., Graner, F., et al. (2012). Mechanical control of morphogenesis by fat/dachsous/four-jointed planar cell polarity pathway. *Science*, 336(6082):724–727.

[Butler et al., 2009] Butler, L. C., Blanchard, G. B., Kabla, A. J., Lawrence, N. J., Welchman, D. P., Mahadevan, L., Adams, R. J., and Sanson, B. (2009). Cell shape changes indicate a role for extrinsic tensile forces in drosophila germ-band extension. *Nature Cell Biology*, 11(7):859–864.

[Calzolari et al., 2014] Calzolari, S., Terriente, J., and Pujades, C. (2014). Cell segregation in the vertebrate hindbrain relies on actomyosin cables located at the interhombomeric boundaries. *The EMBO journal*, 33(7):686–701.

[Campos-Ortega and Hartenstein, 1997] Campos-Ortega, J. A. and Hartenstein, V. (1997). The embryonic development of drosophilae melanogaster.

[Casali and Struhl, 2004] Casali, A. and Struhl, G. (2004). Reading the hedgehog morphogen gradient by measuring the ratio of bound to unbound patched protein. *Nature*, 431(7004):76–80.

[Casanova, 2007] Casanova, J. (2007). The emergence of shape: notions from the study of the drosophila tracheal system. *EMBO reports*, 8(4):335–339.

[Chang et al., 2003] Chang, T., Shy, D., and Hartenstein, V. (2003). Antagonistic relationship between dpp and egfr signaling in drosophila head patterning. *Developmental biology*, 263(1):103–113.

[Colas and Schoenwolf, 2001] Colas, J.-F. and Schoenwolf, G. C. (2001). Towards a cellular and molecular understanding of neurulation. *Developmental dynamics*, 221(2):117–145.

[Colombelli and Solon, 2013] Colombelli, J. and Solon, J. (2013). Force communication in multicellular tissues addressed by laser nanosurgery. *Cell and tissue research*, 352(1):133–147.

[Costa et al., 1994] Costa, M., Wilson, E. T., and Wieschaus, E. (1994). A putative cell signal encoded by the folded gastrulation gene coordinates cell shape changes during drosophila gastrulation. *Cell*, 76(6):1075–1089.

[Cramer et al., 1997] Cramer, L. P., Siebert, M., and Mitchison, T. J. (1997). Identification of novel graded polarity actin filament bundles in locomoting heart fibroblasts: implications for the generation of motile force. *The Journal of cell biology*, 136(6):1287–1305.

[Davidson, 2012] Davidson, L. A. (2012). Epithelial machines that shape the embryo. *Trends in cell biology*, 22(2):82–87.

[de Matos Simões et al., 2010] de Matos Simões, S., Blankenship, J. T., Weitz, O., Farrell, D. L., Tamada, M., Fernandez-Gonzalez, R., and Zallen, J. A. (2010). Rho-kinase directs bazooka/par-3 planar polarity during drosophila axis elongation. *Developmental cell*, 19(3):377–388.

[Dickinson et al., 2011] Dickinson, D. J., Nelson, W. J., and Weis, W. I. (2011). A polarized epithelium organized by β-and α-catenin predates cadherin and metazoan origins. *Science*, 331(6022):1336–1339.

[Duffy, 2002] Duffy, J. B. (2002). Gal4 system in drosophila: a fly geneticist's swiss army knife. *genesis*, 34(1-2):1–15.

[Even-Ram et al., 2007] Even-Ram, S., Doyle, A. D., Conti, M. A., Matsumoto, K., Adelstein, R. S., and Yamada, K. M. (2007). Myosin iia regulates cell motility and actomyosin–microtubule crosstalk. *Nature cell biology*, 9(3):299–309.

[Eyckmans et al., 2011] Eyckmans, J., Boudou, T., Yu, X., and Chen, C. S. (2011). A hitchhiker's guide to mechanobiology. *Developmental cell*, 21(1):35–47.

[Farhadifar et al., 2007] Farhadifar, R., Röper, J.-C., Aigouy, B., Eaton, S., and Jülicher, F. (2007). The influence of cell mechanics, cell-cell interactions, and proliferation on epithelial packing. *Current Biology*, 17(24):2095–2104.

[Fernandez-Gonzalez et al., 2009] Fernandez-Gonzalez, R., de Matos Simoes, S., Röper, J.-C., Eaton, S., and Zallen, J. A. (2009). Myosin ii dynamics are regulated by tension in intercalating cells. *Developmental cell*, 17(5):736–743.

[Fernandez-Gonzalez and Zallen, 2009] Fernandez-Gonzalez, R. and Zallen, J. A. (2009). Cell mechanics and feedback regulation of actomyosin networks. *Science signaling*, 2(101):pe78.

[Fletcher et al., 2014] Fletcher, A. G., Osterfield, M., Baker, R. E., and Shvartsman, S. Y. (2014). Vertex models of epithelial morphogenesis. *Biophysical journal*, 106(11):2291–2304.

[Foe and Alberts, 1983] Foe, V. E. and Alberts, B. M. (1983). Studies of nuclear and cytoplasmic behaviour during the five mitotic cycles that precede gastrulation in drosophila embryogenesis. *Journal of cell science*, 61(1):31–70.

[Fossett et al., 2003] Fossett, N., Hyman, K., Gajewski, K., Orkin, S. H., and Schulz, R. A. (2003). Combinatorial interactions of serpent, lozenge, and u-shaped regulate crystal cell lineage commitment during drosophila hematopoiesis. *Proceedings of the National Academy of Sciences*, 100(20):11451–11456.

[Foty et al., 1996] Foty, R. A., Pfleger, C. M., Forgacs, G., and Steinberg, M. S. (1996). Surface tensions of embryonic tissues predict their mutual envelopment behavior. *Development*, 122(5):1611–1620.

[Franke et al., 2005] Franke, J. D., Montague, R. A., and Kiehart, D. P. (2005). Nonmuscle myosin ii generates forces that transmit tension and drive contraction in multiple tissues during dorsal closure. *Current biology*, 15(24):2208–2221.

[Friedl and Gilmour, 2009] Friedl, P. and Gilmour, D. (2009). Collective cell migration in morphogenesis, regeneration and cancer. *Nature reviews Molecular cell biology*, 10(7):445–457.

[Fromental-Ramain et al., 2008] Fromental-Ramain, C., Vanolst, L., Delaporte, C., and Ramain, P. (2008). pannier encodes two structurally related isoforms that are differentially expressed during drosophila development and display distinct functions during thorax patterning. *Mechanisms of development*, 125(1):43–57.

[Gates and Peifer, 2005] Gates, J. and Peifer, M. (2005). Can 1000 reviews be wrong? actin, α-catenin, and adherens junctions. *Cell*, 123(5):769–772.

[Ghysen and Dambly-Chaudière, 2007] Ghysen, A. and Dambly-Chaudière, C. (2007). The lateral line microcosmos. *Genes & development*, 21(17):2118–2130.

[Gimbrone et al., 1972] Gimbrone, M. A., Leapman, S. B., Cotran, R. S., and Folkman, J. (1972). Tumor dormancy in vivo by prevention of neovascularization. *The Journal of experimental medicine*, 136(2):261–276.

[Grether et al., 1995] Grether, M. E., Abrams, J. M., Agapite, J., White, K., and Steller, H. (1995). The head involution defective gene of drosophila melanogaster functions in programmed cell death. *Genes & development*, 9(14):1694–1708.

[Guillot and Lecuit, 2013] Guillot, C. and Lecuit, T. (2013). Mechanics of epithelial tissue homeostasis and morphogenesis. *Science*, 340(6137):1185–1189.

[Hakeda-Suzuki et al., 2002] Hakeda-Suzuki, S., Ng, J., Tzu, J., Dietzl, G., Sun, Y., Harms, M., Nardine, T., Luo, L., and Dickson, B. J. (2002). Rac function and regulation during drosophila development. *Nature*, 416(6879):438–442.

[Halbleib and Nelson, 2006] Halbleib, J. M. and Nelson, W. J. (2006). Cadherins in development: cell adhesion, sorting, and tissue morphogenesis. *Genes & development*, 20(23):3199–3214.

[Harden et al., 1999] Harden, N., Ricos, M., Ong, Y. M., Chia, W., and Lim, L. (1999). Participation of small gtpases in dorsal closure of the drosophila embryo: distinct roles for rho subfamily proteins in epithelial morphogenesis. *Journal of cell science*, 112(3):273–284.

[Heisenberg and Bellaïche, 2013] Heisenberg, C.-P. and Bellaïche, Y. (2013). Forces in tissue morphogenesis and patterning. *Cell*, 153(5):948–962.

[Hildebrand, 2005] Hildebrand, J. D. (2005). Shroom regulates epithelial cell shape via the apical positioning of an actomyosin network. *Journal of cell science*, 118(22):5191–5203.

[Honda et al., 2008] Honda, H., Nagai, T., and Tanemura, M. (2008). Two different mechanisms of planar cell intercalation leading to tissue elongation. *Developmental Dynamics*, 237(7):1826–1836.

[Hopyan et al., 2011] Hopyan, S., Sharpe, J., and Yang, Y. (2011). Budding behaviors: Growth of the limb as a model of morphogenesis. *Developmental Dynamics*, 240(5):1054–1062.

[Howard et al., 2001] Howard, J. et al. (2001). Mechanics of motor proteins and the cytoskeleton.

[Hu et al., 1998] Hu, Z., Chen, Y., Wang, C., Zheng, Y., and Li, Y. (1998). Polymer gels with engineered environmentally responsive surface patterns. *Nature*, 393(6681):149–152.

[Hummel et al., 1999] Hummel, T., Schimmelpfeng, K., and Klämbt, C. (1999). Commissure formation in the embryonic cns ofdrosophila: I. identification of the required gene functions. *Developmental biology*, 209(2):381–398.

[Hutson et al., 2003] Hutson, M. S., Tokutake, Y., Chang, M.-S., Bloor, J. W., Venakides, S., Kiehart, D. P., and Edwards, G. S. (2003). Forces for morphogenesis investigated with laser microsurgery and quantitative modeling. *Science*, 300(5616):145–149.

[Jacinto et al., 2002] Jacinto, A., Wood, W., Woolner, S., Hiley, C., Turner, L., Wilson, C., Martinez-Arias, A., and Martin, P. (2002). Dynamic analysis of actin cable function during drosophila dorsal closure. *Current biology*, 12(14):1245–1250.

[Karess et al., 1991] Karess, R. E., Chang, X.-j., Edwards, K. A., Kulkarni, S., Aguilera, I., and Kiehart, D. P. (1991). The regulatory light chain of nonmuscle myosin is encoded by spaghetti-squash, a gene required for cytokinesis in drosophila. *Cell*, 65(7):1177–1189.

[Karpova et al., 2006] Karpova, N., Bobinnec, Y., Fouix, S., Huitorel, P., and Debec, A. (2006). Jupiter, a new drosophila protein associated with microtubules. *Cell motility and the cytoskeleton*, 63(5):301–312.

[Kee and Robinson, 2008] Kee, Y.-S. and Robinson, D. N. (2008). Motor proteins: myosin mechanosensors. *Current Biology*, 18(18):R860–R862.

[Keller, 2013] Keller, P. J. (2013). Imaging morphogenesis: technological advances and biological insights. *Science*, 340(6137):1234168.

[Keller, 2006] Keller, R. (2006). Mechanisms of elongation in embryogenesis. *Development*, 133(12):2291–2302.

[Keller et al., 2003] Keller, R., Davidson, L. A., and Shook, D. R. (2003). How we are shaped: the biomechanics of gastrulation. *Differentiation*, 71(3):171–205.

[Keller and Shook, 2011] Keller, R. and Shook, D. (2011). The bending of cell sheets-from folding to rolling. *BMC biology*, 9(1):90.

[Kiehart et al., 2000] Kiehart, D. P., Galbraith, C. G., Edwards, K. A., Rickoll, W. L., and Montague, R. A. (2000). Multiple forces contribute to cell sheet morphogenesis for dorsal closure in drosophila. *The Journal of cell biology*, 149(2):471–490.

[Kovács et al., 2007] Kovács, M., Thirumurugan, K., Knight, P. J., and Sellers, J. R. (2007). Load-dependent mechanism of nonmuscle myosin 2. *Proceedings of the National Academy of Sciences*, 104(24):9994–9999.

[Kozlova and Thummel, 2003] Kozlova, T. and Thummel, C. S. (2003). Essential roles for ecdysone signaling during drosophila midembryonic development. *Science*, 301(5641):1911–1914.

[Landsberg et al., 2009] Landsberg, K. P., Farhadifar, R., Ranft, J., Umetsu, D., Widmann, T. J., Bittig, T., Said, A., Jülicher, F., and Dahmann, C. (2009). Increased cell bond tension governs cell sorting at the drosophila anteroposterior compartment boundary. *Current Biology*, 19(22):1950–1955.

[Lecuit et al., 2011] Lecuit, T., Lenne, P.-F., and Munro, E. (2011). Force generation, transmission, and integration during cell and tissue morphogenesis. *Annual review of cell and developmental biology*, 27:157–184.

[Lienkamp et al., 2012] Lienkamp, S. S., Liu, K., Karner, C. M., Carroll, T. J., Ronneberger, O., Wallingford, J. B., and Walz, G. (2012). Vertebrate kidney tubules elongate using a planar cell polarity-dependent, rosette-based mechanism of convergent extension. *Nature genetics*, 44(12):1382–1387.

[Lye and Sanson, 2011] Lye, C. M. and Sanson, B. (2011). 5 tension and epithelial morphogenesis in drosophila early embryos. *Current topics in developmental biology*, 95:145.

[Major and Irvine, 2006] Major, R. J. and Irvine, K. D. (2006). Localization and requirement for myosin ii at the dorsal-ventral compartment boundary of the drosophila wing. *Developmental dynamics*, 235(11):3051–3058.

[Mammoto and Ingber, 2010] Mammoto, T. and Ingber, D. E. (2010). Mechanical control of tissue and organ development. *Development*, 137(9):1407–1420.

[Marder, 1987] Marder, M. (1987). Soap-bubble growth. *Physical Review A*, 36(1):438.

[Martin, 2010] Martin, A. C. (2010). Pulsation and stabilization: contractile forces that underlie morphogenesis. *Developmental biology*, 341(1):114–125.

[Martin et al., 2010] Martin, A. C., Gelbart, M., Fernandez-Gonzalez, R., Kaschube, M., and Wieschaus, E. F. (2010). Integration of contractile forces during tissue invagination. *The Journal of cell biology*, 188(5):735–749.

[Martin and Lewis, 1992] Martin, P. and Lewis, J. (1992). Actin cables and epidermal movement in embryonic wound healing.

[McCartney and Fehon, 1996] McCartney, B. M. and Fehon, R. G. (1996). Distinct cellular and subcellular patterns of expression imply distinct functions for the drosophila homologues of moesin and the neurofibromatosis 2 tumor suppressor, merlin. *The Journal of cell biology*, 133(4):843–852.

[Merrill et al., 1989] Merrill, V., Diederich, R., Turner, F., and Kaufman, T. (1989). A genetic and developmental analysis of mutations in labial, a gene necessary for proper head formation in drosophila melanogaster. *Developmental biology*, 135(2):376–391.

[Mishra et al., 2012] Mishra, M., Huang, Y., Srivastava, P., Srinivasan, R., Sevugan, M., Shlomovitz, R., Gov, N., Rao, M., and Balasubramanian, M. (2012). Cylindrical cellular geometry ensures fidelity

of division site placement in fission yeast. *Journal of cell science*, 125(16):3850–3857.

[Monier et al., 2015] Monier, B., Gettings, M., Gay, G., Mangeat, T., Schott, S., Guarner, A., and Suzanne, M. (2015). Apico-basal forces exerted by apoptotic cells drive epithelium folding. *Nature*.

[Monier et al., 2010] Monier, B., Pélissier-Monier, A., Brand, A. H., and Sanson, B. (2010). An actomyosin-based barrier inhibits cell mixing at compartmental boundaries in drosophila embryos. *Nature cell biology*, 12(1):60–65.

[Monier et al., 2011] Monier, B., Pélissier-Monier, A., and Sanson, B. (2011). Establishment and maintenance of compartmental boundaries: role of contractile actomyosin barriers. *Cellular and Molecular Life Sciences*, 68(11):1897–1910.

[Müller and Newman, 2003] Müller, G. B. and Newman, S. A. (2003). Origination of organismal form.

[Nassif et al., 1998] Nassif, C., Daniel, A., Lengyel, J. A., and Hartenstein, V. (1998). The role of morphogenetic cell death duringdrosophilaembryonic head development. *Developmental biology*, 197(2):170–186.

[Nishimura et al., 2012] Nishimura, T., Honda, H., and Takeichi, M. (2012). Planar cell polarity links axes of spatial dynamics in neural-tube closure. *Cell*, 149(5):1084–1097.

[Nishimura and Takeichi, 2008] Nishimura, T. and Takeichi, M. (2008). Shroom3-mediated recruitment of rho kinases to the apical cell junctions regulates epithelial and neuroepithelial planar remodeling. *Development*, 135(8):1493–1502.

[Ntwasa et al., 2001] Ntwasa, M., Aapies, S., Schiffmann, D. A., and Gay, N. J. (2001). Drosophila embryos lacking n-myristoyltransferase

have multiple developmental defects. *Experimental cell research*, 262(2):134–144.

[Odell et al., 1981] Odell, G. M., Oster, G., Alberch, P., and Burnside, B. (1981). The mechanical basis of morphogenesis: I. epithelial folding and invagination. *Developmental biology*, 85(2):446–462.

[Olofsson and Page, 2005] Olofsson, B. and Page, D. T. (2005). Condensation of the central nervous system in embryonic drosophila is inhibited by blocking hemocyte migration or neural activity. *Developmental biology*, 279(1):233–243.

[Page and Olofsson, 2008] Page, D. T. and Olofsson, B. (2008). Multiple roles for apoptosis facilitating condensation of the drosophila ventral nerve cord. *genesis*, 46(2):61–68.

[Pocha and Knust, 2013] Pocha, S. M. and Knust, E. (2013). Complexities of crumbs function and regulation in tissue morphogenesis. *Current Biology*, 23(7):R289–R293.

[Pollard and Cooper, 1986] Pollard, T. D. and Cooper, J. A. (1986). Actin and actin-binding proteins. a critical evaluation of mechanisms and functions. *Annual review of biochemistry*, 55(1):987–1035.

[Pouille et al., 2009] Pouille, P.-A., Ahmadi, P., Brunet, A.-C., and Farge, E. (2009). Mechanical signals trigger myosin ii redistribution and mesoderm invagination in drosophila embryos. *Science signaling*, 2(66):ra16–ra16.

[Prehoda, 2009] Prehoda, K. E. (2009). Polarization of drosophila neuroblasts during asymmetric division. *Cold Spring Harbor perspectives in biology*, 1(2):a001388.

[Rehorn et al., 1996] Rehorn, K.-P., Thelen, H., Michelson, A. M., and Reuter, R. (1996). A molecular aspect of hematopoiesis and endoderm development common to vertebrates and drosophila. *Development*, 122(12):4023–4031.

[Reichert and Boyan, 1997] Reichert, H. and Boyan, G. (1997). Building a brain: developmental insights in insects. *Trends in neurosciences*, 20(6):258–264.

[Rogers and Kaufman, 1996] Rogers, B. T. and Kaufman, T. C. (1996). Structure of the insect head as revealed by the en protein pattern in developing embryos. *Development*, 122(11):3419–3432.

[Roh-Johnson et al., 2012] Roh-Johnson, M., Shemer, G., Higgins, C. D., McClellan, J. H., Werts, A. D., Tulu, U. S., Gao, L., Betzig, E., Kiehart, D. P., and Goldstein, B. (2012). Triggering a cell shape change by exploiting pre-existing actomyosin contractions. *Science (New York, NY)*, 335(6073):1232.

[Röper, 2012] Röper, K. (2012). Anisotropy of crumbs and apkc drives myosin cable assembly during tube formation. *Developmental cell*, 23(5):939–953.

[Röper, 2013] Röper, K. (2013). Supracellular actomyosin assemblies during development. *Bioarchitecture*, 3(2):45–49.

[Rørth, 2009] Rørth, P. (2009). Collective cell migration. *Annual Review of Cell and Developmental*, 25:407–429.

[Salbreux et al., 2012] Salbreux, G., Charras, G., and Paluch, E. (2012). Actin cortex mechanics and cellular morphogenesis. *Trends in cell biology*, 22(10):536–545.

[Sanson, 2001] Sanson, B. (2001). Generating patterns from fields of cells. *EMBO reports*, 2(12):1083–1088.

[Schilling et al., 2011] Schilling, S., Willecke, M., Aegerter-Wilmsen, T., Cirpka, O. A., Basler, K., and von Mering, C. (2011). Cell-sorting at the a/p boundary in the drosophila wing primordium: a computational model to consolidate observed non-local effects of hh signaling. *PLoS computational biology*, 7(4):e1002025.

[Sherrard et al., 2010] Sherrard, K., Robin, F., Lemaire, P., and Munro, E. (2010). Sequential activation of apical and basolateral contractility drives ascidian endoderm invagination. *Current Biology*, 20(17):1499–1510.

[Simons and Mlodzik, 2008] Simons, M. and Mlodzik, M. (2008). Planar cell polarity signaling: from fly development to human disease. *Annual review of genetics*, 42:517.

[Sink, 2006] Sink, H. (2006). *An Introduction to Muscle Development in Drosophila*. Springer.

[Slováková et al., 2012] Slováková, J., Speicher, S., Sánchez-Soriano, N., Prokop, A., and Carmena, A. (2012). The actin-binding protein canoe/af-6 forms a complex with robo and is required for slit-robo signaling during axon pathfinding at the cns midline. *The Journal of Neuroscience*, 32(29):10035–10044.

[Steinberg, 1963] Steinberg, M. S. (1963). Reconstruction of tissues by dissociated cells. *Science*, 141(3579):401–408.

[Suzanne et al., 2010] Suzanne, M., Petzoldt, A. G., Spéder, P., Coutelis, J.-B., Steller, H., and Noselli, S. (2010). Coupling of apoptosis and l/r patterning controls stepwise organ looping. *Current Biology*, 20(19):1773–1778.

[Tabata et al., 1992] Tabata, T., Eaton, S., and Kornberg, T. (1992). The drosophila hedgehog gene is expressed specifically in posterior compartment cells and is a target of engrailed regulation. *Genes and Development*, 6:2635–2635.

[Tateno et al., 2000] Tateno, M., Nishida, Y., and Adachi-Yamada, T. (2000). Regulation of jnk by src during drosophila development. *Science*, 287(5451):324–327.

[Teng and Toyama, 2011] Teng, X. and Toyama, Y. (2011). Apoptotic force: active mechanical function of cell death during morphogenesis. *Development, growth & differentiation*, 53(2):269–276.

[Tepass et al., 2000] Tepass, U., Truong, K., Godt, D., Ikura, M., and Peifer, M. (2000). Cadherins in embryonic and neural morphogenesis. *Nature Reviews Molecular Cell Biology*, 1(2):91–100.

[Therianos et al., 1995] Therianos, S., Leuzinger, S., Hirth, F., Goodman, C. S., and Reichert, H. (1995). Embryonic development of the drosophila brain: formation of commissural and descending pathways. *Development*, 121(11):3849–3860.

[Thompson et al., 1942] Thompson, D. W. et al. (1942). On growth and form. *On growth and form.*

[Trichas et al., 2012] Trichas, G., Smith, A. M., White, N., Wilkins, V., Watanabe, T., Moore, A., Joyce, B., Sugnaseelan, J., Rodriguez, T. A., Kay, D., et al. (2012). Multi-cellular rosettes in the mouse visceral endoderm facilitate the ordered migration of anterior visceral endoderm cells. *PLoS biology*, 10(2):e1001256.

[Trier and Davidson, 2011] Trier, S. M. and Davidson, L. A. (2011). Quantitative microscopy and imaging tools for the mechanical analysis of morphogenesis. *Current opinion in genetics & development*, 21(5):664–670.

[VanHook and Letsou, 2008] VanHook, A. and Letsou, A. (2008). Head involution in drosophila: genetic and morphogenetic connections to dorsal closure. *Developmental Dynamics*, 237(1):28–38.

[Villar et al., 2013] Villar, G., Graham, A. D., and Bayley, H. (2013). A tissue-like printed material. *Science*, 340(6128):48–52.

[Walck-Shannon and Hardin, 2014] Walck-Shannon, E. and Hardin, J. (2014). Cell intercalation from top to bottom. *Nature Reviews Molecular Cell Biology*, 15(1):34–48.

[Wang et al., 2012] Wang, Y.-C., Khan, Z., Kaschube, M., and Wieschaus, E. F. (2012). Differential positioning of adherens junctions is

associated with initiation of epithelial folding. *Nature*, 484(7394):390–393.

[Warga and Kimmel, 1990] Warga, R. M. and Kimmel, C. B. (1990). Cell movements during epiboly and gastrulation in zebrafish. *Development*, 108(4):569–580.

[Weliky et al., 1991] Weliky, M., Minsuk, S., Keller, R., and Oster, G. (1991). Notochord morphogenesis in xenopus laevis: simulation of cell behavior underlying tissue convergence and extension. *Development*, 113(4):1231–1244.

[White et al., 1994] White, K., Grether, M. E., Abrams, J. M., Young, L., Farrell, K., and Steller, H. (1994). Genetic control of programmed cell death in drosophila. *Science*, 264(5159):677–683.

[Wood and Jacinto, 2007] Wood, W. and Jacinto, A. (2007). Drosophila melanogaster embryonic haemocytes: masters of multitasking. *Nature Reviews Molecular Cell Biology*, 8(7):542–551.

[Wood et al., 2002] Wood, W., Jacinto, A., Grose, R., Woolner, S., Gale, J., Wilson, C., and Martin, P. (2002). Wound healing recapitulates morphogenesis in drosophila embryos. *Nature cell biology*, 4(11):907–912.